Development of a Generic Model for Real - time Simulation and Assessment of the Dynamic Performance of a Large Scale Offshore Transmission Network

Saran Ganesh

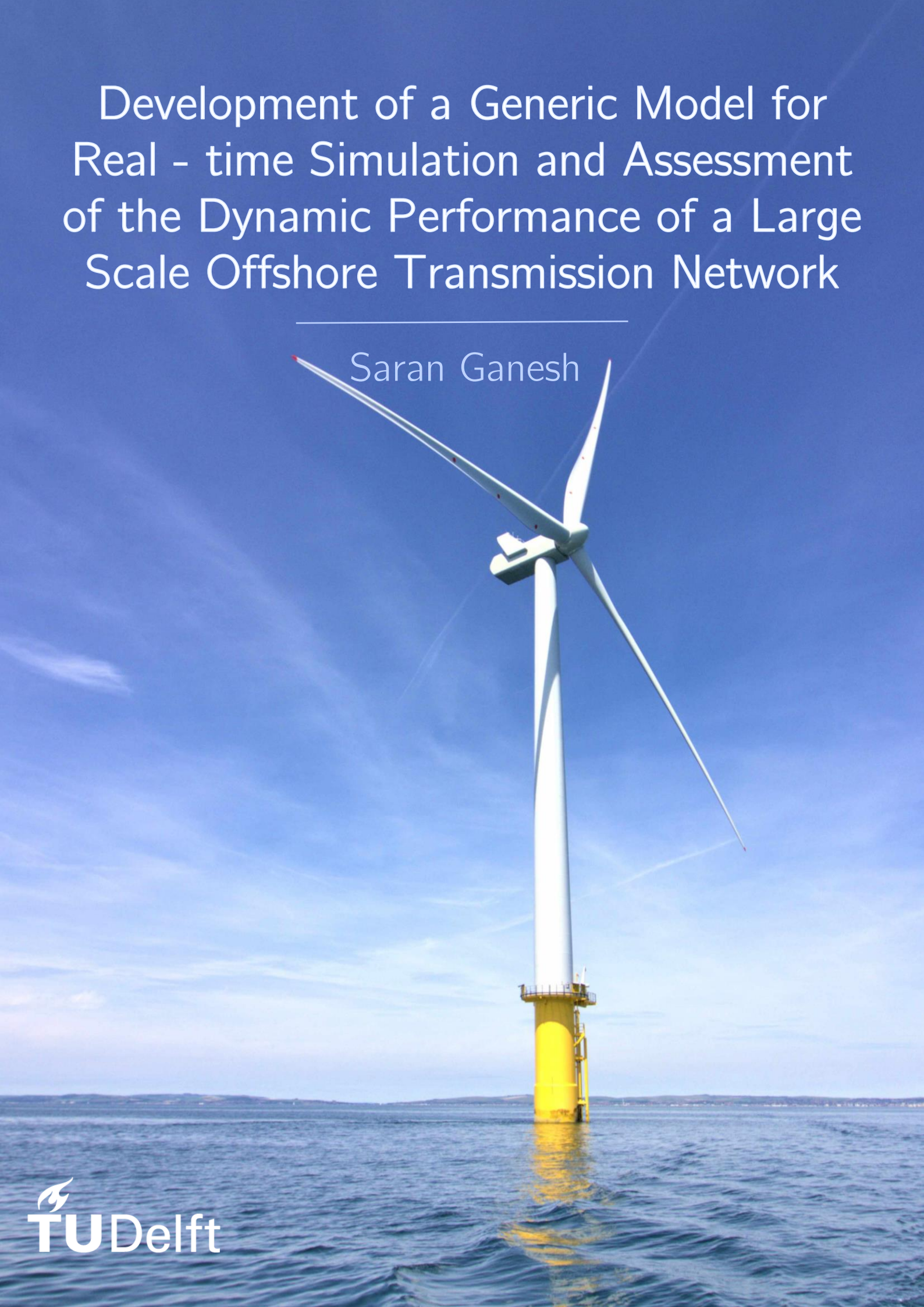

TU Delft

Development of a Generic Model for Real-time Simulation and Assessment of the Dynamic Performance of a Large Scale Offshore Transmission Network

by

Saran Ganesh

in partial fulfillment of the requirements for the degree of

Master of Science
in Electrical Power Engineering

at the Delft University of Technology,
to be defended on October 29, 2020 at 10:00 AM.

Supervisor:	Dr. ir. J.L. (Jose) Rueda Torres	
Thesis committee:	Prof. ir. M.A.M.M. (Mart) van der Meijden,	IEPG
	Dr. ir. J.L. (Jose) Rueda Torres,	IEPG
	Dr. T. (Thiago) Batista Soeiro	DCES

TU Delft Delft University of Technology

Acknowledgement

There are many people to thank for the successful completion of my thesis. Firstly, I would like to thank Dr. Jose Rueda Torres for providing me with this opportunity to work on such an interesting topic and guiding me throughout the research. His inputs and suggestions have been extremely valuable. All the constructive criticisms through his comments for my report and presentations has helped in developing me as a good researcher and a good human being. My sincere gratitude to Prof. Mart van der Meijden for believing in me and for the constant support. He has always made me aware of the bigger picture of the work I was doing. I am incredibly thankful to both my supervisors for their support and goodwill during this thesis. Moreover, I thank Dr. Thiago Batista for being a part of my thesis committee and taking time to review and assess my work.

I am indebted to my daily supervisor Arcadio Perilla for holding the torch to light my path all along this uphill journey. I am grateful for all the discussions, explanations and proposed ideas for the successful completion of this project. He has been a great teacher to me from the start of my thesis and this work would not have been possible without his help and contribution.

A special thanks to Dr. Abdul Korai from DIgSILENT GmbH and Shubham Sethi from Hitachi ABB Power Grids, whose works served as an inspiration for the development of this thesis and for their insights on the report. I also extend my gratitude to Nidarshan, Dr. Zameer Ahmad and Ajay for their sharp comments given during the break discussions. Every time I hit a roadblock, they assured me that 'this too shall pass'. Also, thanks for the free coffee!

I am extremely grateful for my friends Preetha, Vishal, Medha, Nived, Devika chechi, Adeep and Lee for being my support system and keeping my sanity intact. They are now family to me and have played a huge role in the last two years of my life in Delft. Thank you so much people! A big shout out to Medha and Nived for helping me with the cover picture.

Finally, I extend my gratitude to Varun and Veena manni for their love and support. Last but not the least, I take this opportunity to thank Amma and Appa for letting me pursue my ambition, supporting and encouraging me to achieve my dreams. Thank you so much Amma and Appa!

To the Class of 2020..

Saran Ganesh
Delft, October 2020

Abstract

The Paris Agreement, which calls for countries to channel their efforts to limit global warming would require the deployment of large scale offshore wind energy in the North Sea. This includes the possibility of developing offshore infrastructure for deploying offshore wind power generation with installed capacity ranging from 70 to 150 GW by 2040 and increasing up to 180 GW by 2045. Presently, the Voltage Source Converter (VSC) based - High Voltage Direct Current (HVDC) transmission is considered the most suitable for transfer of offshore wind power from distant offshore wind farms (OWFs) to the onshore system. Amidst the available VSC topologies, Modular Multi-level Converter (MMC) topology is the most appropriate solution for the transfer of offshore wind power to onshore systems due to their enhanced performance during offshore and onshore disturbances. However, the currently deployed state-of-the-art MMC-HVDC transmission has a maximum capacity of 1.2 GW. Compatibility of this available technology for complex systems, with the working of parallel units contributing to the increase in power transfer capacity is still unknown. Hence, this demands the development and analysis of a generic model with parallel operation of MMC-HVDC transmission systems to transfer the bulk amount of power from large scale OWFs.

Additionally, the implementation of large scale offshore networks leads to an increase in the penetration of power electronic (PE) converters in the electrical power system. The increase in PE converters causes technical challenges (e.g. due to unprecedented fast dynamic phenomena) related to voltage and frequency stability, and power flow coordination in the power system. In OWFs, the currently available current injection-based voltage control for PE converters are not suitable for voltage control in large scale PE dominated systems due to the absence of continuous voltage control and ineffectiveness during islanding. Moreover, in such power systems, the conventional controllers are not suitable for frequency control due to the absence of dynamic frequency control. Therefore, better control strategies are required in large scale offshore networks to enhance the dynamic characteristics of the power system.

Conventionally, the OWFs are coupled to an AC collector platform through 33 kV High Voltage Alternating Current (HVAC) cables. The voltage is stepped-up to 145 kV at the collector platform, and power is transferred to the offshore converter station using 145 kV HVAC cables. However, in the upcoming projects, the rated voltage levels are expected to increase from 33 kV to 66 kV to avoid the use of such a collector platform and directly transfer power from OWFs to the offshore converter station using 66 kV HVAC cables. Hence, it would be better to understand the performance of large scale offshore networks developed with 66 kV voltage rating.

This thesis proposes a digital twin model of a 2 GW offshore network with the parallel operation of two MMC-HVDC transmission links connecting four OWFs to two onshore systems representing a large scale power system. The MMCs are connected to a common bus on the AC side of the network, with one MMC creating the voltage reference for the common bus and the other MMC following this reference. Additionally, to mitigate the challenges corresponding to voltage and frequency stability in large scale offshore networks, a Direct Voltage Control (DVC) strategy is implemented in the Type-4 Wind Generators (WGs) representing the OWFs. After analyzing the need for 66 kV HVAC transmission from the OWFs to the offshore converter stations, a 66 kV offshore network is developed to achieve 2 GW offshore wind power transfer. The electrical power system is developed in the power system simulation software, RSCAD^{TM} Version 5.011.1, in order to perform Electro-Magnetic Transient (EMT) based simulations.

Initially, a single OWF with DVC implemented in the WG connected to an AC equivalent system is modelled to test the performance of DVC in a digital twin of a 66 kV HVAC network. The DVC provides continuous voltage control that improves the dynamic performance of the power system. As mentioned in most of the grid codes, the important requirement of reactive power injection by the OWF during dynamic conditions is satisfied by the controller. DVC also avoids the need for an external controller to perform such an action. To validate the working of the implemented DVC in RSCAD, a similar 66 kV HVAC network with the benchmark DVC model is developed in DIgSILENT PowerFactory^{TM} 2019 SP2 (x64), for EMT simulations and tested under severe dynamic conditions. Both the models provide similar results, confirming the validation of the RSCAD model. Moreover, the RSCAD model provides a better representation of the real-world operation.

To achieve the overall goal of developing a 2 GW offshore transmission network, a hybrid system with the hub-and-spoke principle is utilized in this thesis. The 2 GW offshore network is achieved by a modular approach, connecting four OWFs to a common bus, to which two MMCs are connected in parallel. The coordination between the implemented DVC in WGs and the control structures in MMCs is evaluated for different scenarios in the network. The performance of the 2 GW network in terms of short-term voltage stability and power flow during severe dynamic conditions in the grid is analyzed. The two most severe dynamic conditions chosen for assessment are; the disconnection of one OWF, and a three-phase fault in the middle of an HVAC cable. In the analysis, it is observed that even after the loss of generation from one OWF, the voltage at Point of Common Coupling (PCC) of other OWFs remains stable within

the tolerance limit of ± 10 %. Additionally, the loss of generation decreases the active power flow in MMC-1 since it is the one that creates the voltage reference. The power flow in MMC-2 is maintained with the corresponding active power reference. For the event of a three-phase fault, the OWF is islanded by the operation of a circuit breaker. During this event, with implemented DVC, the important requirement of reactive power injection from the islanded OWF as stated in most of the grid codes is achieved. This leads to the conclusion that the voltage control in MMC-1 provides the voltage reference in the network during the pre-fault and post fault conditions. However, DVC implemented in the WGs of OWFs take up the role of providing the voltage reference at corresponding PCCs when the OWFs are islanded from the network during the time of the fault.

Contents

List of Figures

List of Abbreviations

AC Alternating Current

DC Direct Current

dq Direct Quadrature

DVC Direct Voltage Control

EMT Electro-Magnetic Transient

EU European Union

FSC Full Scale Converter

GSC Grid Side Converter

HPF High Pass Filter

HV High Voltage

HVAC High Voltage Alternating Current

HVDC High Voltage Direct Current

IGBT Insulated Gate Bipolar Transistors

LSC Line Side Converter

LV Low Voltage

MMC Modular Multi-level Converter

MPPT Maximum Power Point Tracking

MSC Machine Side Converter

NPC Neutral Point Clamped

OWF Offshore Wind Farm

PCC Point of Common Coupling

PE Power Electronic

PI Proportional Integral

PLL Phase Locked Loop

PMSG Permanent Magnet Synchronous Generator

PWM Pulse Width Modulation

RES Renewable Energy Sources

RTDS Real Time Digital Simulator

VDAPR Voltage Dependent Active Power Reduction

VSC Voltage Source Converter

WECS Wind Energy Conversion Systems

WG Wind Generator

1 Introduction

This chapter discusses the motivation, specific context, research gaps of literature, goals and research questions, overall methodological approach, and the list of scientific contributions.

1.1. Background and Motivation

To combat climate change, the production of greenhouse gas emissions must be reduced to significant levels and shift to the use of Renewable Energy Sources (RES) must be accomplished. In numbers, the European Union's (EU) Nationally Determined Contribution (NDC) under the Paris Agreement is to reduce greenhouse gas emissions by at least 40% by 2030 when compared to 1990 [1].

The plans involve a future target of nearly 70 GW to 150 GW offshore wind power in the North Sea by 2040. A scope of 140 to 450 GW of offshore wind power in the EU by 2050 is seen from the latest European Commission situations. Going with the current pace, the rate of offshore wind energy deployment is deficient in reaching the objectives of the Paris Agreement. To comply with these objectives, an extraordinary jump in offshore wind energy is required, as shown in Figure 1.1. A practical solution calls for an increase in large scale offshore wind energy deployment in the North Sea [2]. As part of the North Sea Wind Power Hub Programme [3], the Transmission System Operator (TSO) of the Netherlands, TenneT, has already entered into an innovation partnership with its suppliers to establish a 2 GW offshore platform to bring in their contribution towards the Paris Agreement. Likewise, Denmark is progressing with the first hub-and-spoke energy island with a vision of connecting at least 10 GW of offshore wind power in the North Sea [4]. While the requirement for large scale offshore networks is appealing, the technical challenges that could be encountered should also be considered.

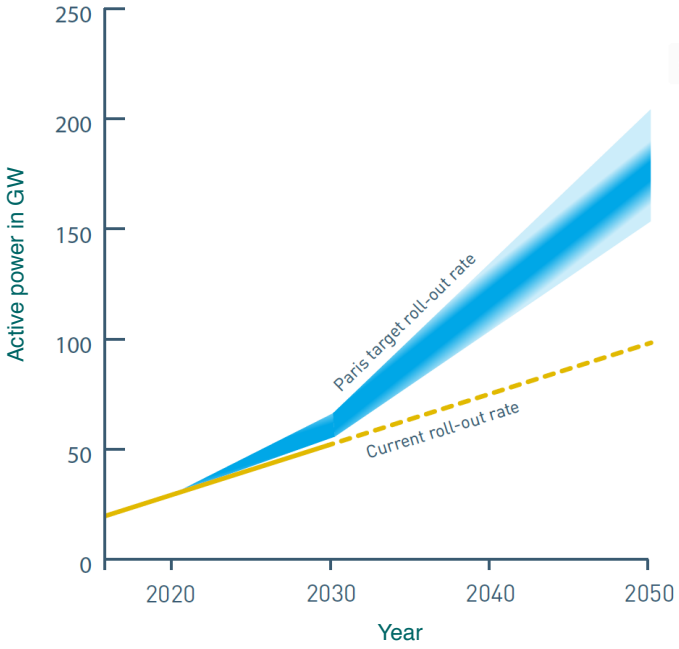

Figure 1.1: Installed wind capacity in the North Sea in GW [2]

RES are connected to the power system through Power Electronic (PE) converters as shown in Figure 1.2. The PE converters do not possess inherent inertial response characteristics. Until now, the integration of RES to power system has not created major problems since the stability of the system is maintained by the synchronous machines in power plants. Traditionally, the inertia for the power system is provided by these synchronous machines connected to the network (Figure 1.3). However, an increase in RES in the future causes an increase in PE converter based generation units. Simultaneously, the synchronous machines in conventional power plants need to be disconnected from the network. This makes the power systems weak due to low short circuit power and low system inertia. Therefore, the consequence of disconnecting the synchronous generators leads to the requirement of the PE converter based generation units to take up the role of governing the stability of the power system.

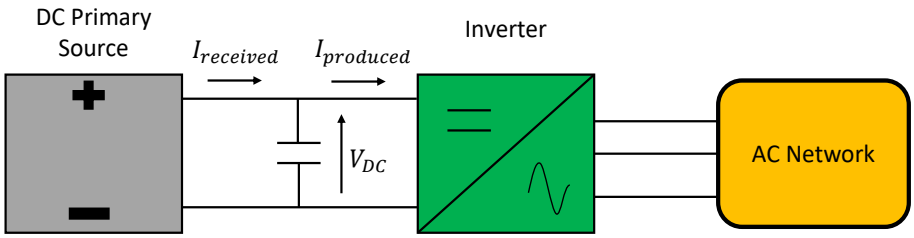

Figure 1.2: PE converter-based generation connection to the AC network [5]

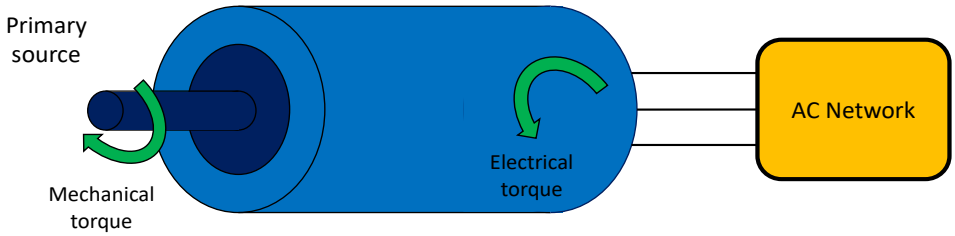

Figure 1.3: Synchronous machine connection to the AC network [5]

The majorly contributing source among the available RES is wind energy. Specifically, offshore wind energy is predicted to be the most significant source of energy among the North Sea countries by 2040 [6]. As a result, the deployment of offshore wind energy technology is expected to grow further. With the increase in integration of offshore wind energy, the inherent characteristics of offshore wind energy conversion systems will affect the nature of the power system. The vulnerable wind speed conditions due to the uncertain behaviour of wind could lead to variations in the supply and demand, and therefore, fluctuations in voltages and frequency are bound to occur. Moreover, as the power systems become weak due to the decommissioning of synchronous generators in conventional power plants that use non-renewable energy sources, the integration of offshore wind power plants to such weak power systems pose various research challenges on the power system stability.

One of the challenges is related to voltage stability. The continuous variation in offshore wind speed causes a constant change in the active power output of the offshore wind power plant. This could lead to an increase in the reactive power output and consequently, the voltage at the point of common coupling (PCC). The conventional current control methods using Proportional Integral (PI) controllers in the modern Wind Generators (WGs) are capable of providing voltage control by injecting reactive currents when connected to a strong network [1]. However, these controllers are not suitable for operation in highly PE converter dominated grids as the connected network is weak and is not capable of absorbing the injected currents. Furthermore, during the scenario of islanding, voltage control by the conventional current controllers is ineffective due to the absence of continuous voltage control, and the deviation in voltage is not high enough to activate an effective voltage reduction mechanism. There are challenges in terms of frequency stability as well since the conventional current controllers in the WGs are not equipped to provide frequency control of the network during islanding.

Currently, the state-of-the-art technology for the transfer of offshore wind power to the onshore system is Voltage Source Converter (VSC) based - High Voltage Direct Current (HVDC) transmission links. Presently, Modular Multilevel Converter (MMC) topology that falls under the classification of VSC topologies is the most suitable solution. Few among the advantages of MMC are [7]; (1) ease of integration with Offshore Wind Farms (OWF)s, (2) supporting the bi-directional flow of power between the offshore network and onshore system, and (3) independent control of active

[1] SCR = SC_{MVA}/P; where SC_{MVA} is the short circuit power of the network and P is the active power generation.
If SCR = 100 to 250, it is a strong grid. If SCR = 5 to 25, it is a weak grid.

and reactive powers in the network. However, with the available technology, MMC-HVDC transmission are limited to a rated capacity of 1.2 GW [8].

The implementation of large scale offshore networks (greater than or equal to 2 GW) creates a highly PE converter dominated network. The challenges mentioned above in terms of voltage and frequency control by the PE converters without the presence of conventional units are prominent in large scale offshore networks.

The absence of conventional generators would mean that the PE converters will have to take into account the decreasing inertia of the system that leads to faster dynamic behaviour and needs controllers with faster time response. Moreover, in large scale offshore networks, distant OWFs would be connected in parallel. With the parallel operation of the conventional current controllers in WGs, interactions can persist among them and could lead to instability of the network. Additionally, the restoration of the grid, following disturbances by the PE converter units is a serious matter of concern. With the conventional current control approach, grid restoration is challenging without the help of auxiliary diesel generators. However, in the case of large scale offshore networks, the role of grid restoration must be taken up by PE converters. There can be arguments that storage facilities such as battery and thermal can be a realizable solution in case when there are no conventional generators available. Huge investment costs, low lifetime and low efficiency when compared to controller modifications are the drawbacks that make these storage facilities practically unusable in large scale offshore networks [9].

Traditionally, the transmission of power from OWF to the offshore converter station uses a combination of 33 kV and 145 kV High Voltage Alternating Current (HVAC) cables. The OWFs are connected to an Alternating Current (AC) offshore platform using 33 kV HVAC cables. The platform holds a power transformer that is used to step-up voltage from 33 kV to 145 kV, and power is transferred from the AC platform to the offshore converter station using 145 kV HVAC cables [10]. However, the upcoming projects are expected to have a higher voltage level of 66 kV for transmission to allow twice the amount of power transferred compared to 33 kV. Therefore, this would only require 66 kV HVAC cables to directly connect OWFs to offshore converter station, avoiding the use of an AC collector platform [11]. Hence, advancing towards large scale offshore networks, it would be more appropriate to assess the performance of these networks developed with 66 kV HVAC transmission.

With the available MMC-HVDC transmission technology, multiple MMC-HVDC transmission links connected in parallel would be required to transfer the bulk amount of offshore wind power generated from large scale offshore networks to the onshore system. In such networks, the power flow between the parallel operated MMCs and the OWFs must be coordinated during steady state and dynamic conditions. The major challenges regarding voltage and frequency control during islanding of the OWFs must be taken into account. The scenario of reactive current injection that needs to be provided by the WGs during dynamic conditions as demanded by majority of the grid codes must also be taken into consideration [12]. Therefore, the progress towards the development of large scale offshore networks calls for a generic model with a suitable layout with the available technology that is capable of tackling the aforementioned technical challenges and providing stable operation during steady state and dynamic conditions.

1.2. Literature Review

As seen in Section 1.1, the significant challenges are; development of large scale offshore networks with the available technology, no much knowledge about 66 kV HVAC transmission available, and new control strategies are required that can provide better control of voltage and frequency. Hence, a generic model for large scale offshore networks with the latest trend in available technology, and enhanced control strategies is a crucial research requirement.

Based on MMC-HVDC transmission technology, there are mainly three configurations available for the connection of offshore and onshore converter stations [7], [13]:

- Point-to-point connection: The configuration connects one OWF to the offshore converter station, which is then connected using HVDC link to the onshore converter station.
- Multi-infeed connection: The configuration involves connecting one OWF to two different onshore systems by connecting two offshore converter stations on a common bus on the AC side and transmitting power through two HVDC links. Such a configuration allows for increasing the rating of the OWF beyond the capacity of a single offshore converter station. The drawback of such a configuration is that it allows the connection of only one OWF to the network.
- Multi-Terminal Direct Current (MTDC) connection: In this configuration, the HVDC links of multiple offshore converter stations are connected to the main Direct Current (DC) link. Such a configuration enables the transfer of active power to onshore system depending on the capacity of the main DC link. However, the major drawback is that complete shutdown and restart of connected MMCs is required for a fault on the DC side.

The multi-infeed and the MTDC connections allow for parallel operation of MMCs, which is a significant requirement for large scale offshore networks with the available technology. However, both the configurations have the drawback of being able to connect only one OWF to the network. Therefore, configurations that utilize several OWFs with

parallel operation of MMCs are currently unavailable and is a key area of research. The topology mentioned in [14] embraces the utilization of 66 kV HVAC transmission from the OWFs (all connected in parallel) to the offshore converter station. However, the topology examined does not utilize parallel operation of MMCs and uses only one MMC-HVDC link with a maximum power transfer capacity of 1 GW.

Typically, PE converters in the WGs are connected to the network for parallel operation using present state-of-the-art technology, current control strategies. In such control strategies, the regulation of power output of the converters is achieved by measuring the angle of the grid voltage. The drawback of these control strategies is that they require an already existing reference voltage. There are control strategies that create the reference voltage and are termed as voltage control strategies. One among the voltage control strategies is the V/F (voltage/frequency) control that is utilized for operation in the islanded mode. The drawback with V/F control is that it is not equipped for the parallel operation of various voltage forming converter units [15]. Therefore, there need to be new control strategies in the WGs that can create the reference voltage and work in parallel operation. Such control strategies are an emerging area of research and studies are being performed in this regard. Few among the new control strategies are mentioned as follows:

- Virtual Synchronous Machines (VSM): The PE converter control is modelled with the characteristics of a synchronous machine in terms of inertia and voltage support by correspondingly deriving the equivalent equations [16], [17], [18].
- Modified Droop Control: This strategy is common for standalone grids, where the parallel operation of voltage forming units is developed recently using the f/P (frequency/active power) and V/Q (voltage/reactive power) droop controls similar to the control in synchronous generators [19]. Few authors have named these droop control concepts as Virtual Synchronous Machines Without Inertia (VSCM0H) [20].
- Direct Voltage Control (DVC): DVC is a representation of the conventional current control approach towards a voltage control. DVC allows for the direct control of the AC converter voltage which in turn varies the current injected by the converter [21], [22]. This approach provides continuous voltage control both in steady-state and dynamic scenarios.
- Extended Current Control: The control is similar to the conventional current control with an additional inertia control in the outer control loop by using a synthetic inertia controller that gives a behaviour similar to that of a synchronous machine [23] [24].

Studies performed by I. Erlich et al. and A. Korai et al. in [22] and [21] show appealing results of the implemented DVC for highly PE dominated systems. The simulations are tested for different grids based on real-world data and provide promising outcomes with effective voltage and frequency control. Hence, with such proven results and available models, the DVC strategy was chosen to be incorporated for this work. Moreover, the real-time implementation of DVC in Type-4 WG is attempted in [25], but the latest trend of 66 kV HVAC transmission and the major requirement of reactive current injection by the WGs during dynamic conditions is lacking.

It is also good to analyze the effectiveness of other control strategies mentioned above. With a generic offshore network model, different control strategies can be implemented in the OWFs, and the complexity related to the interoperability of the controllers can be assessed. However, this lies beyond the scope of this project.

1.3. Objectives and Research Questions

The overall goal of the thesis is to develop a generic digital twin model of 2 GW, 66 kV HVAC offshore network and to perform analysis on the dynamics of voltage and power at various locations in the network. The thesis makes use of the Electro-Magnetic Transient (EMT) simulation-based software tools such as RSCAD and DIgSILENT PowerFactory to analyze the performance of the developed control models. The average model of Type-4 WG available in RSCAD is used as a starting point. The thesis provides a detailed description of the different available features in RSCAD that are employed to develop the 2 GW model. To achieve the overall goal, the following research questions are defined:

- How effective is the Direct Voltage Control (DVC) when implemented in an EMT average model of Type-4 WG connected to a 66 kV equivalent HVAC system in RSCAD?
- What insights can be attained by the EMT average model of Type-4 WG with DVC in 66 kV network in RSCAD in comparison with a similar network modelled with a simplified Type-4 WG configuration with DVC in DIgSILENT PowerFactory?
- How can Type-4 WGs with implemented DVC work in coordination with offshore MMCs within a multi-gigawatt offshore transmission network?

- How effectively do Type-4 WGs with implemented DVC perform when connected in an offshore network for parallel operation?

1.4. Thesis Contribution

On behalf of the thesis objectives defined above, the major contributions from this thesis are presented in this section.

- Implementation of the DVC in Type-4 WG model in RSCAD for an offshore 66 kV HVAC network. With proper documentation provided in this report, the developed 66 kV HVAC model in RSCAD can be utilized for future work.
- Development of a 66 kV HVAC offshore network in PowerFactory by adapting the benchmark DVC model in Type-4 WGs. With proper documentation provided in this report, the developed 66 kV HVAC model in PowerFactory model can be utilized for future work.
- Development of a digital twin of 2 GW, 66 kV HVAC offshore network with DVC implemented in Type-4 WGs connected to two offshore converter stations in RSCAD. With proper documentation provided in this report, the developed 2 GW model in RSCAD can be utilized for future work.
- Automation script for the operation of the developed 2 GW offshore network model using the interface between RSCAD and MATLAB is created.

1.5. Thesis Outline

A brief outline of the methodology is structured in several chapters, which sequentially describe the performed tasks as follows:

- Chapter 2: The chapter presents the concepts of wind energy conversion system and the classification of wind turbines. The overview of the OWF network with all the major equipment and the latest trend in technology is explained. The issues with the present current control strategies and the necessity to move towards better control strategies are addressed. The new control strategy, DVC, to be implemented in Type-4 WG is formulated.
- Chapter 3: The implementation of DVC in [21] and [25] for a digital twin of 66 kV HVAC offshore network in RSCAD is detailed. The performance of Type-4 WG with DVC, in terms of short-term voltage stability and reactive current injection, under severe disturbances is analyzed. Modelling of a similar 66 kV HVAC offshore network in DIgSILENT PowerFactory tool is also addressed. The comparison of the dynamic performance of DVC in two EMT platforms (RSCAD and PowerFactory) for a 66 kV HVAC offshore network during severe disturbances is carried out.
- Chapter 4: The development of a large scale digital twin model of a 2 GW offshore network in RSCAD is detailed. The modifications in the control structures of the MMCs to work in coordination with the implemented DVC in WGs are addressed.
- Chapter 5: The operation of the developed large scale 2 GW network is discussed. The interplay of offshore MMCs and Type-4 WGs in terms of dynamic power flow control within the offshore network (by analyzing the voltage and current profiles in the electrical path between the WGs and the MMCs) is performed.
- Chapter 6: The significant conclusions for the research questions are provided. The future scope and recommendations are also added.

A figurative representation of the thesis workflow is presented in Figure 1.4.

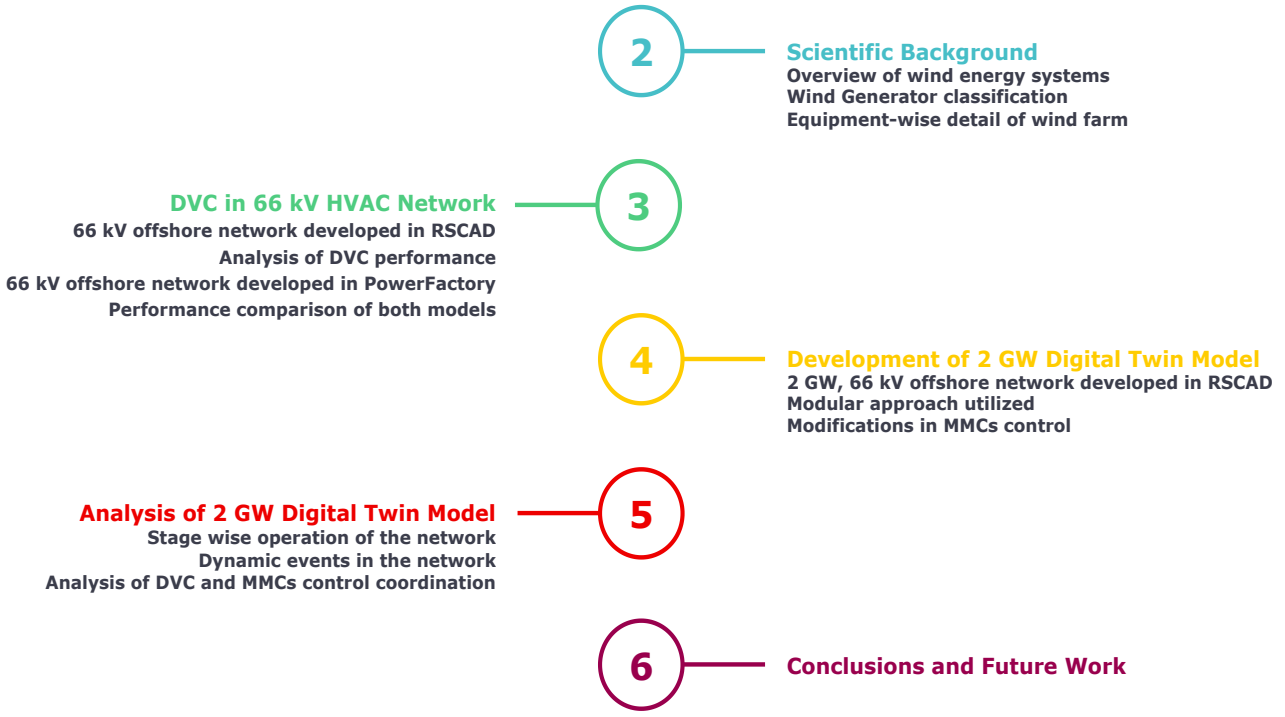

Figure 1.4: Work flow of thesis

2

Scientific Background

An outline of the scientific concepts required for this thesis work is presented in this chapter. Firstly, the basics of wind energy conversion systems are explained. All components that are a part of an offshore wind farm network are depicted and explained. The conventional control topologies in the PE converters of WGs are also explained.

2.1. Wind Energy Conversion Systems (WECS)

The WECS is a mixture of various engineering fields such as mechanical, electrical and control systems. The WECS consists of several components that convert the kinetic energy of the wind into electrical energy and transfer power efficiently and systematically. The major mechanical equipment in the WECS are the turbine tower, nacelle, rotor blades, hub, drives, gearbox, drive-train and mechanical brakes [26]. The PE converters, electrical generator, transmission cables, power transformers and transmission towers constitute the electrical part. The control systems govern both the electrical and mechanical systems [27]. The basic structure of the WECS is depicted in Figure 2.1.

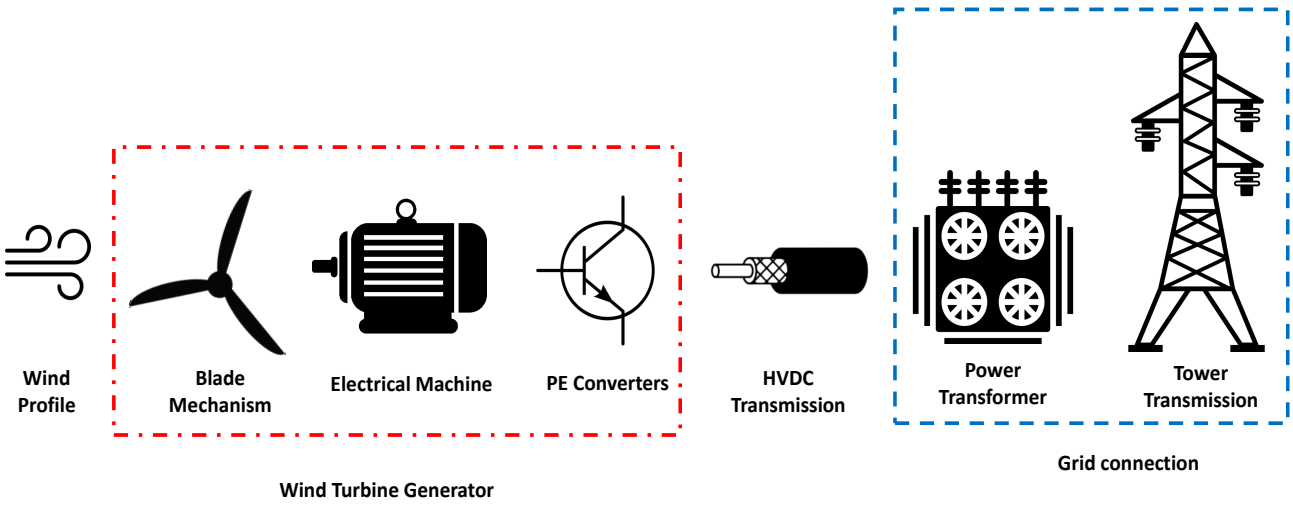

Figure 2.1: Schematic of offshore wind power transmission

2.2. Power from Wind Energy

The wind energy converts kinetic energy of the wind to mechanical energy or electrical energy. Wind energy is represented as the kinetic energy of moving air mass. The mechanical power extracted from practical wind turbines can be depicted as in Equation 2.1 [28].

$$P_m = \frac{1}{2} C_p(\lambda, \beta) \rho A v_m^3 = C_p P_w \tag{2.1}$$

where P_m is the power from wind, C_p is the power coefficient, λ is the tip speed ratio, β is the blade pitch angle in degrees, ρ is the air density and v_m being wind speed.

The tip speed ratio, λ is defined as,

$$\lambda = \frac{R\omega}{v} \tag{2.2}$$

where R is the turbine blade radius in meters and ω is the mechanical angular velocity in rad/s and v is the wind speed in m/s.

The coefficient of performance, C_p, is not a constant value and is a function of λ and β. The C_p-λ characteristics are represented for different pitch angle (β) values in Figure 2.2. As can be seen, there exists a maximum mechanical power that can be achieved for a specific tip speed ratio and pitch angle.

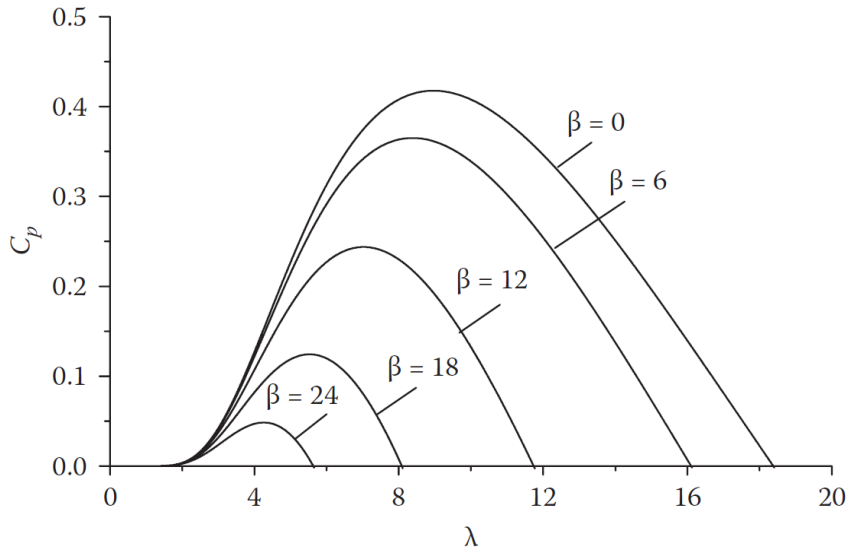

Figure 2.2: Characteristics of C_p-λ for various pitch angle [28]

2.3. Wind Turbine Generator

The Wind Turbine Generator (also termed as Wind Generator (WG)) consists of the mechanical equipment, the electrical generator and the PE converters mentioned in Section 2.1 and depicted in Figure 2.1. Depending on the speed of operation, WGs can be classified as follows [28]:

- **Type 1 - Fixed speed Induction Generator (FSIG) :** Type 1 WG has a fixed speed of operation. Hence, maximum power extraction at all times is not possible.
- **Type 2 - Slip Ring Induction Generator (SRIG) :** Type 2 WG is a variable speed technology that uses a variable resistor in the rotor windings to adjust the rotor speed. However, the variation of speed is limited in this technology, and higher heat dissipation exists due to the variable resistance.
- **Type 3 - Doubly-Fed Induction Generator (DFIG) :** Type 3 WG also comes under variable speed technology. The configuration is depicted in Figure 2.3. The grid transformer is directly connected to the stator of the DFIG, and the rotor is connected through a partially rated PE converter. This configuration adds variable frequency AC excitation (instead of only resistance) to the rotor circuit. The additional excitation for the rotor is provided through slip rings by the Voltage Source Converter (VSC) which controls rotor currents and thereby controls the torque and reactive power of the generator. This VSC is the Machine Side Converter (MSC) and is connected back-to-back with a Grid Side Converter (GSC), which provides control of the DC link voltage and the reactive power flow to the grid. The downside of this topology is that it requires gearbox for operation and hence the chances of wear and tear is high.

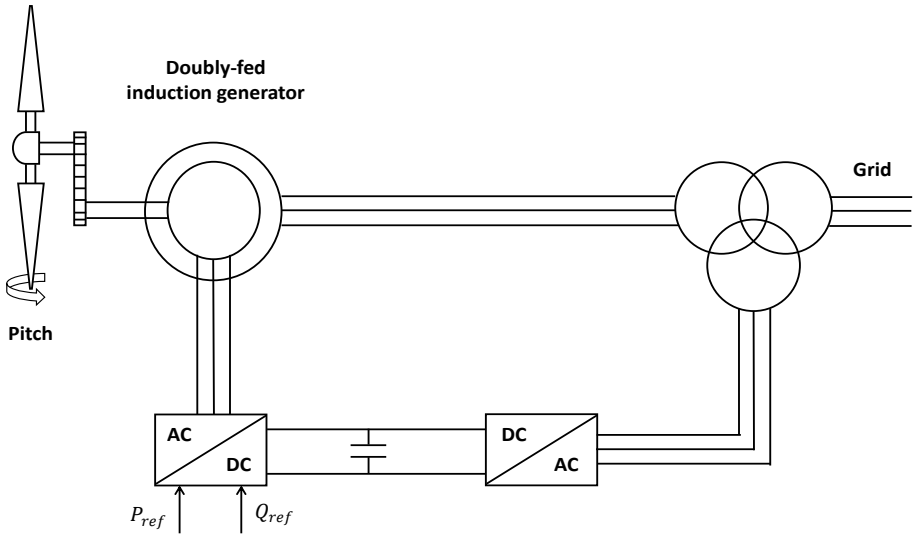

Figure 2.3: Type 3 WG configuration [28]

- **Type 4 - Permanent Magnet Synchronous Generator (PMSG) :** Type-4 WG also has a variable speed configuration, as shown in Figure 2.4. PMSG is connected to the grid transformer through a full-scale back-to-back power converter. There is no speed limit in this topology when compared to Type-3 configuration. Another advantage in Type-4 WG is that the gearbox can be avoided. The control structures of the converters are explained in the following sections.

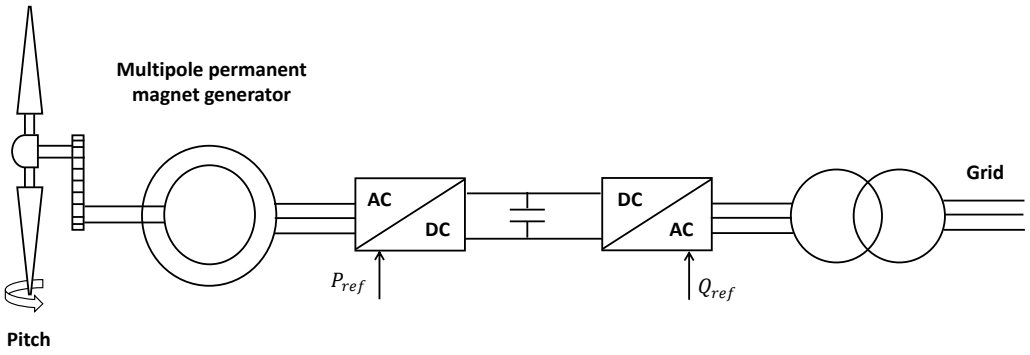

Figure 2.4: Type-4 WG configuration [28]

Type-4 WGs are employed for this thesis work, and hence the components involved for this architecture are explained further.

2.3.1. Permanent Magnet Synchronous Generator (PMSG)

As shown in Figure 2.5, PMSG consists of stator, rotor and windings. The rotor is generally a permanent magnet that creates the magnetic flux. The stator consists of windings that are sinusoidally distributed. Generally, wound-field synchronous generators require DC excitation to be provided by an external source. Whereas in PMSG, external DC excitation is not required, as it is created using the permanent magnets present in the rotor. Based on the direction of flux lines, PMSG can be classified as radial flux, axial flux and transverse flux. Another classification is based on the location of permanent magnets on the rotor as inset PMSGs and surface mounted PMSGs [29].

The mathematical model of PMSG is based on Direct-Quadrature (dq) theory. The differential equations for the PMSG in dq frame are depicted in Equation 2.3 [29].

$$\begin{aligned} v_d &= r_s.i_d + \frac{d}{dt}\Psi_d + \omega_r.\Psi_q \\ v_q &= r_s.i_q + \frac{d}{dt}\Psi_q + \omega_r.\Psi_d \end{aligned} \tag{2.3}$$

where i_d and i_q are the stator d and q axes currents respectively, v_d and v_q are the stator d and q axes voltages respectively. r_s is the stator resistance and ω_r is electrical speed in rad/s. Ψ_d and Ψ_q are the d and q axes flux linkages

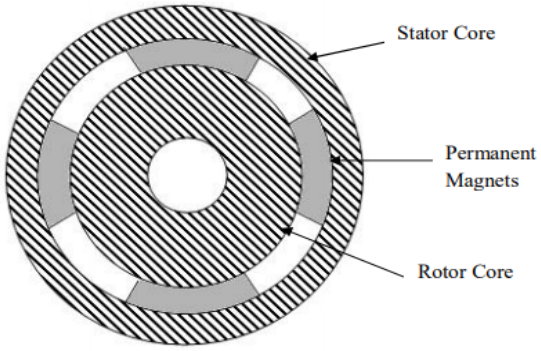

Figure 2.5: Cross section of a PMSG [29]

respectively.

The flux linkages Ψ_d and Ψ_q are given by the Equation 2.4 [30].

$$\begin{aligned} \Psi_d &= L_d.i_d + L_{md}.i_D + \Psi_m \\ \Psi_q &= L_q.i_q + L_{mq}.i_Q \end{aligned} \tag{2.4}$$

where L_d and L_q are the inductances in d and q axes respectively, L_{md} and L_{mq} are mutual inductances and Ψ_m is the permanent magnet flux linkage.

2.3.2. Voltage Source Converter (VSC)

The stator of the PMSG is connected directly to the AC side of a VSC as seen in Figure 2.4. This VSC which works as a rectifier during generation operation is termed as MSC. It is interfaced back to back with another VSC that works as an inverter during generation operation and is called GSC.

VSC consists of self-commutated switching devices such as the Insulated Gate Bipolar Transistors (IGBTs) and anti-parallel diodes and hence allows the bidirectional flow of power between the AC and DC sides. The output voltage is obtained by switching off the IGBTs in a synchronized manner. The VSCs are classified as two-level or multi-level depending on the number of voltage levels they can generate [31].

Two-level VSC

The two-level VSC is the most commonly used type of converter in various applications because of the simplicity of its operation. The configuration of a two-level VSC is depicted in Figure 2.6. Voltages of (1/2 V_{dc}, -1/2 V_{dc}) can be obtained using two-level VSC as shown in the graph in Figure 2.6. The operation of switches S_1 and S_2 in two-level VSC are operated complementary to prevent short circuit across the DC link, hence protecting the PE devices from being subjected to over-current.

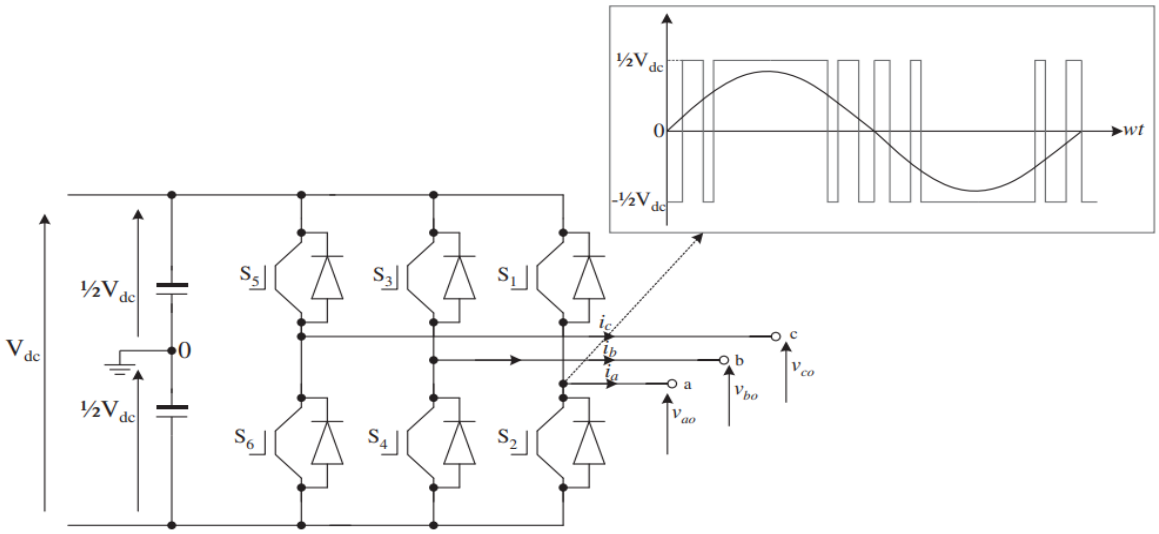

Figure 2.6: Two-level VSC [31]

Multi-level VSC

VSCs with three or more levels are termed as multi-level VSCs. The three-level VSC is among the first multi-level configuration used on large scale and is also termed as Neutral Point Clamped (NPC) converter [13]. The topology of a NPC converter is shown in Figure 2.7. The voltage levels of (1/2 V_{dc} , 0 , -1/2 V_{dc}) can be obtained using a NPC converter. This provides a better sinusoidal nature and also reduces the Total Harmonic Distortion (THD) when compared to a two-level VSC. The switches (S_{a1},S_{a3}) and (S_{a2},S_{a4}) are operated complementary in a NPC converter. This means, turning on switch S_{a1} eliminates S_{a3} from being turned on and the same pattern is followed for the latter complementary pair. The summary of switching operation for a NPC converter is shown in Table. 2.1.

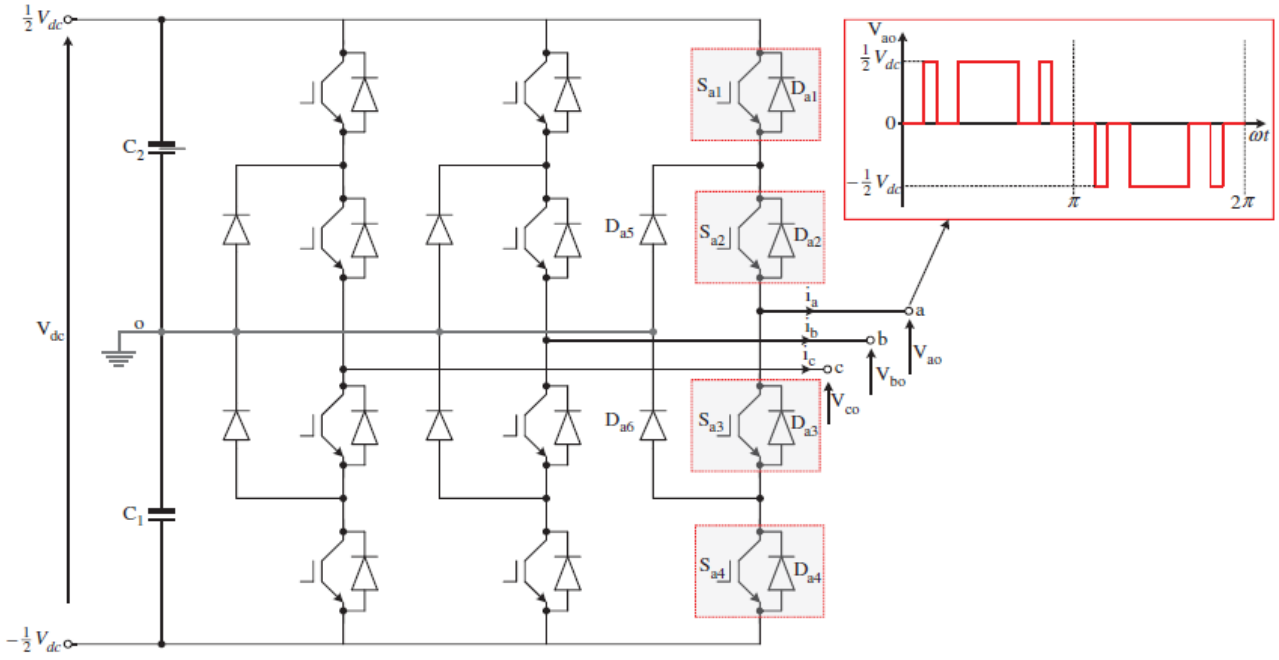

Figure 2.7: Three-level VSC or NPC Converter [31]

	Switch state			
Voltage level	S_{a1}	S_{a2}	S_{a3}	S_{a4}
$\frac{1}{2}V_{dc}$	ON	ON	OFF	OFF
0	OFF	ON	ON	OFF
$-\frac{1}{2}V_{dc}$	OFF	OFF	ON	ON

Table 2.1: Switching operation of a three-level VSC [31]

Pulse Width Modulation (PWM)

The switching of the valves has to be configured using a control mechanism to ensure proper operation. To reduce the harmonic content and to control the magnitude of output voltage, many Pulse Width Modulation (PWM) techniques are developed. Few of them used currently are, Selective Harmonic Elimination (SHE), Sinusoidal Pulse Width Modulation (SPWM) and Space Vector Modulation (SVM). SPWM technique is employed in this thesis and is explained further. SPWM is one of the simplest methods to be implemented and provides high effectiveness in modulation by suppressing the harmonic contents that are farther from the fundamental frequency component. SPWM can be termed to be a multi-pulse based modulation technique that changes the pulse width of the output voltage of the converter in a sinusoidal fashion with respect to a corresponding reference voltage. The implementation of this concept is done by comparing a particular reference signal of low-frequency with a carrier signal of higher frequency. The reference signal frequency is set to the required fundamental frequency, which is normally 50 Hz or 60 Hz, and the carrier signal frequency should be higher than the reference signal frequency. An example of SPWM in two-level VSC is shown in Figure 2.8.

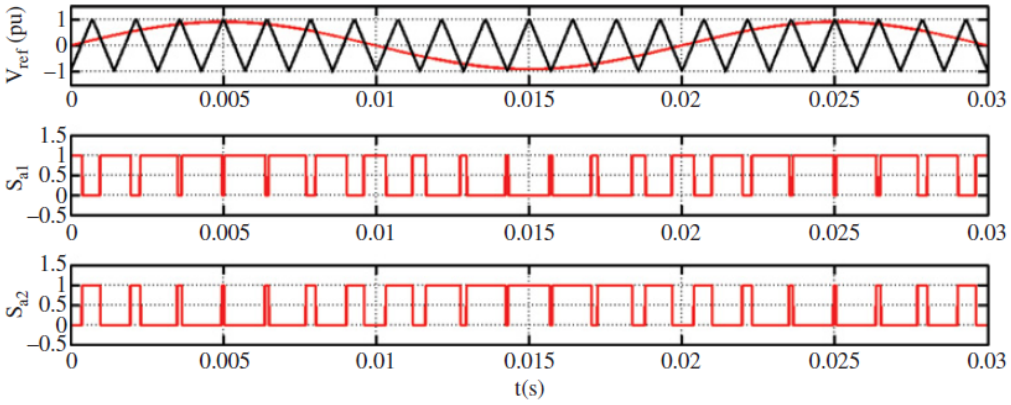

Figure 2.8: SPWM for phase A in two-level VSC [31]

Reference frame transformation

PI controllers are widely used for the control operation of VSCs in power systems. It is therefore relevant to translate from three-phase abc frame to a rotating dq frame in order to have a two signal representation of three-phase AC signals. Figure 2.9 shows the Clarke-Park transformation used for this purpose. The three-phase measured signals from the node are translated to a stationary reference frame ($\alpha\beta$) using the Clarke transform. It is then translated to a synchronous rotating dq frame using the Park transform. The reference signal for control is provided to the corresponding frame, and after the control process is established, it is translated back to the three-phase signals. In real-world, during translation to a rotating dq frame, the d-axis is aligned with the grid voltage, and q-axis is aligned to zero. The alignment is done by the voltage angle determined by the Phase Locked Loop (PLL). Such an approach provides control of active power or DC voltage using d-axis current component of the converter, while the reactive power or AC voltage can be controlled using the q-axis current component of the converter.

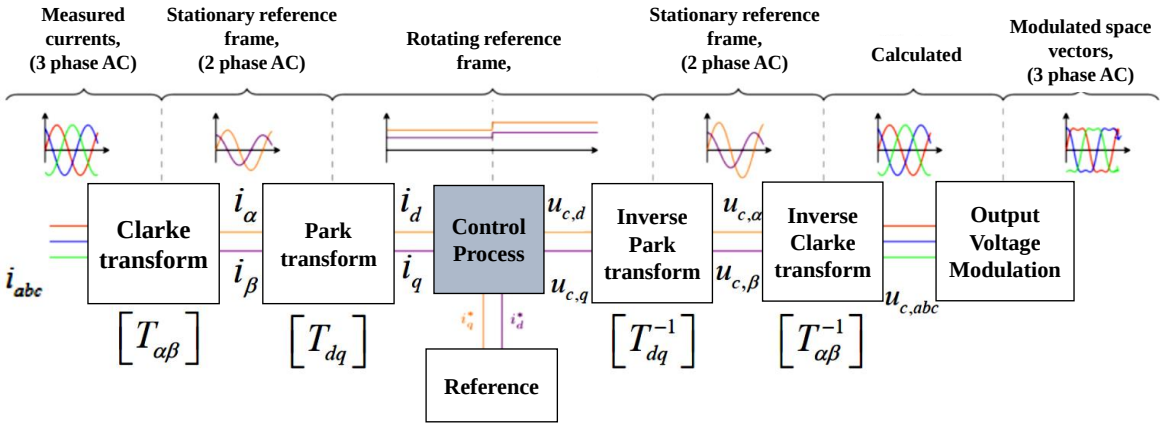

Figure 2.9: Reference frame transformation for control of VSC [32]

2.3.3. Machine Side Converter (MSC) Control

The MSC controller is in charge of optimizing the rotor speed to increase the amount of wind energy being captured continuously [33]. The following equation gives the electromagnetic torque of the PMSG.

$$T_e = \frac{3}{2} P_n [\Psi_m . i_q - (L_d - L_q) i_d . i_q] \tag{2.5}$$

where P_n is the number of pole pairs.
The majorly used mechanisms for the control of MSC are the following three control schemes [34]:

- Zero d-axis Control (ZDC): As the name suggests, this control involves setting the d-axis component of stator current to zero. If i_d= 0 in Equation 2.5, the electromagnetic torque will be proportional to the q-axis component of stator current (i_q).
- Maximum Torque per Ampere (MTPA) control: The concept of MTPA control is to generate a required torque with a minimum stator current. Thereby, the use of stator current is increased, and the losses across the stator

windings are reduced. In case of non-salient pole generators, the inductances in d and q axes are the same ($L_d = L_q$). On substituting $L_d = L_q$ in Equation 2.5, this simplifies to the fact that electromagnetic torque is proportional to the q-axis current component. Therefore, the MTPA control is the same as the ZDC in case of non-salient pole generators.

- Unity Power Factor (UPF) control: The stator voltage and current phase angles are calculated initially. To achieve UPF, the angle between the stator voltage and current, i.e. the stator power factor angle must be zero. The equations are then solved for both the d and q axes stator currents.

Additionally, the generator is also governed by the Maximum Power Point Tracking (MPPT) mechanism to extract the maximum power possible. There are two ways of implementing this mechanism; the first involves measuring the speed of the WG shaft, and the maximum mechanical power that can be extracted is calculated. The error obtained by comparing the maximum mechanical power with the actual power achieved is provided for the MSC control. The next method is through measurement of wind speed. If for a given speed, the ratio of optimum tip speed ratio and the radius of the blade is known, the optimal rotational speed of the rotor ($v\lambda_{opt}$ /R) can be calculated. The error obtained on comparing this speed with the measured speed is used to calculate the $i_{q,ref}$ component [28]. The detailed implementation of MSC control in RSCAD is given in Appendix A.1.2.

2.3.4. Grid Side Converter (GSC) or Line Side Converter (LSC) Control

The GSC is connected back to back with the MSC through a DC link. The GSC is mainly responsible for providing DC voltage control and the AC side reactive power control.

Conventional Current Control

The conventional control of GSC implemented in power systems follows the current control strategy. This involves an outer loop to control the DC voltage (V_{dc}) in d-axis, and AC voltage (V_{ac}) or reactive power (Q) control in q-axis as shown in the blue box in Figure 2.10. The outer loop provides reference set points (i_{d_ref} and i_{q_ref}) for the inner current control loop which is represented by the orange coloured box in Figure 2.10. The inner loop consists of PI controllers and feed-forward term (V_T) that form the major part of the control. The decoupling terms (x) are added at the end of the current regulator output to improve the dynamic performance of the system.

The conventional current control strategy has not led to any major issues until now, because the synchronous generators in power plants were capable of absorbing the injected currents. However, this is not the case for a network that is dominantly connected using PE interface. An example of such a situation is an OWF network. The effect could also be severe for a large scale OWF network involving more PE converters to be connected to the network. Hence this calls for the need for better control strategies.

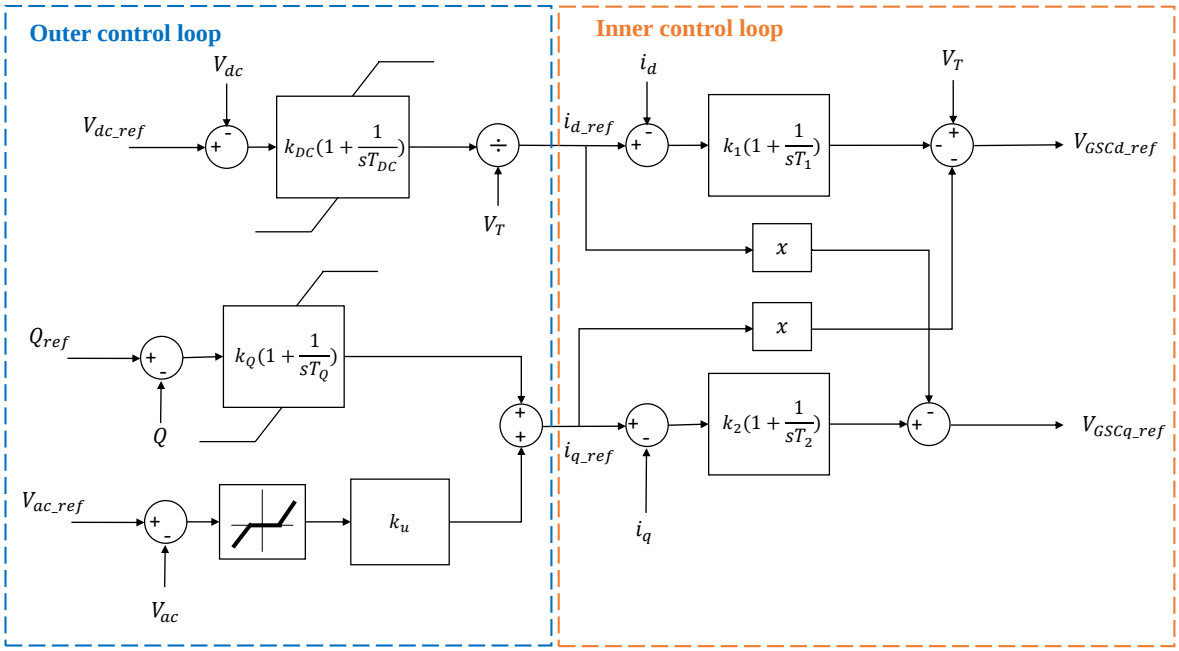

Figure 2.10: Conventional current control in GSC [21]

Direct Voltage Control (DVC)

The major issue with conventional control is the wind up of the integrator that causes the voltage to rise. This happens because the reference value of current (i_{d_ref} and i_{q_ref}) remains non-zero and the measured current (i_d and i_q) following islanding nearly falls to zero. To overcome this issue, the inner control loop in Figure 2.10 is modified as shown in Figure 2.11. In Figure 2.11, the integrator term is avoided, and the proportional term is moved to the output end. However, this causes the set points to differ in the absence of the integral component. The main role of set points is to limit the PE converter current. Nevertheless, the current limitation would be based on the grid situation, and hence the performance of the controller is not affected in the absence of the integral component [21], [22].

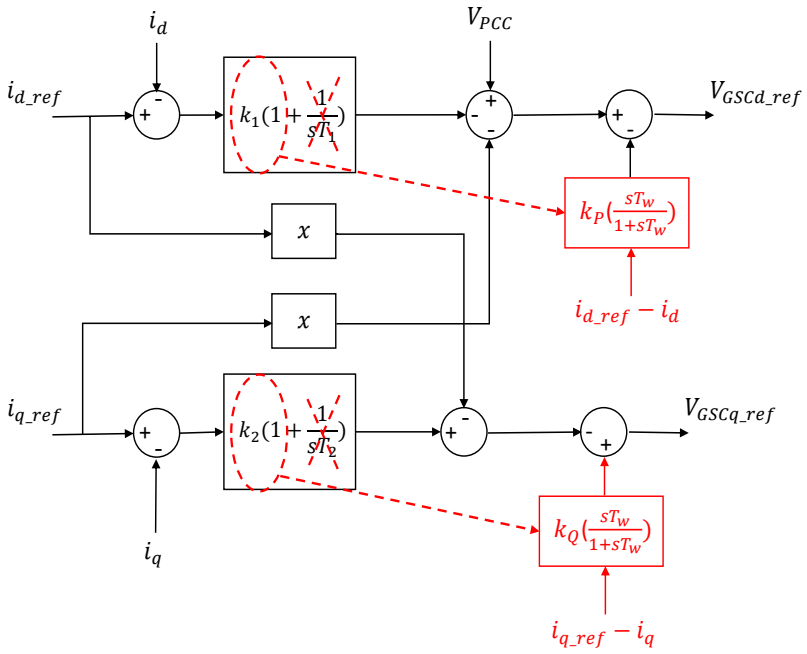

Figure 2.11: Development of new voltage controller strategy by modifications in the inner control loop of conventional current controller [22]

The damping of transient scenarios is provided by imitating the use of a resistor in series in the PE converter circuit. In the real scenario, damping can be depicted as the power loss across a resistor. However, placing a physical resistor in the circuit causes loss of active power which is not desired. In order to achieve the damping effect without power loss, the controller is formulated to mimic the drop in voltage using a virtual resistor [22]. The value of the virtual resistors in d and q axes are the gains (k_P and k_Q) of the washout filers depicted in red boxes in Figure 2.11.

The control strategy developed in [21] uses a vector control strategy similar to the conventional current control. The transformation in d and q axis allows the independent control of active and reactive powers. This control strategy is adapted for this thesis and is explained in detail in Section 3.3.1.

Power Balance Equation

The power balance equation at the WG is given as follows:

$$P_{inverter,input} = P_{rectifier,output} + P_{capacitor} \tag{2.6}$$

where rectifier is the MSC and inverter is the GSC. For steady-state conditions, the voltage across the DC capacitance is steady. Thereby, the active power input for the inverter (GSC) equals the active power output from the rectifier (MSC). During the fault condition, the active power output from the inverter is decreased, whereas the output from the rectifier tends to be the same. The capacitors are charged during this scenario, and the DC link voltage increases to maintain the power balance.

2.4. High Voltage Direct Current (HVDC) Transmission

As the name suggests, a High Voltage Direct Current (HVDC) transmission system uses DC for bulk transmission of electrical power. The electrical power from the offshore AC network is stepped-up using a power transformer and is converted to DC at the converter station, which is transmitted to onshore locations using subsea cables or overhead lines [35]. The commercial utilization of HVDC transmission was started in 1954 [36], [37]. HVDC technology employs VSCs to convert power from AC to DC and vice versa, as explained in Section 2.3.2, and hence the systems that employ this technology are termed as VSC-HVDC systems.

As explained in Section 2.3.2, the classification for VSCs can be termed as two-level and multi-level. The two-level VSCs are an economical solution for low power rating applications up to 1 MVA. The main drawbacks of two-level VSCs include increased power losses, high harmonic content on the AC side voltages and require expensive filters to mitigate the harmonics. On the other hand, multi-level converters provide notable improvements for the above mentioned issues as can be seen in Figure 2.12 [13].

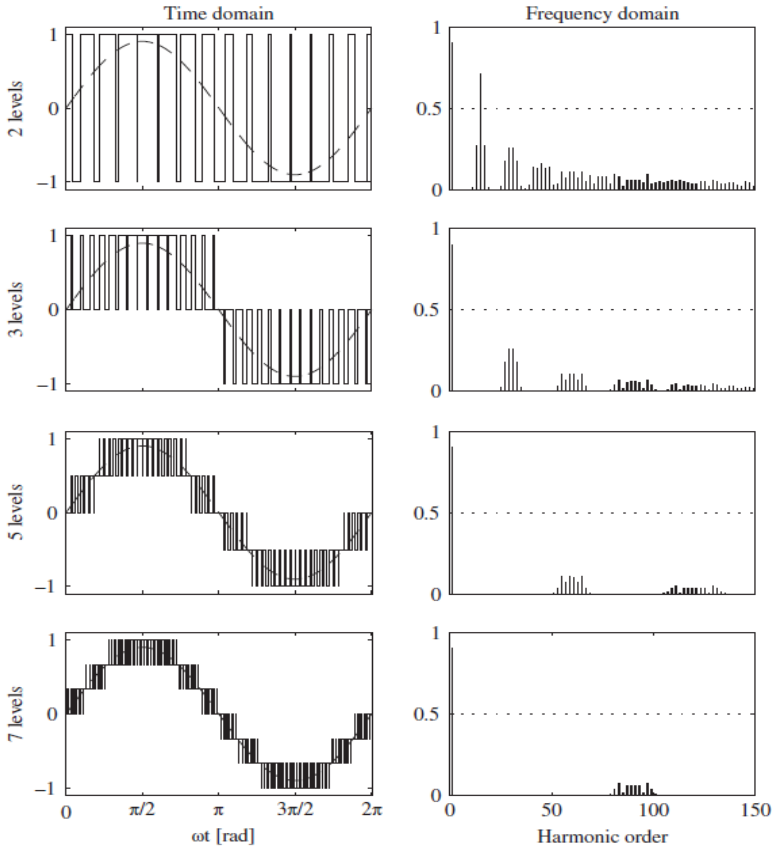

Figure 2.12: Effect of moving towards multi-level converters [13]

The most common multi-level converters for high voltage applications in recent times are the Modular Multi-level Converters (MMC)s. The significant component in an MMC is the switching submodule that can be either half-bridge or full-bridge submodules. The half-bridge submodule has one two-level phase leg parallel to a DC capacitor that maintains the DC voltage. The voltage level can be increased by connecting the submodules in series. The DC power at the output of MMC is transmitted to the onshore converter using subsea HVDC cables. It is converted back to AC at the onshore converter station and sent to the distribution network.

Having understood the basics of various equipment in an OWF and VSC-HVDC transmission, the goal of modelling a multi-gigawatt offshore network with identified control strategies needs to be achieved. Implementation of the control strategy for a single WG model is taken as the starting step and is explained in the following chapter.

3

Modelling and Analysis of DVC in a Digital Twin of 66 kV HVAC Offshore Network

In this chapter, the basics of EMT software utilized is explained briefly. Then the model consisting of a Type-4 WG with implemented DVC from [21] in a 66 kV HVAC offshore network in RSCAD is detailed. The performance of the control strategy is tested for severe dynamic conditions. Lastly, the performance of the DVC modelled in RSCAD is then validated with the benchmark DVC model in DIgSILENT PowerFactory software [38] (based on a qualitative comparison because of the unavoidable differences between the software packages) for a similar 66 kV HVAC offshore network.

3.1. Real Time Digital Simulator (RTDS) Tool

Real Time Digital Simulator (RTDS) Hardware is equipped to perform EMT simulations. The overall network solution in RTDS is based on the nodal analysis. The simulator can work in the range from DC to 3 kHz of frequency. It can simulate a time step of 25 - 50 μs for even complex power systems. This is termed as a large time step. RTDS gives the option for a small time step environment to incorporate PE components simulation. These blocks have time steps in the range of 1400 - 3750 ns. The hardware consists of two generations of processor cards, namely, PB5 and NovaCor [30].

RTDS provides a user-friendly Guided User Interface (GUI) called RSCAD wherein the network is modelled, run and analyzed. There are modules available in RSCAD for the actions mentioned above (Figure 3.1). These are explained in [30] in detail. The majorly used modules for this thesis are the Draft, Runtime, Cable and Tline modules. The modelling of the system is performed in the Draft module, which contains a drawing canvas whose size can be adjusted. The working of the Cable and Tline modules are illustrated in Sections 3.2.2 and 4.3.2, respectively. After the model is developed, the simulation is run in the Runtime module. RTDS also allows for Hardware In Loop (HIL) and Software In Loop (SIL) simulations to test the working of controllers in real-world scenario [39].

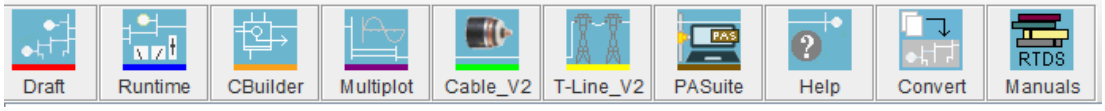

Figure 3.1: Modules available in RSCAD

A simple network model in the Draft module layout is shown in Figure 3.2. The time step, plot duration and the canvas size is assigned by right-clicking on anywhere on the canvas area and choosing the "Circuit Options" as shown in Figure 3.2.

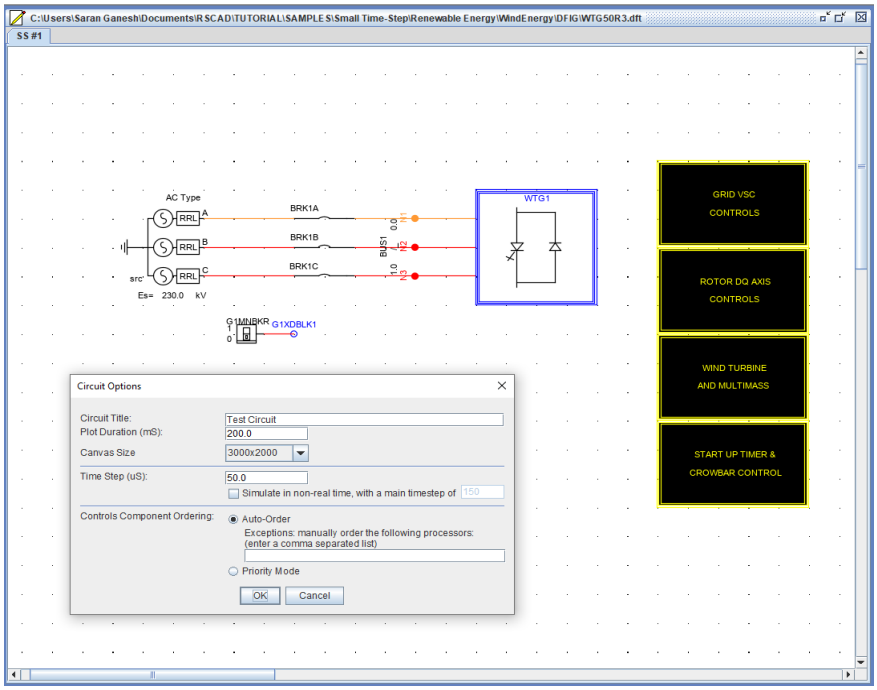

Figure 3.2: Example of a power system in Draft module in RSCAD

There are different libraries available in the Draft module to select the components. The major libraries that were used are [30]:

- Power system library (Figure 3.3(a)) - Consists of power component models such as transformer, transmission line, cables etc. These components are to be used in the large time step in the workspace.
- Small time step library - This library consists of components that are used to model in the small time step environment. The mainly used components are the VSC bridge box, VSC interface transformers, Tline block to interface between small time step environment and large time step environment.
- Controls library (Figure 3.3(b)) - The most important block for modelling control strategies. Consists of transfer functions, logic functions, math functions and so forth.

(a) Power system library in Draft module

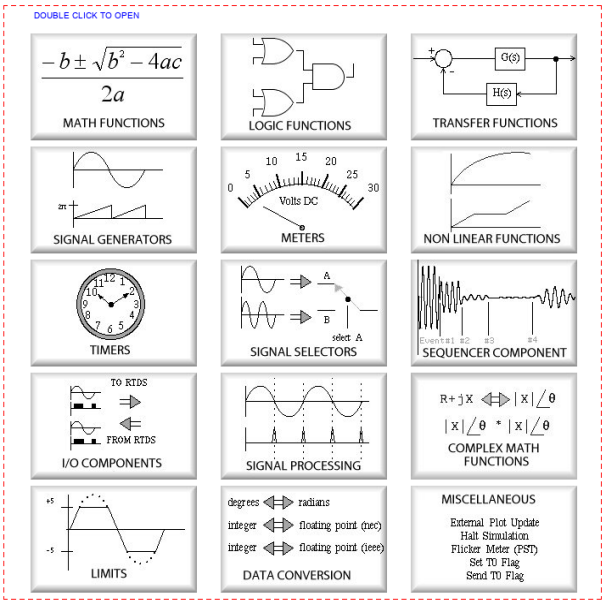

(b) Controls library in Draft module

Figure 3.3: Libraries available in Draft module in RSCAD

After the model has been developed in the Draft module as shown in Figure 3.2, the user has to compile the file by clicking on "Compile" [1]. The processor calculates the actual time step, and the initial conditions are stored in the MAP file which is available by right-clicking on the white space in the draft module. The user is notified of errors or warnings during simulation through a pop-up box at the end of file compilation. The processor assignment and the controls assignment can be viewed by clicking the "Processor Assignment" [2] tab. There are some important data in the RSCAD configuration files that hold information about the configuration of hardware in RTDS. IP addresses of all rack ports and the processor cards are the data available in the configuration file. It can be accessed using the "Tool" menu in the main tab of RSCAD. Improper configuration of these files will result in no simulation of the test case [30].

The real-time interaction of the user with the system is done through the Runtime module available in RSCAD. The user can accomplish tasks like measuring signals, plotting graphs, adjusting sliders and creating faults in this interface. An example of the Runtime module with the scenarios mentioned above is shown in Figure 3.4.

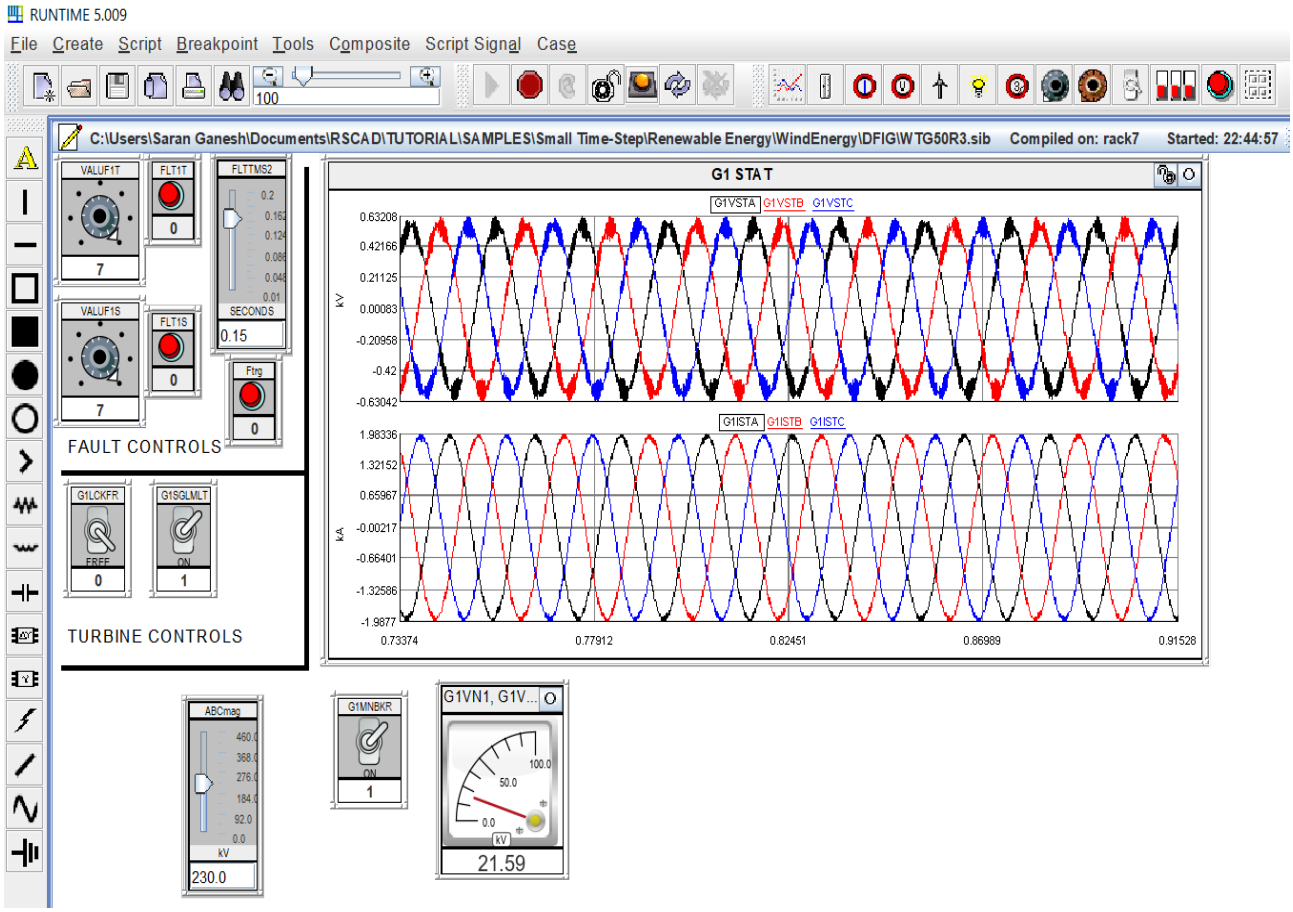

Figure 3.4: Example of the Runtime module with plots, switches, sliders etc. in RSCAD

The overall working of RSCAD can be understood as depicted by the flowchart in Figure 3.5.

[1] Compile icon in RSCAD:

[2] Processor Assignment icon in RSCAD

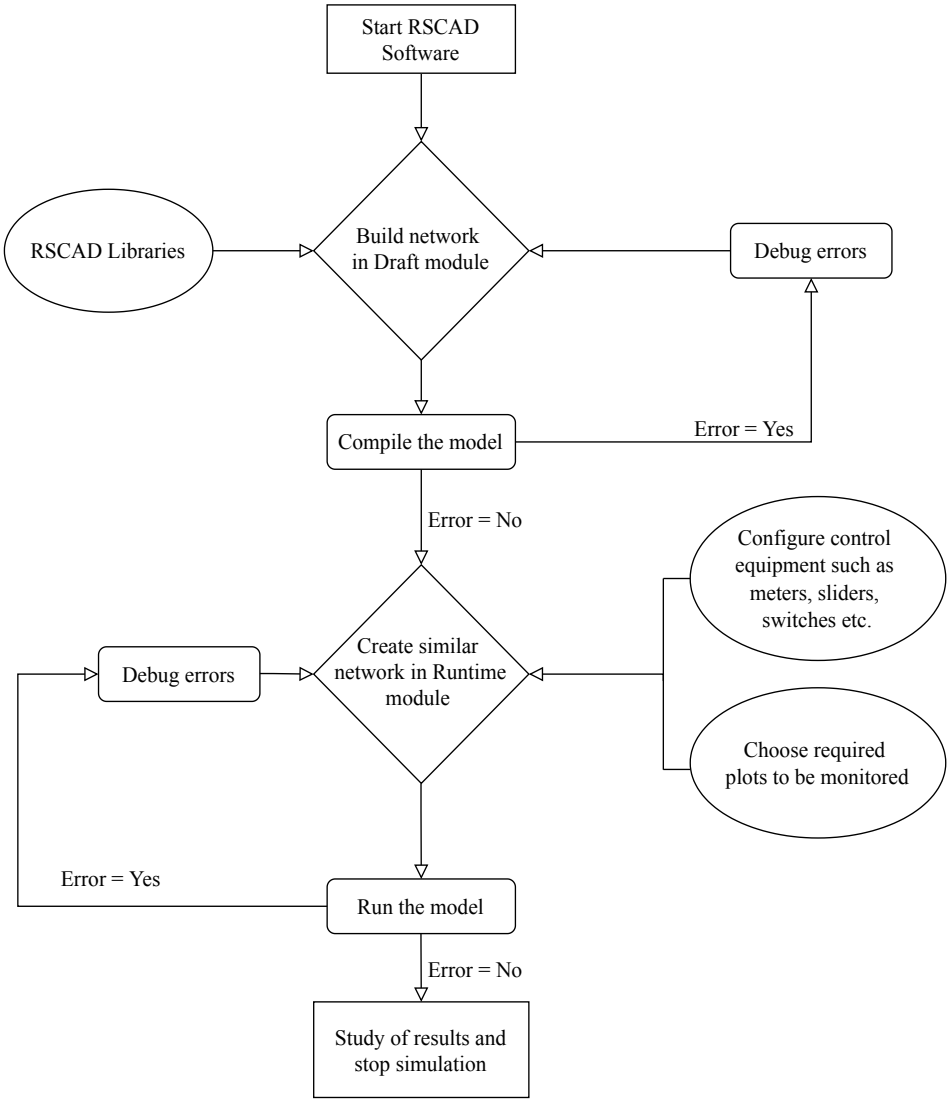

Figure 3.5: Flowchart representation of RSCAD working

3.2. Layout of the 66 kV HVAC Test System in RSCAD

After understanding the basics of RSCAD software, a 66 kV offshore network, as shown in Figure 3.6 is developed. The network consists of the following components.

- An aggregated representation of ~ 700 MW installed capacity OWF is modelled with the following elements:
  - A single Wind Generation System with
    - Permanent Magnet Synchronous Generator (PMSG)
    - Machine Side Converter (MSC)
    - DC circuit
    - Grid Side Converter (GSC)
  - High Pass filter (HPF) with series reactor
  - OWF transformer
- HVAC cables
- External AC system

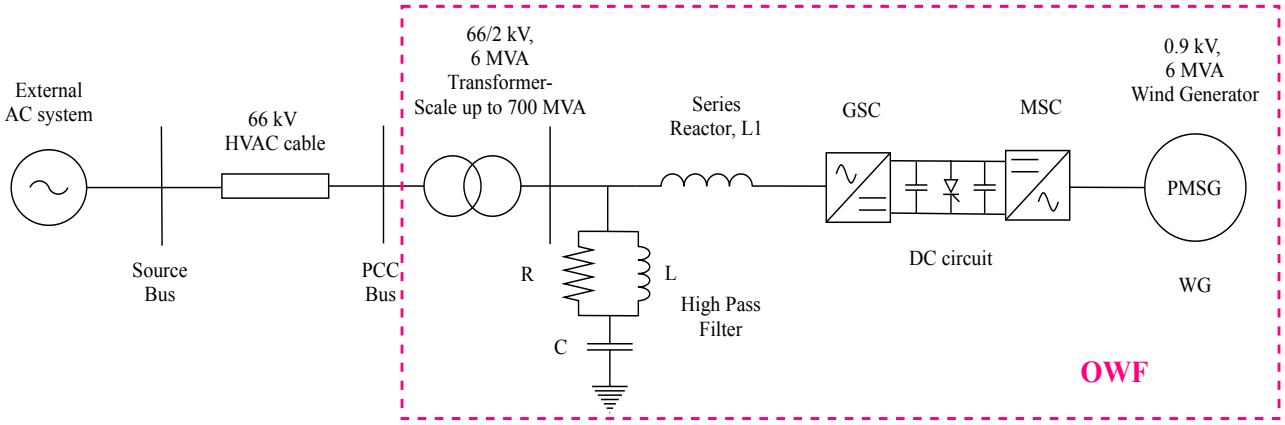

Figure 3.6: Single line diagram of the 66 kV HVAC offshore test network in RSCAD

3.2.1. Aggregated Offshore Wind Farm (OWF)

The ~ 700 MW offshore wind power is represented by a single OWF consisting of 116 WGs, each rated 6 MW connected in parallel. Type-4 WGs are used for all units. The RSCAD representation of aggregated OWF is utilized in this work. The aggregated model consists of PE components which require high switching frequency and hence is modelled in a small time step environment by selecting the "VSC Bridge Box" (Figure 3.7) available in the small time step library in the Draft module. The box contains the PMSG, MSC, DC capacitors, chopper circuit, GSC, HPF with a series reactor and OWF transformer as illustrated in Figure 3.8. As mentioned in Section 3.1, the block can be assigned to have a time step value between 1400 to 3750 ns. Hence, a value of 2500 ns is chosen for this model. The value can be entered by right-clicking on the small time step block and choosing "Edit" and then "Parameters" as shown in Figure 3.7. Also, it must the noted that the above specified time step is only for initialization and the actually used time step can be viewed in the Map file which is accessible by right-clicking on any white space in the Draft file and selecting "View" then, "Map File". It is also worth mentioning that the ratio of the large time step to the small-time step in a network in RSCAD must be higher than 12 when using NovaCor and must be higher than 17 when using PB5 racks [30].

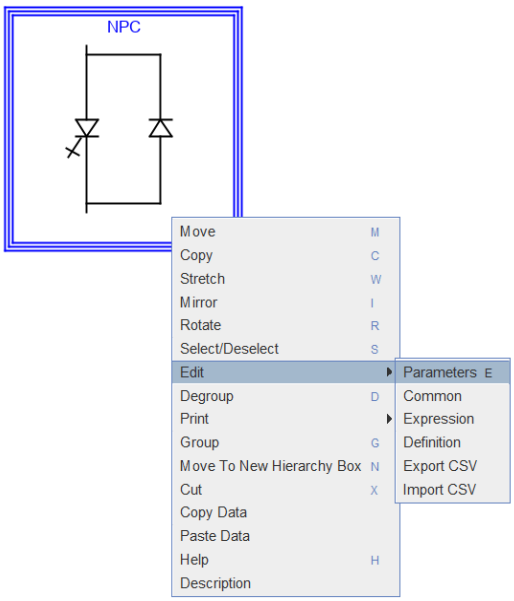

Figure 3.7: Small time step block

Wind Generation System

The Wind Generation System consists of PMSG, MSC, DC circuit and GSC. The EMT model of Type-4 WG with detailed modelling of MSC, DC circuit and GSC represented by three-level VSCs are utilized for this work. The basic models available in IEPG Section of Delft University of Technology (TU Delft), developed as a part of the MIGRATE project [40] is considered for this work. The detailed description of the PMSG, MSC and DC circuit models along with the control structures are explained in Appendix A. The control for GSC developed in [25] is modified and implemented in this thesis work. This is explained in detail in Section 3.3.1.

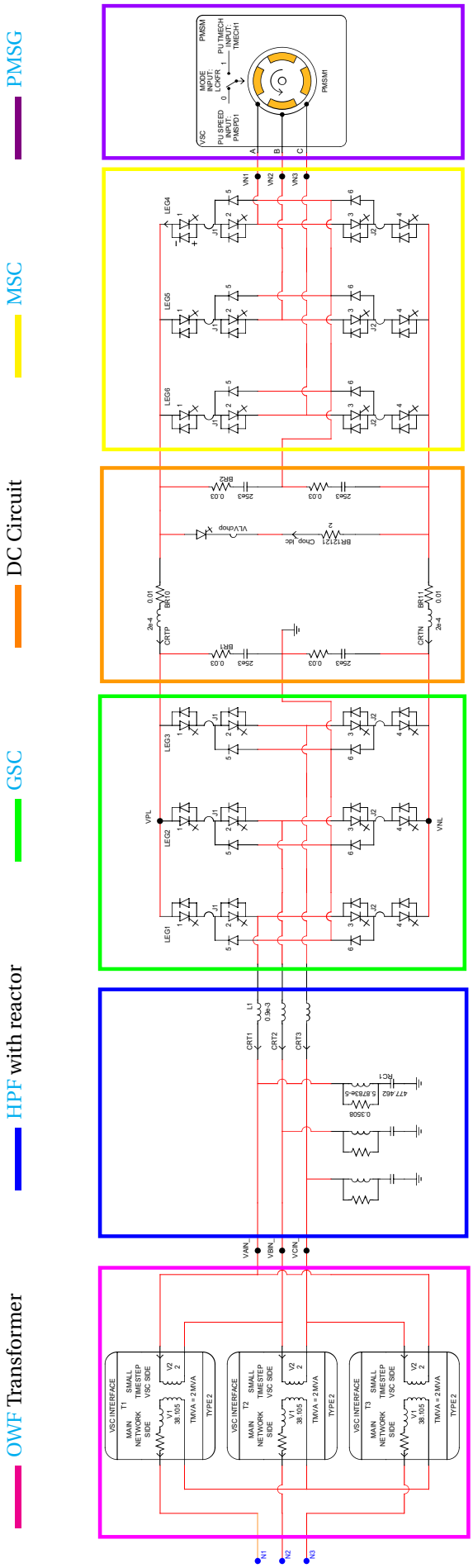

Figure 3.8: Overview of OWF model in small time step environment

High Pass Filter (HPF) with Series Reactor

The switching operation of PE converters leads to the generation of harmonics. Thereby, to mitigate these harmonics, filters are provided at the output of the GSC. There are various types of filters available for this application. The common ones are the LCL filter, L filter and high pass filter [41]. In RSCAD, there is a HPF block readily available in the small time step library, as shown in Figure 3.9 [30]. It is chosen by selecting the VSC branch model in this library and changing the branch type to "HIPASS". A three-phase inductance branch is chosen by selecting the branch type to "L" and connected as the series reactor, as depicted in the blue box in Figure 3.8. After the HPF parameters are calculated and set, then it would only be required to tune the inductance of the series reactor to limit the flow of current and thereby stabilizing the voltage. Hence, it was decided to go with HPF.

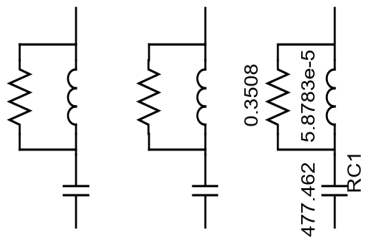

Figure 3.9: High Pass Filter in RSCAD

The base impedance on the low voltage side of transformer is calculated in ohms as in Equation 3.1.

$$Z_{baseLV} = \frac{LV^2}{BaseMVA} = \frac{(2kV)^2}{6MVA} = 0.6667\Omega \tag{3.1}$$

The HPF should have a high impedance value at the nominal frequency (50 Hz) so that it works as an open circuit. Therefore, a higher value of 10 times base impedance is chosen. The impedance of the capacitor at 50 Hz is computed by the following equation.

$$Z_c = 10 \times Z_{baseLV} = 10 \times 0.6667\Omega = 6.667\Omega \tag{3.2}$$

Hence, the value of capacitance at 50 Hz in Farad is calculated by using Equation 3.3,

$$C = \frac{1}{2\pi f \times Z_c} = \frac{1}{2\pi \times 50Hz \times 6.667\Omega} = 4.77462 \times 10^{-4} F \tag{3.3}$$

The next step is to calculate the inductance 'L'. Inductance must be selected such that the impedance of the inductor and capacitor cancel each other during the switching or modulating frequency (950 Hz in this case). The switching and higher frequencies can be passed to the ground and thereby purely sinusoidal signals will be transferred to the PCC. The impedance of the inductor, resistor and capacitor must be equal at the switching frequency in order to pass the high frequencies to the ground. Therefore, to calculate inductance, it is considered as a series LC circuit. The resonant frequency of the LC circuit is given by Equation 3.4.

$$\omega = \frac{1}{\sqrt{LC}} \tag{3.4}$$

Hence, the inductance value can be calculated as per the following equation.

$$L = \frac{1}{\omega^2 C} = \frac{1}{(2\pi \times 950Hz)^2 \times 4.77462 \times 10^{-4} F} = 5.8783 \times 10^{-5} H \tag{3.5}$$

Upon deriving the inductance, the resistance is selected to match the impedance of the parallel inductor at the modulating frequency.

$$R = \omega L = (2\pi \times 950Hz) \times 5.8783 \times 10^{-5} H = 0.3508\Omega \tag{3.6}$$

The series reactor is used for limiting the current to the AC network. The impedance value of the reactor is selected based on sensitivity analysis. A value of 0.9 mH is chosen to achieve a voltage of 1 p.u. at the PCC.

OWF Transformer

The GSC is connected in series to a three-phase offshore 66/2 kV, 6 MVA transformer with leakage reactance of 10 %, through a series reactor and a shunt HPF as seen in Figure 3.8. Single-phase VSC interface transformer shown in Figure 3.10 available in the small time step library is used for this approach. Three transformers each rated 2 MVA are connected in wye-delta configuration with as seen in Figure 3.8. In RSCAD, the scaling up of power is done at this transformer. The option for scaling up the primary current of the transformer is available in the VSC interface transformer block as shown in Figure 3.11(a) [30]. The user can control the amount of scaling, i.e. the number of parallel units by a slider, as shown in Figure 3.11(b). The user can model the components in the secondary side of the transformer as required for a single WG and then scale it to the required power (~ 700 MW in this case).

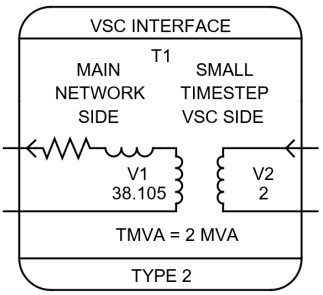

Figure 3.10: VSC interface transformer

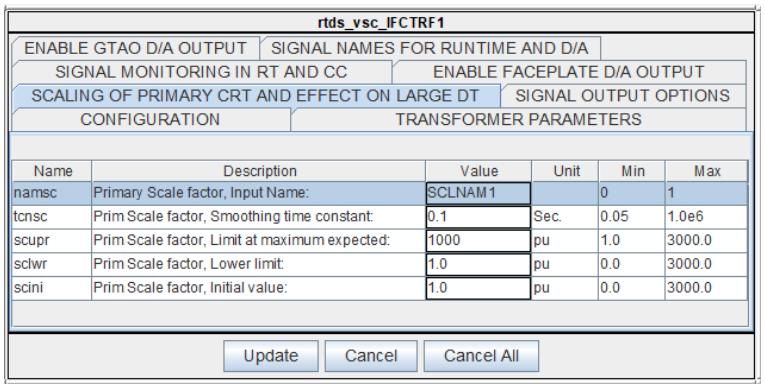

(a) Option for scaling in VSC transformer

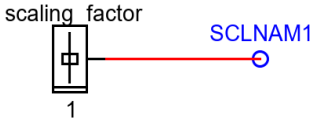

(b) Scaling factor

Figure 3.11: Scaling up of power in RSCAD

3.2.2. HVAC Cables

The HVAC cables transfer power from the OWF transformer to the external AC system. The HVAC cables are rated at 66 kV and modelled in the large time step environment. When compared to 33 kV cables, 66 kV cables allow twice the amount of power to be transferred for the same area of cross-section and require lower array cabling [11].

RSCAD allows cables to be modelled as Frequency Dependent Phase, Bergeron and Pi models [30]. The Frequency Dependent Phase and the Bergeron are travelling wave models. Pi model representation of cable is chosen for this research in RSCAD. To ease the goal of comparing the performance of models in two EMT software, which is explained later in this chapter, a Pi cable model was chosen. In RSCAD, cable parameters can be entered using the Cable module available in the RSCAD modules section as denoted by a red box in Figure 3.12.

In the Draft module, the cable model is added in the circuit using the unified model shown in Figure 3.13 available in RSCAD power system library. The unified model consists of the following components:

- Calculation Block
- Sending End Terminal
- Receiving End Terminal

The detailed representation of the cable parameters in Cable module, and the representation of the cable model using the calculation block, sending end terminal and receiving end terminals in the Draft module is shown in Appendix D.4.

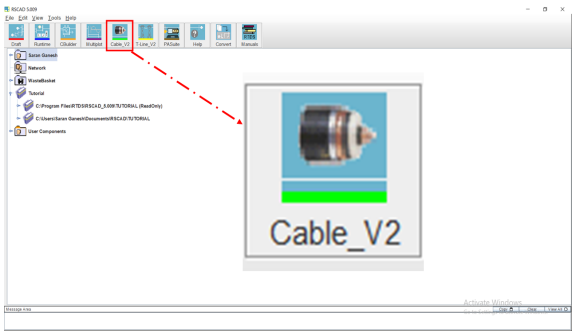

Figure 3.12: Cable module in RSCAD

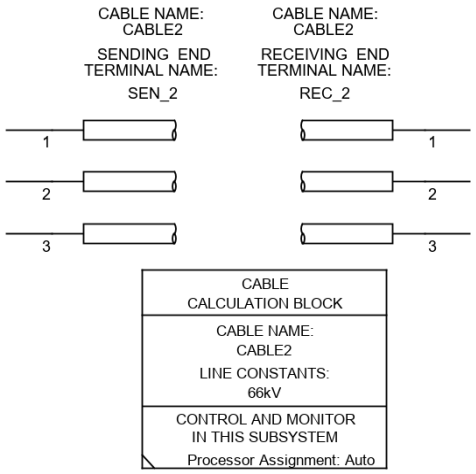

Figure 3.13: Cable configuration in Draft module in RSCAD

3.2.3. External AC system

The external AC system represents the infinite grid connection and is modelled as an AC voltage source. The infinite grid is similar to the representation of a synchronous generator with high inertia constant. For a strong grid, typical values of inertia constant of 5 MW/MVA^2 depicting a synchronous generator is chosen from [42]. The commonly represented damping constant is the frequency-dependent load damping constant. However, the damping constant is zero in this case as no loads and a lossless machine is considered. Alternatively, for short circuit calculations, the reference parameters given in [43] can be chosen for representing an infinite grid. The parameters include short circuit power of 30 GVA and X/R of [3] 10. The AC source voltage is rated at 66 kV.

3.3. Control Structures

The control strategies are implemented for the MSC, DC circuit and GSC of the Type-4 WG. The conventional current control architecture utilized in MSC is explained in Appendix A.1.2. The major area of interest for this thesis is the control strategy of GSC. The DVC illustrated in Section 2.3.4.2 is implemented in the GSC.

3.3.1. Implementation of DVC in RSCAD

The control strategy depicted in [21] is achieved in RSCAD software. The control was implemented in RSCAD in [25] for a 33 kV HVAC transmission network, but the final goal of achieving reactive current injection during severe dynamic conditions was lacking. The primary reason was due to the avoidance of the current limiter block that is explained later in this section. However, the block is implemented successfully in this work, and the results are illustrated. Since RSCAD allows modelling of the secondary side of the transformer as required for one WG as explained in Section 3.2.1.3, the control loop parameters of GSC remain the same as 33 kV for a 66 kV offshore network and are based on the benchmark values provided in [38]. The control strategy described in Section 2.3.4.2 is incorporated in the reactive power and active power control loops defined in the following section.

[3] X/R = the amount of reactance X divided by the amount of resistance R

Reactive Power Control

From the control structure, it can be seen that, unlike in conventional current control, the reactive current is not directly utilized for voltage control. The converter voltage is directly controlled here, and this allows the current to modify on its own according to varying network conditions. This strategy is similar to the voltage control in conventional synchronous generators. The reactive control loop consists of an outer loop based on a slow VAR controller that tracks the changes in set points required by the system-wide demand. The inner loop consists of a fast-acting controller, as the name suggests, that responds towards crucial changes in voltage where quick action is required [21].

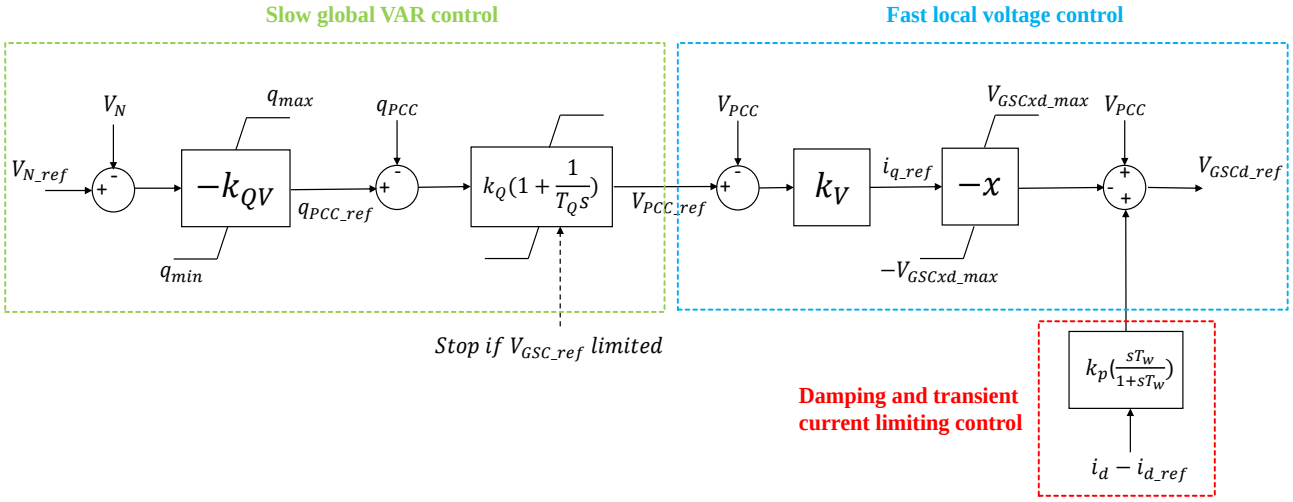

Figure 3.14: Reactive power control loop [21]

Slow global VAR control : It is the upper-level controller and can be modelled as a power factor, reactive power or voltage controller. The reference values can be directly sent as inputs to the PI controller if the controller is made to use for reactive power or power factor control. The voltage controller is used here, and this requires reactive power reference (q_{PCC_ref}) to be determined from a predefined voltage versus reactive power droop characteristic. A voltage value for which the injection of reactive power is zero is obtained from this characteristic. The obtained reactive power reference output is provided as input to the PI controller having a small proportional gain (k_Q) and ample time constant (T_Q) in order to avoid transformer tap changes and not very fast in order to avoid unwanted controller interactions. The automatic adjustment of reactive power in relation to varying voltage using the proportional gain, (k_{QV}) is significant. There is no dead band present in order to ensure continuous voltage control. The proportional gain that represents the droop can be obtained from the following relation,

$$k_{QV} = \frac{\Delta q}{\Delta V_N} \tag{3.7}$$

In theory, the proportional gain can be varied with changes in power flow. However, this is not practically feasible and hence it is recommended to set the reactive power reference based on load flow calculation in the network and corresponding optimum power flow (OPF) calculations. The values could be updated at regular intervals. V_{N_ref} can be determined from q_{PCC_ref} as,

$$V_{N\_ref} = -\frac{q_{PCC\_ref}}{k_{QV}} + V_N \tag{3.8}$$

where V_N is desired voltage and V_{N_ref} is the voltage at which no reactive power injection is required. The reactive power limits (q_{max} and q_{min}) are the continuous values in steady state and can be computed from the P-Q diagram of the converter operation. The time constant is chosen in the range of 5-30 s wherein a value in the higher range tends to stabilize, whereas value in the lower range can cause interactions with other controllers.

The slow global VAR controller must be made inactive once the converter current limit is reached and also during cases of large voltage sags or swells by providing a signal to deactivate the controller. A scenario that could lead to the case mentioned above is a three-phase short circuit event. The output from the upper-level controller must be constant because of the chosen high integration time constant or must be limited by a blocking signal [21].

Fast local voltage control : The voltage reference output (V_{PCC_ref}) received from the slow global VAR controller is provided as input to the fast local controller. This controller must be able to provide prompt support for grid voltage during the time of faults. The response of the controller in terms of voltage support must depend on local inputs

sensed at the PCC (V_{PCC}) and not on quantities that need to be measured at remote places using a communication mechanism. A proportional gain (k_V) is used for this purpose. The proportional gain can be obtained from the following relation [21],

$$k_V = \frac{\Delta i_q}{\Delta V_N} \tag{3.9}$$

The primary control action is provided by the feed-forward term, x, which is the reactance of the PE converter (GSC). The voltage output obtained on multiplying the current (i_{q_ref}) with x is the set point voltage of GSC in steady state. The reactive control loop parameters are shown in Appendix D.1.

Active Power Control

The active power control consists of the DC voltage, direct frequency control and Voltage Dependent Active Power Reduction (VDAPR) control, as shown in Figure 3.15. The control of active power is provided using the q-axis component of GSC voltage as per the Equation 3.10. Theoretically, since the DC capacitor provides the active power control, the DC energy barrier should be made higher which is to be done by increasing the capacitor size and DC voltage when in comparison with the conventional PI based current control [21]. However, considering the practical aspect, such an increase in capacitance is not incorporated for this work and the DC voltage is not increased beyond 4 kV. Another significant modification that was done is providing the minimum limit, $V_{a\_lim\_min}$, for the voltage measurement. A small value needs to be set for this parameter in RSCAD software, or else an error causing division by zero would be bound to occur during the start of the simulation. The active power is calculated as follows:

$$p = V_{PCC} i_d = -V_{PCC} \frac{V_{GSC\_q}}{x} \tag{3.10}$$

The direct frequency control provides control in case of under frequency and over frequency. The control is modelled to be activated when the frequency is above 50.2 Hz or below 49.8 Hz. The VDAPR control is provided to control the power injection capacity of the GSC. Since power cannot be injected to the network by the GSC during the time of faults, VDAPR allows in reducing the set point of reference power and thereby refining the dynamic stability of the network. The active control loop parameters are shown in Appendix D.2.

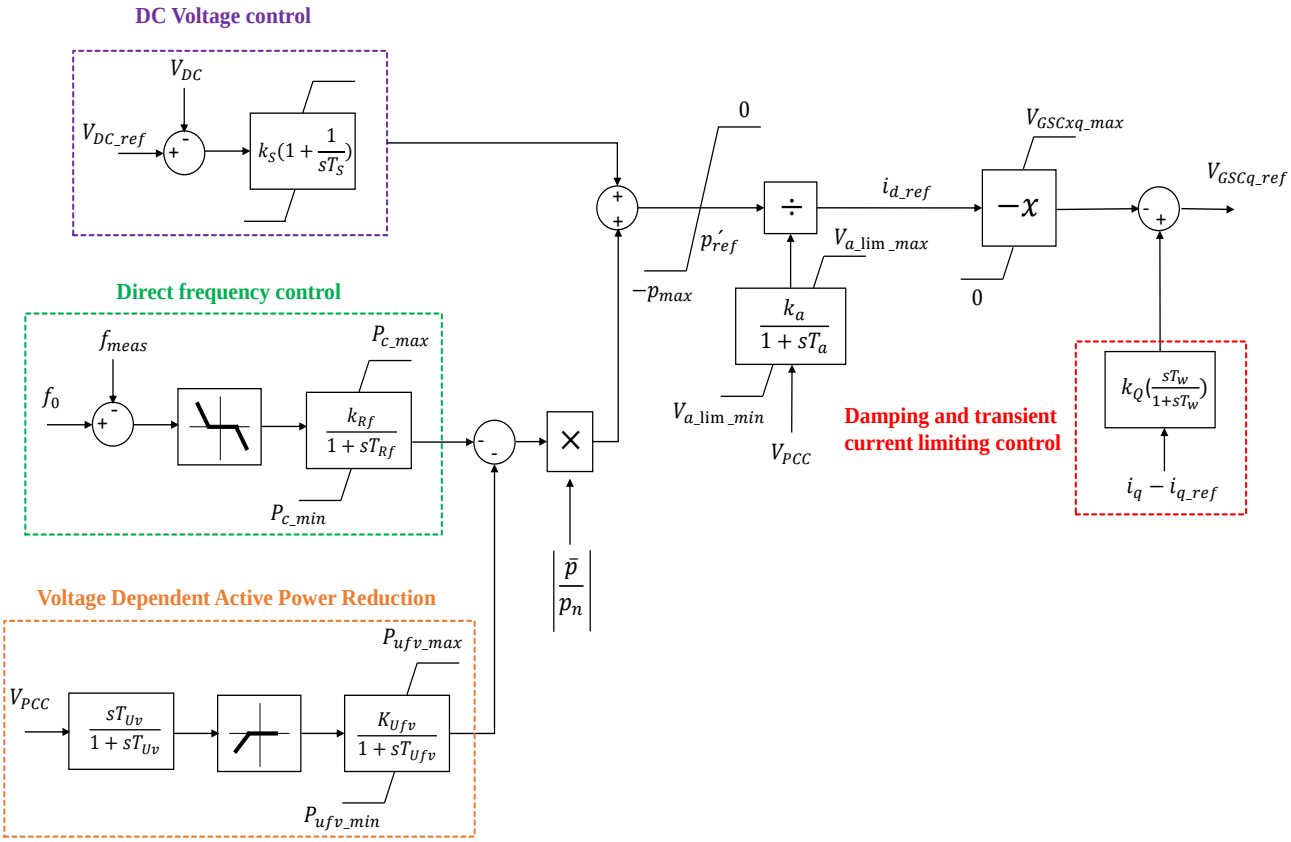

Figure 3.15: Active power control loop [21]

Current Limitation

The current limitation is an important block that protects the PE components from damage due to over current. A new maximum current (i_{max_ref}) value is computed whenever the maximum current (i_{max0_ref}) of the PE converter is exceeded. The current limitation is incorporated in GSC based on Equations 3.11 and 3.12. The upper and lower limits for i_{q_ref} and i_{d_ref} are calculated based on the grid impedance (shown as Priority in Figure 3.16) and the new maximum currents ($i_{d\_ref\_lim}$ and $i_{q\_ref\_lim}$) are computed. Once the reference limits are computed, the converter voltage limits are calculated by Equation 3.13 or by Equations 3.14 and 3.15 [21].

if

$$(|i_d + j i_q| - i_{max0\_ref}) > 0 \longrightarrow i_{max\_ref} = i_{max0\_ref} - k_{red} \times (|i_d + j i_d| - i_{max0\_ref}) \tag{3.11}$$

else

$$i_{max\_ref} = i_{max0\_ref} \tag{3.12}$$

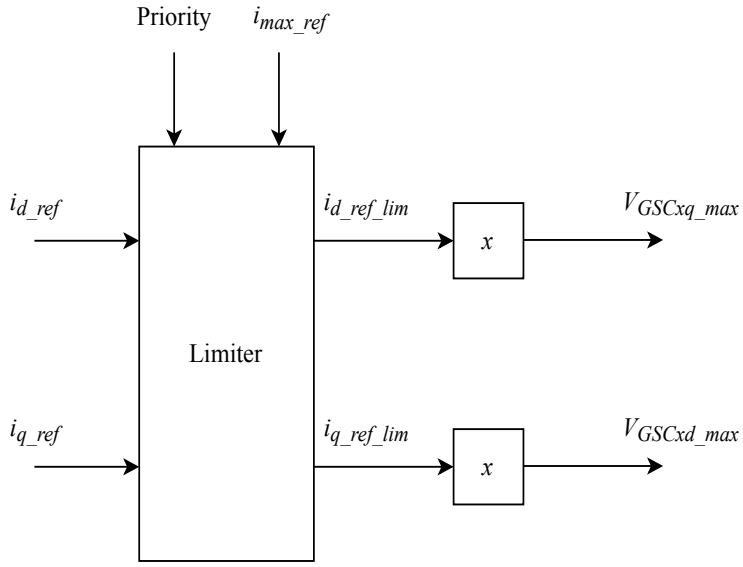

Figure 3.16: Current limitation algorithm in VSC [21]

As long as the reference current is not limited,

$$V_{GSCxq\_max} = V_{GSCxd\_max} = x \times i_{max\_ref} \tag{3.13}$$

else

$$V_{GSCxq\_max} = x \times i_{d\_ref\_lim} \tag{3.14}$$

$$V_{GSCxd\_max} = x \times i_{q\_ref\_lim} \tag{3.15}$$

Voltage Limitation

The AC voltage (V_{AC}) of the GSC is generally limited by the DC voltage (V_{DC}) value. The factor that brings the relationship between the AC and DC voltages is the modulation index. The modulation index is computed, as shown in Equation 3.16. The maximum value of the modulation index is set around to 1, and GSC voltage must be limited at that point to avoid non-saturation of the GSC.

$$m = \frac{2\sqrt{2}V_{AC}}{\sqrt{3}V_{DC}} \tag{3.16}$$

3.4. Analysis of the Dynamic Performance of 66 kV Test System in RSCAD

After the 66 kV system is modelled, it has to be tested for operation in steady state and dynamic conditions. The performance related to short-term voltage stability (fault occurring for a span of 6-10 cycles accounting for 120-200 ms) and reactive power injection by the DVC during the most severe dynamic situation in the network has to be analyzed. A three-phase short circuit in the middle of the HVAC cable is chosen to test the same.

3.4.1. Three-phase Line to Ground Fault

The line to ground fault logic available in the power system library in RSCAD is adapted in this network by splitting the cable model into two halves and implementing the fault logic in the middle of the two halves as shown in Figure 3.17. The Draft module is compiled, and after ensuring no errors, the system is run in the Runtime module. The system is stabilized with the voltage values within the tolerance limit of ± 10% during steady-state operation.

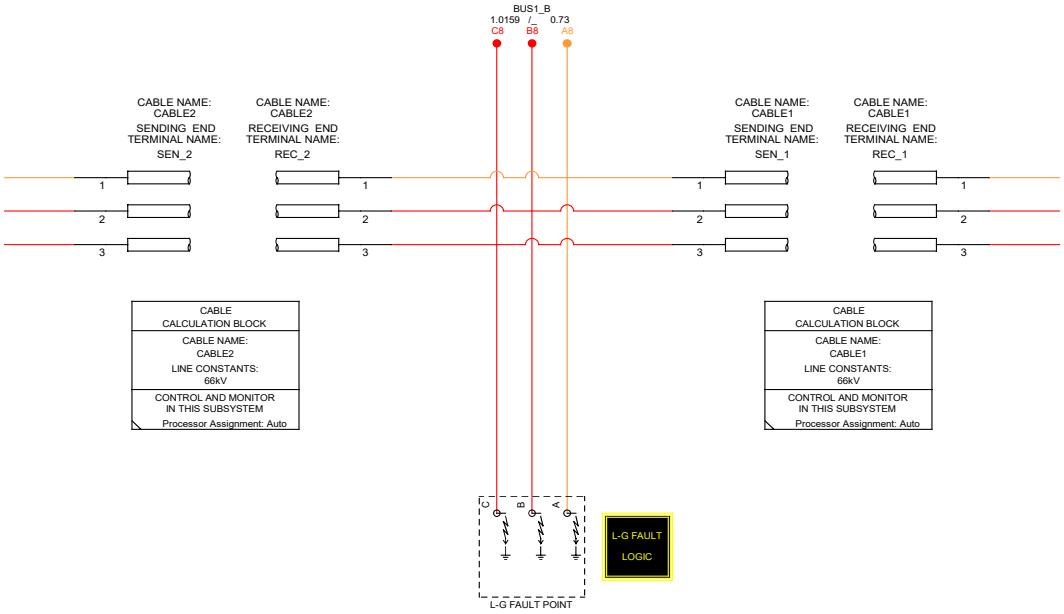

Figure 3.17: Representation of three-phase fault in the middle of the cable in RSCAD

The three-phase line to ground fault is applied at 0.5 s with a fault clearing time of 140 ms. The voltage and frequency responses are plotted for a shorter period (0.3 s to 1.3 s) to have a clearer view of the signals during the occurrence of an event. In the pre-fault condition, the voltage is stabilized at nearly 1.04 p.u., as seen in Figure 3.18. The frequency at the PCC computed by the PLL is set to 50 Hz, and is shown in Figure 3.19. The OWF is generating nearly rated active power, i.e. active current of nearly 1 p.u. is provided by the GSC, as depicted by the green line in Figure 3.20. There is no reactive current or reactive power injection by the GSC during this time, as seen from the purple line in Figure 3.20.

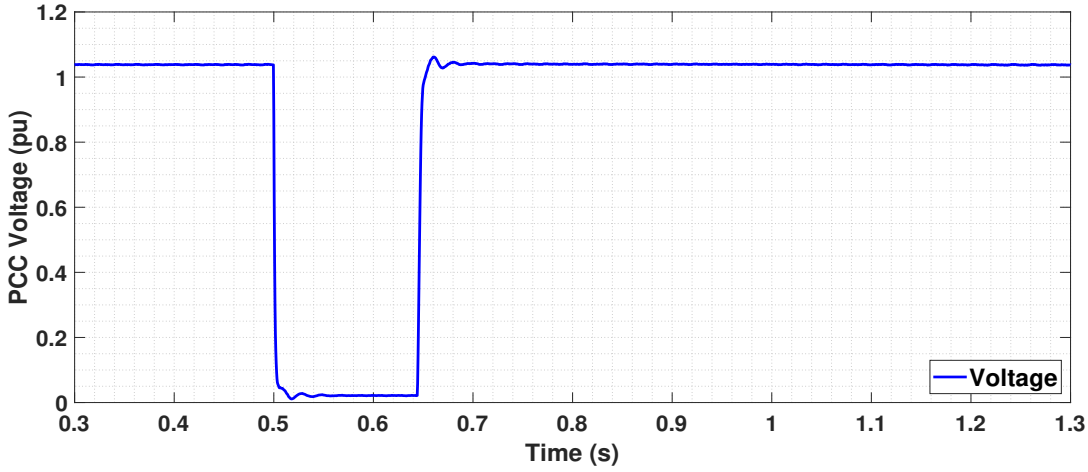

Figure 3.18: Voltage at PCC following a three phase fault in the middle of the cable

During the time of the fault, the voltage drops at PCC as expected for a three-phase line to ground fault. There is no significant drop in frequency since there are no loads connected to the OWF. Hence the frequency control does not get activated since deviation remains within 49.8 Hz and 50.2 Hz. DVC allows reactive current and hence reactive power to be injected by GSC during the time of fault to support the voltage, as shown in Figure 3.20. The corresponding

behaviour is a major requirement as per the grid codes during dynamic conditions, as mentioned in [12]. At the same time, the active current and thus active power is limited, and hence there is no generation from the OWF (Figure 3.20). Simultaneously, the voltage across DC link increases in order to maintain the power balance as per the Equation 2.6. The chopper gets activated when DC voltage goes beyond a particular limit in order to protect the DC link from overvoltage. After the fault is cleared, the DVC allows for quick recovery, the voltage and powers return to the pre-fault values.

The spike in voltage, frequency and currents after the fault is released at 0.64 s is due to the fast dynamics of DVC. Another important observation is the transients in the currents during the time of fault at 0.5 s in Figure 3.20. These are due to the dynamic effects that arise due to the exclusion of an integrator [21]. It can be controlled by proper tuning of washout filters.

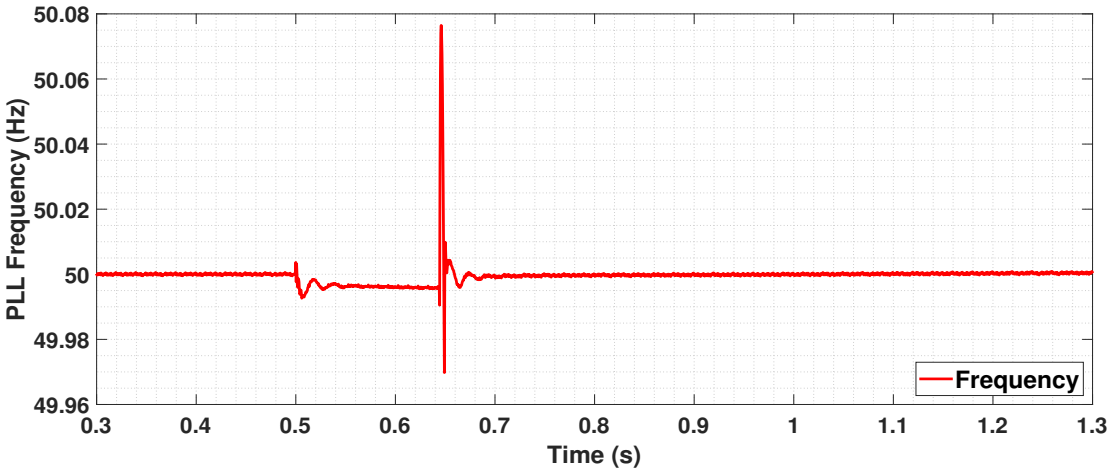

Figure 3.19: Frequency response synthesised by PLL following a three phase fault in the middle of the cable

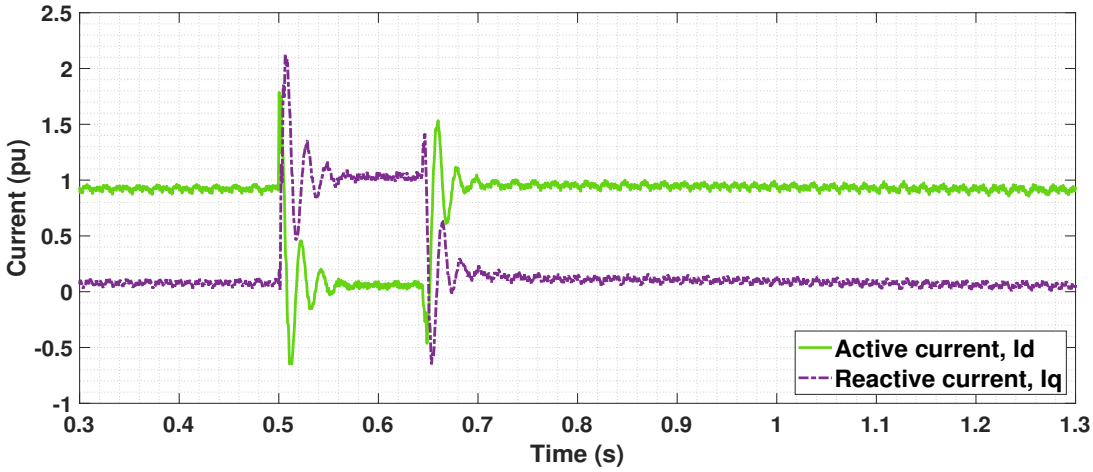

Figure 3.20: Active and reactive currents flowing to the network following a three phase fault in the middle of the cable

Parameter Selection for Washout Filters

The damping during the transient process mentioned in Section 2.3.4.2 is ensured by the washout filters in the reactive power and active power control loops as seen in Figure 3.14 and Figure 3.15 respectively. Parameter sensitivity analysis needs to be performed for the washout filters to ensure fast damping of transients. The output of the washout filter for various proportional gains for a step response is depicted in Figure 3.21. The proportional gain represents values to which the output of the washout filter changes when there is a change in the input. The time constant represents the rate of this change. It can be seen that the output of the washout filter changes proportionally to the gain value specified and comes back to the initial value after a specific time, depending on the time constant mentioned.

Effect of this property of washout filter is observed in the active and reactive currents at the PCC for a similar three-phase fault as performed in the previous section. Measurements are recorded between 0.45 s to 0.65 s in Figure 3.22

and 3.23 for active and reactive currents, respectively to analyze the behaviour of transients. The proportional gain is set as 0.01, 0.03 and 0.05 for comparison, keeping the time constant = 0.01 s for all the three cases. It is observed that faster damping can be achieved for higher proportional gains. It makes sense as the system would try to damp the transients to the maximum possible value in order to have minimum fluctuations and also to limit interactions with other controllers during this period. Thereby, it is worthy to conclude that choosing the right parameters for the washout filter is one among the key factors in this control approach.

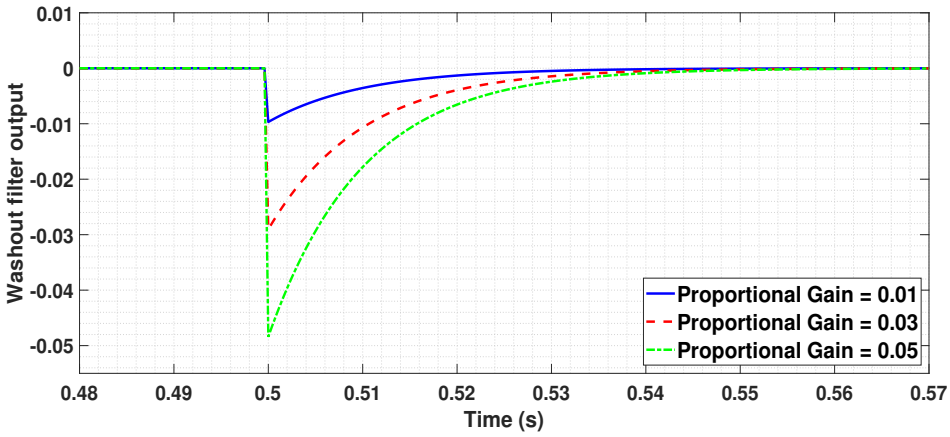

Figure 3.21: Output of a washout filter for different proportional gains for a step response

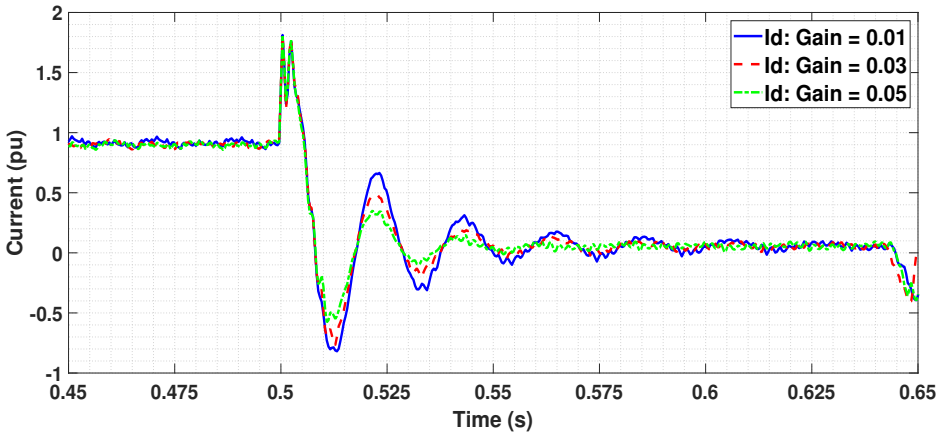

Figure 3.22: Current in d axis following a three phase fault for proportional gains 0.01, 0.03 and 0.05

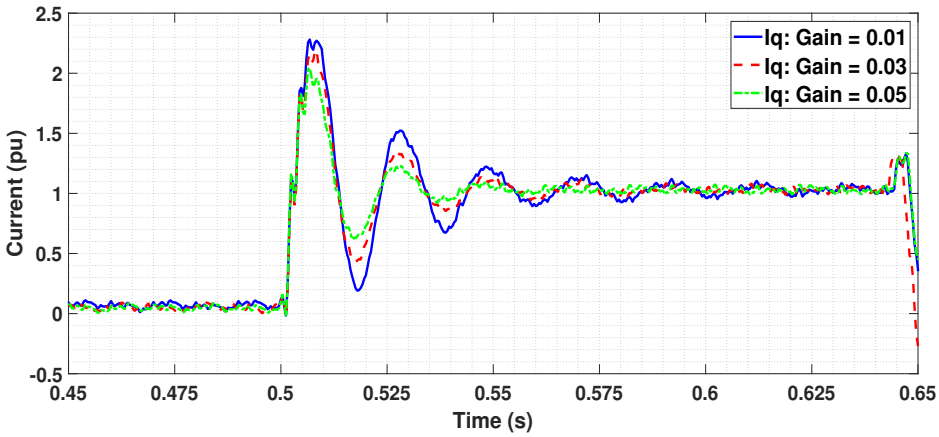

Figure 3.23: Current in q axis following a three phase fault for proportional gains 0.01, 0.03 and 0.05

3.5. DIgSILENT PowerFactory Software

PowerFactory is a software tool developed by DIgSILENT (Germany) that is used for RMS and EMT simulations. It has three integration characteristics; functional integration, vertical integration and database integration. Functional integration explains that PowerFactory is a single executable program and vertical integration means that the models in the power system can exchange all of the analysis functions at one place. PowerFactory uses a Data Manager for database integration that allows all models to be stored under one project file. There are two libraries available in PowerFactory; Global and Project libraries. There are two subsections available within the Project library. They are [44]:

- Equipment Type Library
- User Defined Models

PowerFactory also provides development of user-defined models using DIgSILENT Simulation Language (DSL). These features are utilized, and DVC control is implemented in PowerFactory for a typical configuration of the offshore network in [21]. It is tested and proved to work [21]. The test results achieved in RSCAD in the previous section need to be compared with a similar 66 kV HVAC offshore network in PowerFactory to validate the control action. In this section, a 66 kV HVAC offshore network is developed in PowerFactory with the benchmark DVC model utilized from [21]. Differences in the models are notified, the voltage and current profiles are compared for a three-phase line to ground fault in the middle of the cable.

3.6. Layout of the 66 kV HVAC Test System in PowerFactory

The 66 kV offshore network is modelled in PowerFactory as shown in Figure 3.24. The network consists of the following components:

- A simplified model of Full Scale Converter (FSC) based Type-4 WG system consisting of the following elements:
  - DC circuit
  - Grid Side Converter (GSC) or Line Side Converter (LSC)
- High Pass filter (HPF) with series reactor
- OWF transformer
- HVAC cables
- External AC system

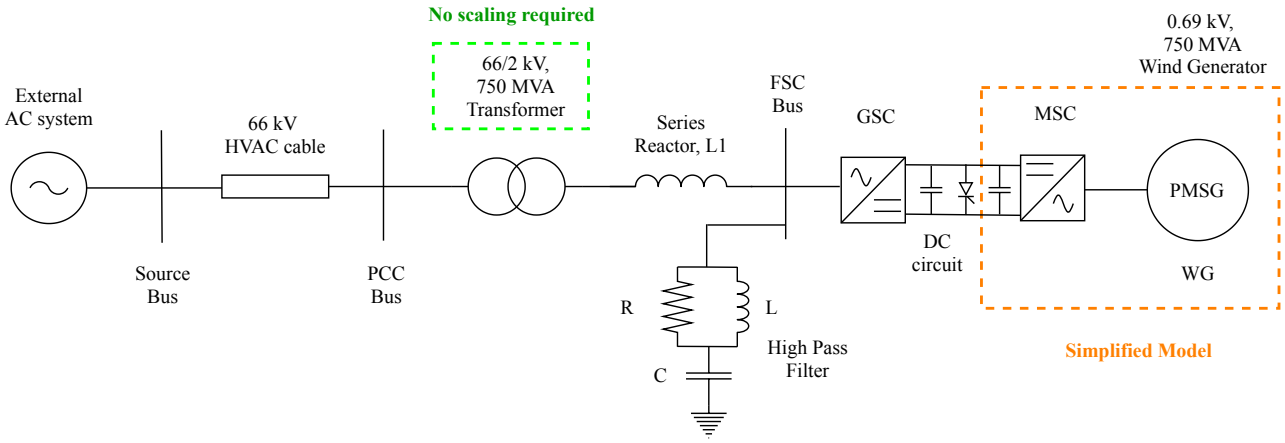

Figure 3.24: Single line diagram of the 66 kV HVAC offshore test network in PowerFactory

3.6.1. Simplified Full Scale Converter (FSC) based WG System

The wind turbine and MSC are simplified since they do not contribute to the dynamics of the network. GSC is modelled in detail. A constant injection of active current is proposed from the MSC to the DC side [21]. Hence it is modelled as a DC current source. The WG unit is represented as a static generator model with 750 MVA nominal apparent power. It is made to operate with constant reactive power (Q) control in order to achieve the active and reactive power set points same as in RSCAD model. The active power flow is set to ~ 700 MW, similar to the RSCAD model.

DC Circuit
The DC circuit is detailed, and the voltage across the capacitor is set to 4 kV, same as the RSCAD model. The chopper activation control is provided when the DC voltage crosses a minimum set value.

GSC
Unlike the RSCAD model, a two-level GSC is utilized in this model. The PWM is not used in this model, and the GSC is modelled as a controlled voltage source. This is one among the major difference with the RSCAD model. The DVC control for GSC developed in [21] is provided in this model as explained in Section 3.3.1. The full representation of DVC with active and reactive power loops in PowerFactory is depicted in Appendix A.2.

3.6.2. HPF with Series Reactor
The shunt filter available in the PowerFactory drawing toolbar is chosen. The values for R, L and C are chosen the same as mentioned in Section 3.2.1.2. A common impedance element available in the drawing tool is chosen for the series reactor and is connected at the output of GSC, as shown in Figure 3.24. The inductance value chosen is the same as the RSCAD model to have an equal impedance for both the models.

3.6.3. OWF Transformer
A two winding transformer available in the equipment library folder of DIgSILENT library is used. The transformer is rated 66/2 kV, 750 MVA with a wye-delta configuration to block zero sequence currents. The leakage inductance and resistance of the transformer are set the same as the RSCAD model.

3.6.4. HVAC Cables
The cables are rated at 66 kV same as the RSCAD model. The cable is modelled from the "Cables" section available in the equipment library in DIgSILENT library. The type of model is chosen to be the Pi model. Pi model is utilized as it is easier to input the cable parameters in terms of RLC in both RSCAD and PowerFactory.

3.6.5. External AC system
The external AC system in PowerFactory also represents an infinite grid. Similar to the model in RSCAD in Section 3.2.3, the infinite grid is modelled as an AC voltage source available in the PowerFactory drawing toolbar.

3.7. Control Structures
As mentioned in Section 3.6.1, the wind turbine and MSC models utilized are simplified and is made to inject constant active current to the DC circuit. Hence, the control of MSC and wind turbine is not required to be modelled. However, control structures are detailed for the DC circuit and the GSC. The benchmark model of DVC from [38] is utilized here for the GSC. The control structures are depicted in Appendix A.2.

3.8. Comparison of Models in RSCAD and PowerFactory
The major differences between the 66 kV HVAC network built in RSCAD and PowerFactory are illustrated in Table 3.1.

Parameters	RSCAD	PowerFactory
WG model	PMSG	Simplified (Constant power model)
MSC control	Conventional current control	Not modelled
GSC model	VSC with PWM	Controlled Voltage Source with no PWM
Generated active power from WG	6 MW	~ 700 MW
Scaling factor at transformer	116 (cf. Section 3.2.1.3)	Not applicable

Table 3.1: Differences in models in RSCAD and PowerFactory

Representation of GSC: One of the differences in both models is the usage of average model representation of VSC with PWM in RSCAD for the GSC, whereas a controlled voltage source model is utilized in the PowerFactory model.

Scaling of power: Another significant difference between the two models is that the components connected to the secondary side of the transformer are modelled for one WG of 6 MW in RSCAD whereas it is directly modelled for ~ 700 MW in PowerFactory. The scaling of power to ~ 700 MW in RSCAD is done at the 66/2 kV OWF transformer, as explained in Section 3.2.1.3. This helps in modelling and analysis in the real-world in terms of single WG.

However, it must be noted that these differences do not affect the performance of the control operation, and both the models have equal impedances that makes the comparison significant.

3.8.1. Selection of Time Step in RSCAD and PowerFactory

Before the start of the simulation, a specific time step value suitable for both the RSCAD and PowerFactory models need to be set. As mentioned in Section 3.2.1, the ratio of large time step to small time step needs to higher than 12 in RSCAD model if NovaCor processor is used. Since the small time step is chosen to be 2500 ns for the RSCAD model, as mentioned in Section 3.2.1, a value of 50 μs is chosen for the large time step. The setting can be done by right-clicking on the Draft module and selecting "Circuit Options" in RSCAD. In PowerFactory, it can be edited in the "Step Size" option available in the "Calculation of initial conditions" tab, as shown in Figure 3.25.

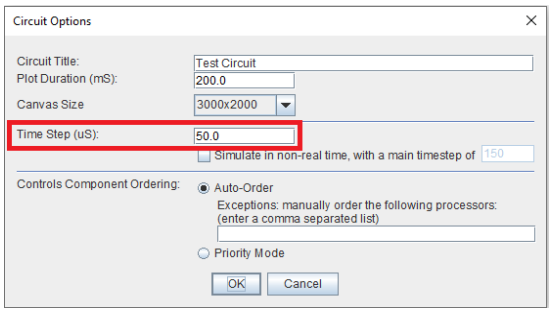

(a) Time step setting in RSCAD

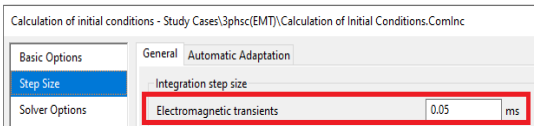

(b) Time step setting in PowerFactory

Figure 3.25: Initialization of time step in RSCAD and PowerFactory

3.8.2. Event Comparison in RSCAD and PowerFactory

The 66 kV offshore network model in RSCAD and PowerFactory are compared for a three-phase line to ground fault in the middle of the cable. A fault is applied at 0.5 seconds with a clearing time of 140 ms. The resulting voltage and current waveforms are as shown in Figure 3.26, 3.27 and 3.28 respectively. As can be observed in Figure 3.26, the voltage measured at PCC drops and the generation is stopped during the fault period. The voltage profile is the same in RSCAD and PowerFactory models during the pre-fault, fault and post fault conditions as can be observed. The drop in voltage in both the graphs is the same due to equal impedance in both the models.

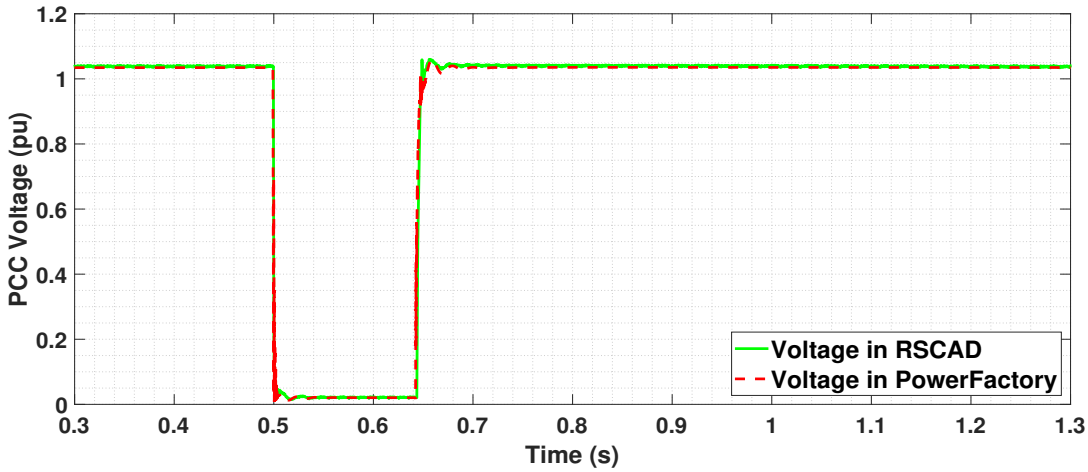

Figure 3.26: Voltage measured at PCC for a three phase fault in the middle of the cable in RSCAD and PowerFactory

Due to the unavoidable modelling differences in the software packages, currents are measured at PCC bus for the RSCAD model and at FSC bus for the PowerFactory model. However, this does not affect the magnitude as the currents are measured in per unit. The currents in both the models have a similar profile, as summarized for the d-axis in Figure 3.27 and q-axis in Figure 3.28. The active and reactive currents generated by the WG have the same set points in both the models during the pre-fault condition, confirming that the power flow in both the models is similar. As the parameters for DVC is same for both the models, reactive power injection in RSCAD model during the time of fault is achieved similar to the PowerFactory model. The transients occurring during the time of fault at 0.5 s can be

damped by controlling the parameters of the washout filters, as seen in Section 3.4.1.1. Spike in the profiles at the time of fault clearance at 0.64 s is due to fast dynamics of PLL in both software packages. It is observed that the currents in RSCAD model have slight transients throughout the simulation. This is due to the detailed model representation of GSC in RSCAD when compared to a simplified representation in PowerFactory. Therefore, it can be concluded that the RSCAD model with the implemented DVC provides similar results as the benchmark PowerFactory model. Moreover, the results from RSCAD model are more detailed and hence can be used as a base model for reference as it provides a better representation of the real-world operation.

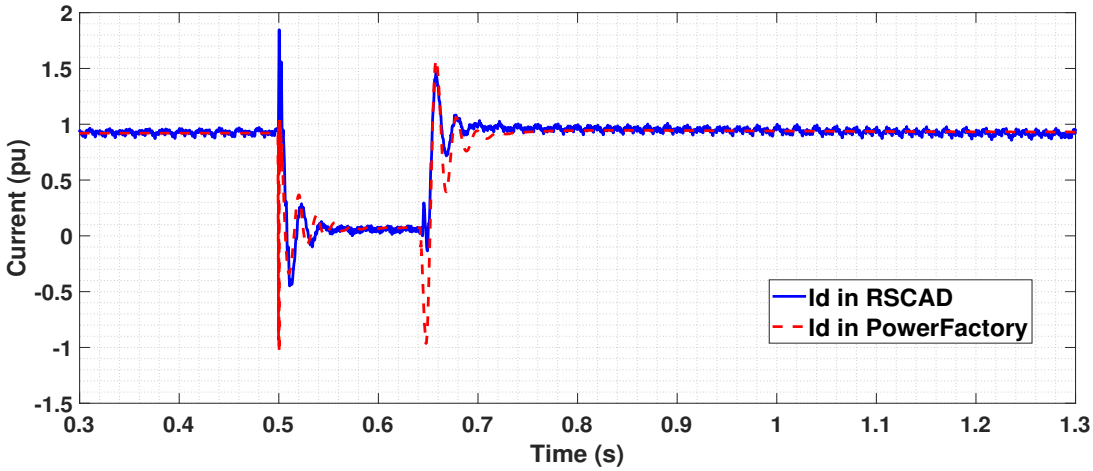

Figure 3.27: Active currents flowing to the network for a three phase fault in the middle of the cable

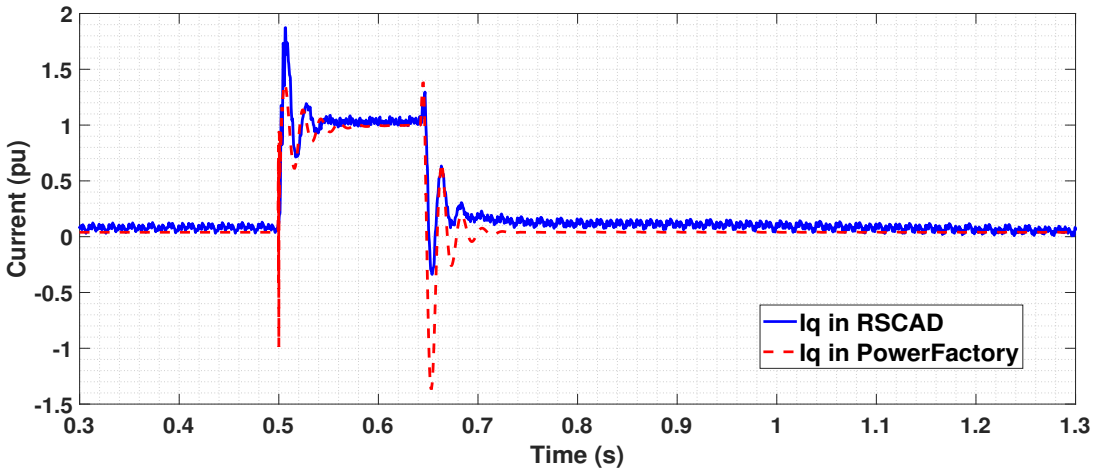

Figure 3.28: Reactive currents flowing to the network for a three phase fault in the middle of the cable

4

Modelling a Digital Twin of 2 GW, 66 kV HVAC Offshore Network with MMC-HVDC Transmission

This chapter details the development of a multi-gigawatt (focus of 2 GW), 66 kV HVAC offshore network connected to two offshore converter stations. Like in Chapter 3, an average EMT modelling depth is used (i.e. focus on the study of three-phase faults occurring in a balanced system), the model is developed, and simulations are conducted in RSCAD. The model depicts the connection of four OWFs through a 66 kV HVAC offshore network contributing a total of 2 GW installed capacity. The power is transferred to the onshore system through MMC based HVDC links. The focus is to investigate the dynamic performance of such a system when subjected to severe disturbances (e.g. three-phase line to ground fault) in the AC part of the network. The role of both DVC in WGs and voltage control in MMC is examined in detail to understand the voltage performance and the power flow distribution based on simulations performed in RSCAD.

4.1. Processors in RSCAD

The simulations in RSCAD can be run in either NovaCor or PB5 processor cards. NovaCor processor is used for this work as they have 2-3 times the simulation capacity of a completely loaded PB5 processor [45]. For an extensive power system network, NovaCor processor requires a part of the system to be placed in a separate subsystem. RSCAD allows provision for splitting of the network into subsystems if the network is large. The splitting is done by right-clicking on the main subsystem tag and choosing "Add Subsystem" as shown in Figure 4.1. This feature is utilized in this section using Tline modules, that are used to connect subsystems. The process is explained in Section 4.3.2 in detail.

There are two NovaCor processors available at TU Delft, and they are equipped with four cores each. These cores are utilized to solve the overall network solution, auxiliary components (such as transformers, cables, generators etc.) and the controls present in the simulation. Assignment of cores for solving various components of the network is an important step that needs to be considered while modelling, as they depict the total load that is distributed over the available cores. The process is detailed in Section 4.3.1.

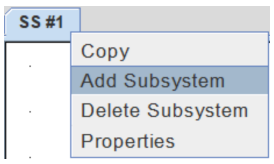

Figure 4.1: Adding subsystems in RSCAD

4.2. Defining the Layout for the 2 GW Offshore Network

The initial aspect that needs to be considered for an offshore network is the topology of the network. The popularity of MMC due to its improved controllability and superior system performances has led the way for the increasing demand of MMC-HVDC transmission to integrate distant OWFs. For the connection of new OWFs in the vicinity of the already existing ones, parallel operation of MMC-HVDC transmission systems can be expected in the near future with multiple connections to the onshore system. Such type of schemes increases the interest in hybrid systems with

the hub-and-spoke principle proposed by ABB [46] and represented in Figure 4.2. The layout in Figure 4.2a) depicts the connection of OWFs to an offshore converter station which in turn transfers power to the onshore system through multi-terminal HVDC connections. However, the scaling of offshore wind power is limited to the installed capacity of MMC unit in such a layout. Another layout involves the OWFs connected through AC links to a back-to-back HVDC converter station as shown in Figure 4.2b). Long distance HVAC transmission is required in this case, for the transfer of power from OWFs to the onshore network and hence contribute to high losses in the network when compared to HVDC transmission for larger distances. Figure 4.2c) represents the connection of multiple OWFs to the offshore converter station, and power is transferred to the onshore system through multiple HVDC links. Such a layout provides contingency in the network by supplying offshore wind power to at least one onshore system if one of the HVDC links gets disconnected [47]. A stage-wise construction of such a HVDC project is easier to be achieved by the developers as well [7].

A specific configuration for a 2 GW offshore network is currently non-existent, and this chapter tries to fill in such a research gap. The idea in this chapter is to expand the single OWF model network in Figure 3.6 for a 2 GW offshore wind power network. This could be made possible by connecting four such OWF models in parallel with each generating ~ 500 MW of power. The reason for choosing four OWFs is to have a symmetrical layout and to test the ability of RSCAD to perform simulations on such a configuration. Correspondingly, a 2 GW offshore converter station capacity is required to transfer this generated amount of power to the onshore system. However, currently deployed (state-of-the-art) MMC-HVDC transmission, has a maximum rated capacity of 1.2 GW [8]. Hence, with the available technology, two MMC offshore stations of 1 GW each will be required for 2 GW power transmission. Taking the aforementioned factors into account, a modified layout of Figure 4.2c) is developed for this work.

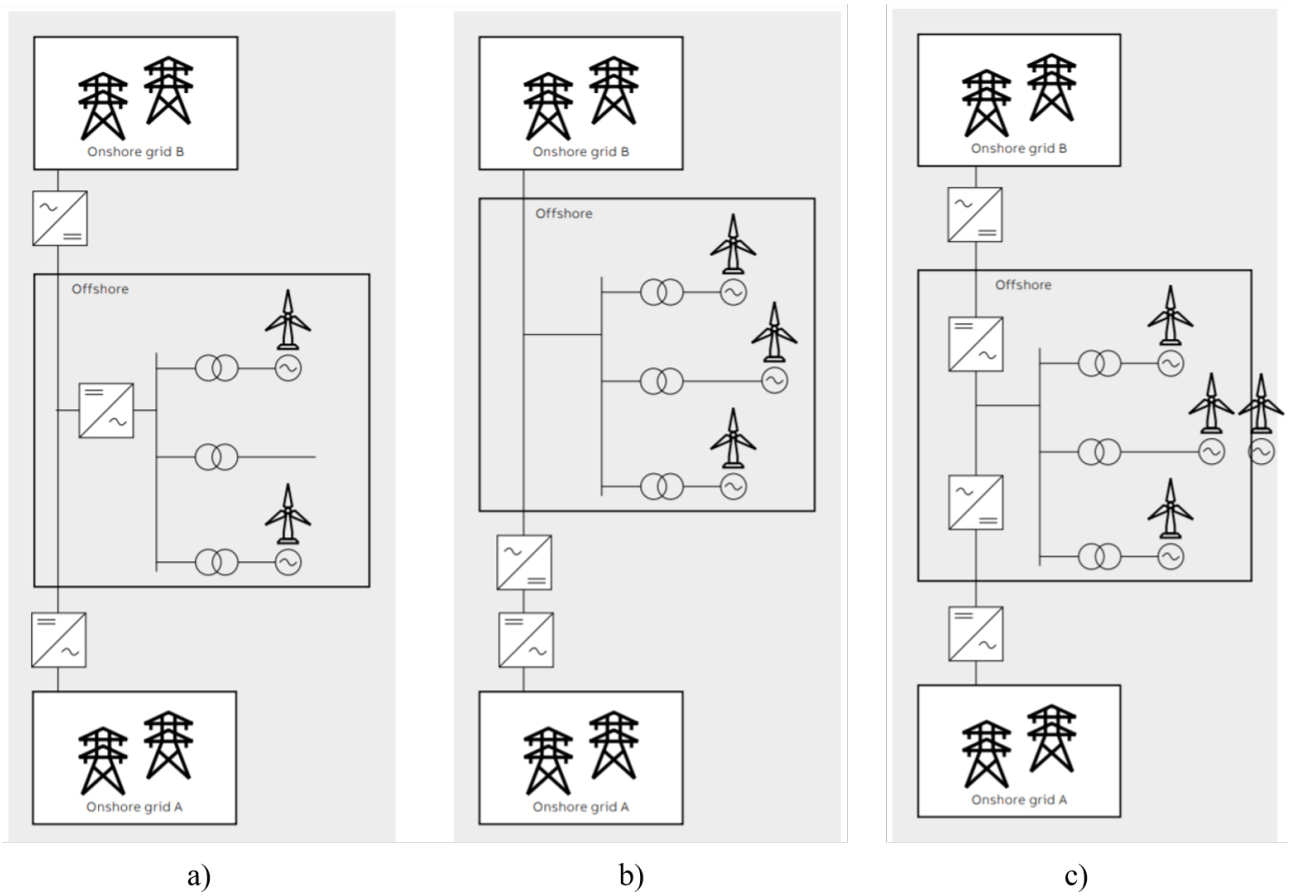

Figure 4.2: a) Hub-and-spoke with multi-terminal HVDC system, b) Hub-and-spoke with AC links and HVDC back-to-back station and c) Hub-and-spoke with multiple HVDC links [46]

4.2.1. Scaling of Single OWF Model for 2 GW Offshore Network

The layout of the 2 GW offshore network is built by resorting to scaling of the aggregated OWF model in Section 3.2.1 of Chapter 3. A modular topology is considered to achieve the capacity of 2 GW.

- The aggregated OWF model in Section 3.2.1 provides a generation of ~ 700 MW. The first step involves reducing this generation to ~ 500 MW as the layout is planned for four OWFs. This is achieved by reducing the number of

parallel WG units from 116 (116 × 6 MW = 696 MW) to 83 (83 × 6 MW = 498 MW) which is done by changing the scaling factor explained in Section 3.2.1.3. Now the OWF generates nearly ~ 500 MW of active power, as shown in Figure 4.3.

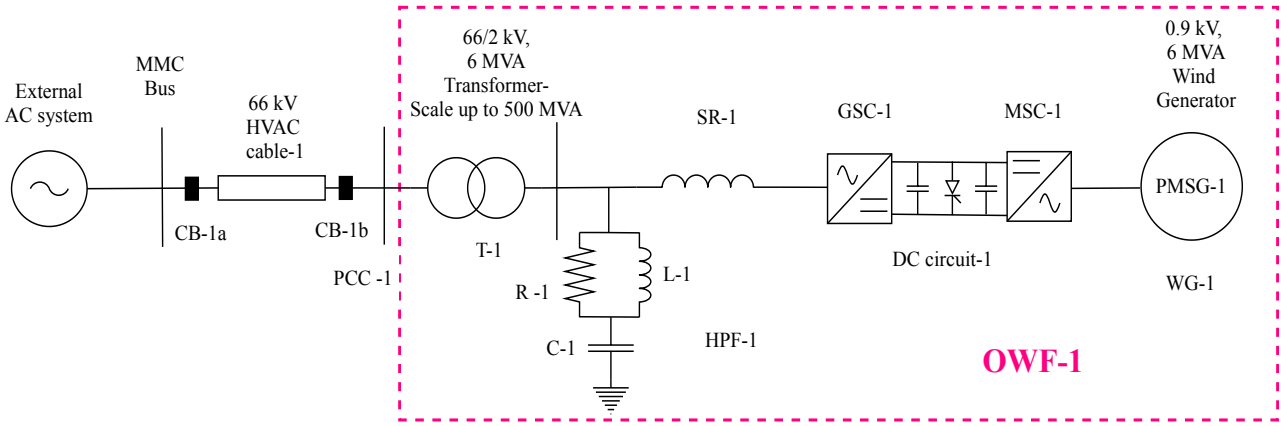

Figure 4.3: OWF-1 connected to external AC system

- The second step involves the connection of two OWFs in parallel to the external AC system in a modular approach. This allows for the generation of 1 GW of power, as depicted in Figure 4.4. All the control structures incorporated in OWF-1 are replicated for OWF-2.

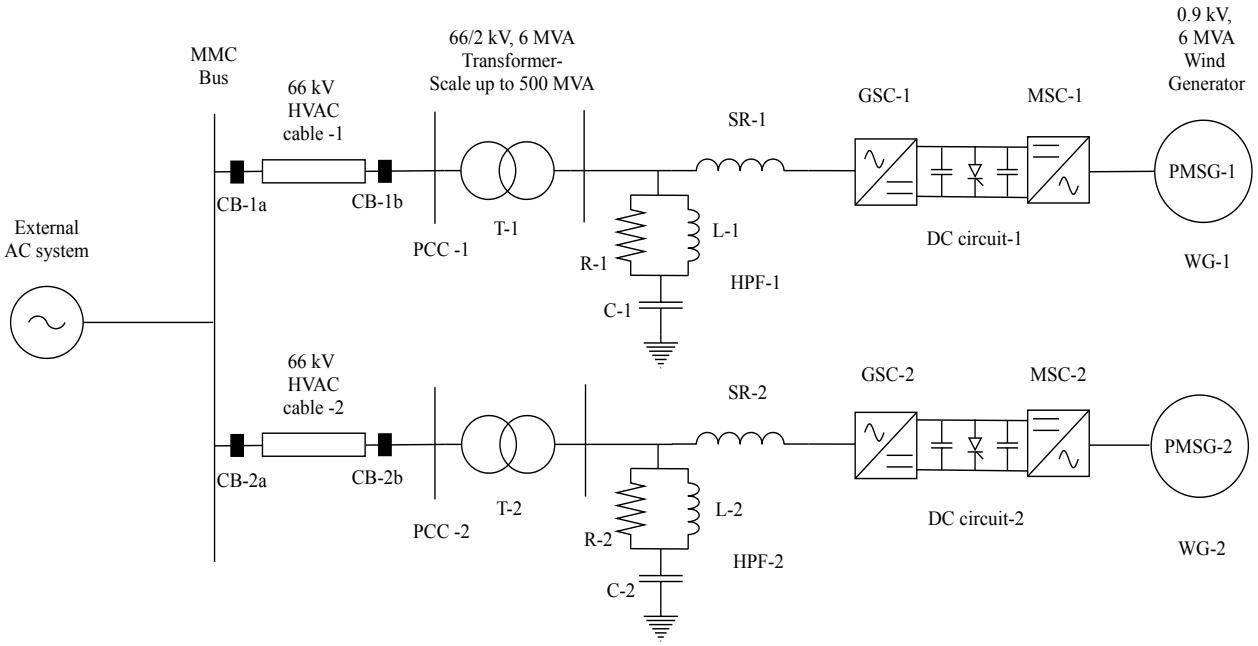

Figure 4.4: OWF-1 and OWF-2 connected in parallel to external AC system

- In the third step, the external AC system is replaced by an offshore converter station consisting of the average EMT model of MMC (MMC-1) and the interface transformer (IT-1) available in the CIGRE B4 DC Grid Test System [48]. The same is depicted in Figure 4.5. As the final layout network would be extensive, it is required to split the network into subsystems, as mentioned in Section 4.1. The splitting into two subsystems is performed in this step. The offshore converter station is modelled in subsystem-1, and the OWFs are modelled in subsystem-2. MMC-1 is designed to operate in V/F control (or grid forming control) which is explained at the end of this chapter.

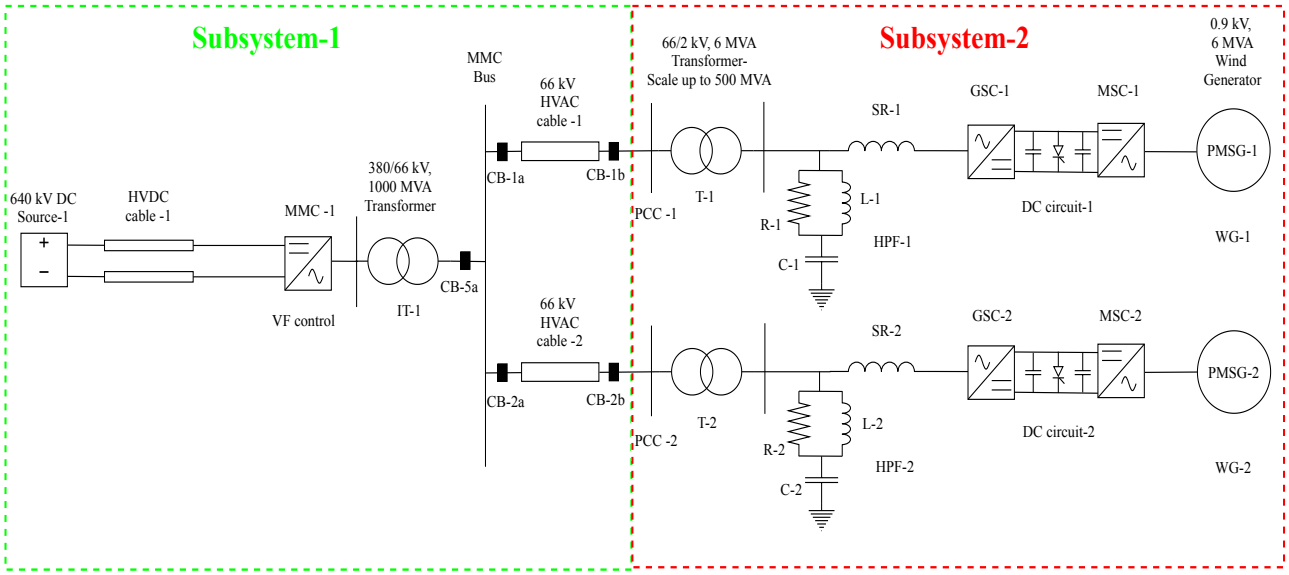

Figure 4.5: OWF-1 and OWF-2 connected in parallel to MMC-1

- The final step involves the parallel connection of two more OWF models (OWF-3 and OWF-4) in a modular approach generating 500 MW each. Additionally, another offshore converter station consisting of a similar average EMT model of MMC (MMC-2) and two interface transformers (IT-2a and IT-2b), is connected in parallel to the previous converter station. The need for two interface transformers in MMC-2 bus is explained at the end of this chapter. Therefore, the final layout shown in Figure 4.6 represents a total of 2 GW offshore wind power transmission.

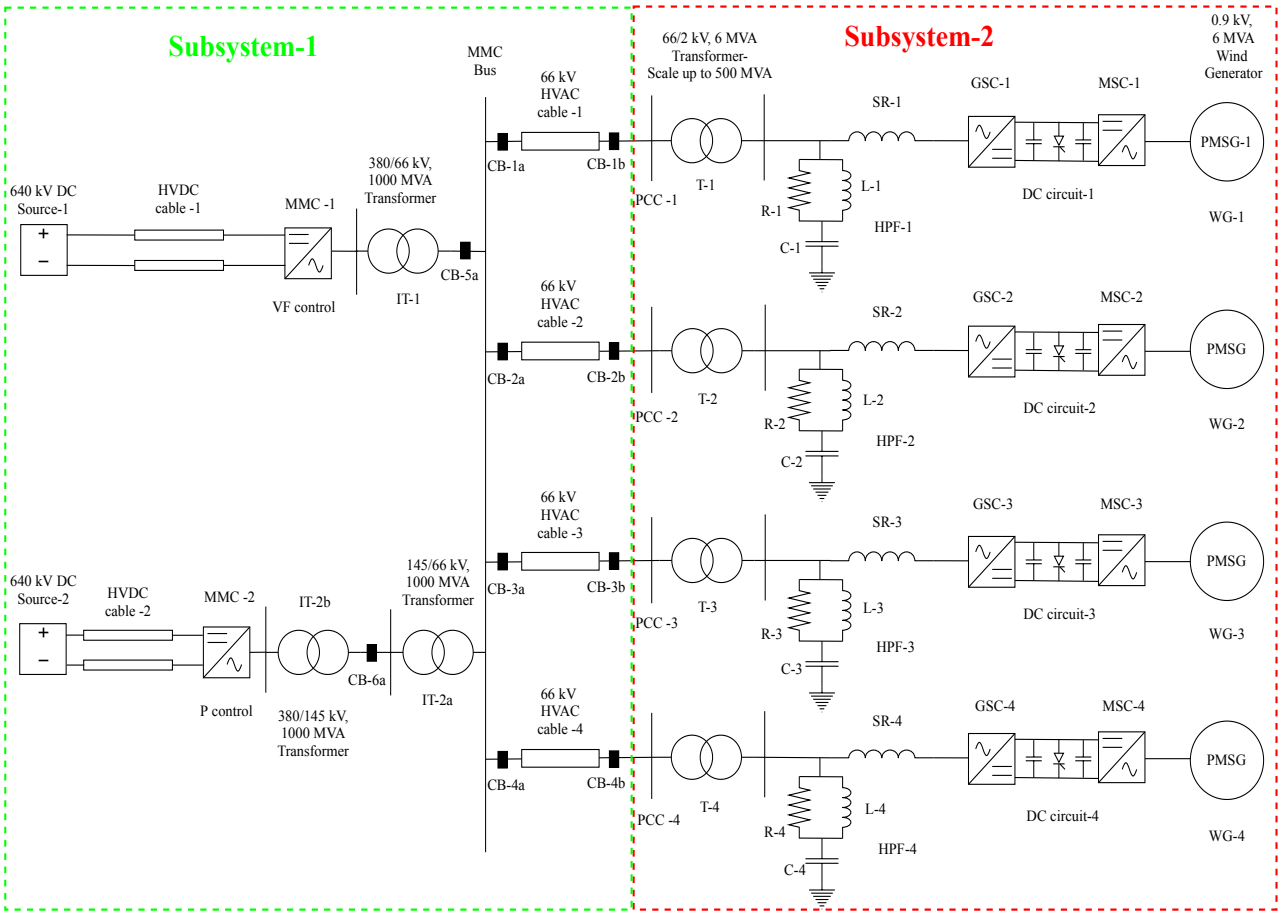

Figure 4.6: Single line diagram of 2 GW, 66 kV HVAC offshore network connected to 2 x 1 GW HVDC links with offshore converter stations in RSCAD

4.3. Layout of 2 GW, 66 kV HVAC Offshore Network in RSCAD

The components in the 2 GW, 66 kV HVAC network is detailed in this section. The single line diagram of the network is depicted in Figure 4.6 and the major components of the network include :

- Four aggregated OWFs, each with 500 MW installed capacity represented by the following components:
  - A single Wind Generation System with
    - Permanent Magnet Synchronous Generator (PMSG)
    - Machine Side Converter (MSC)
    - DC circuit
    - Grid Side Converter (GSC)
  - High Pass filter (HPF) with series reactor
  - OWF transformer
- Four pairs of HVAC cables
- Three interface transformers
- Two MMCs
- Two pairs of HVDC cables

4.3.1. Aggregated OWF

As mentioned in Section 4.2.1, the 2 GW offshore wind power is split into four OWFs with ~ 500 MW rated capacity each. Currently, the largest offshore WG developed by GE Renewable Energy has a rating of 12 MW [49]. However, the standard model available for a Type-4 WG in RSCAD is rated 6 MW. Hence, to represent a ~ 500 MW OWF, 83 WGs are required. All the OWFs are at a distance of 30 km from the MMC bus.

The average model of Type-4 WG available in RSCAD is used for this work as well. The aggregated OWF model represented in a small time step environment described in Section 3.2.1 is used here for all the four OWFs. As the entire network is extensive, it is split into two subsystems in RSCAD, as shown in Figure 4.6 by employing the technique explained in Section 4.1. The four OWFs are modelled in subsystem-2, and the rest of the system is modelled in subsystem-1. Each subsystem requires one rack for operation, and hence two NovaCor racks are used for the network simulation. It is also possible to simulate the network with PB5 processor. However, this requires a total of three subsystems since PB5 racks allow only small network solutions to be solved in one rack [50]. Therefore, two OWFs are to be modelled in subsystem-3, other two OWFs in subsystem-2 and the rest of the network in subsystem-1. Henceforth, the simulations are considered only in NovaCor processor for this study.

Since there need to be four different small time step blocks representing four OWFs, each block needs to be set with different step sizes to avoid conflict during initialization. These step sizes are only used for initialization, and the actual step sizes can be viewed in the "Map File" as mentioned in Section 3.2.1. Moreover, if the time steps are not initialized properly, it could lead to the occurrence of a time step overflow error during the simulation in the Runtime module.

Another essential parameter to be considered here is the assignment of the cores for the small time step blocks. As mentioned in Section 4.1, cores are responsible for solving the entire network solution. NovaCor processor in TU Delft is configured with four cores, and each component used in the network can be assigned to specific cores (1 to 4 in number). Since there are six small time step blocks (OWF-1, 2, 3 and 4; MMC-1 and MMC-2) in total, the cores need to be manually assigned to each block to allocate the load on each processor within their capacity. The core allocation of the small time step blocks representing OWFs for this network is chosen, as shown in Table 4.1.

Small time step block	Core assignment
OWF-1	4
OWF-2	1
OWF-3	3
OWF-4	1

Table 4.1: Core assignment of OWF models in subsystem-2

4.3.2. HVAC Cables

The HVAC cables transfer power from the OWFs to the offshore converter stations. Hence, four pairs of HVAC cables are required to transfer power from four OWFs. The cables are rated at 66 kV and are 30 km of length. In the network layout represented in RSCAD, as shown in Figure 4.6, the HVAC cables connect the OWFs in subsystem-1 with the MMC bus in subsystem-2. To provide such a connection between components placed in different subsystems in RSCAD, a feature called Tline module is available in the RSCAD modules section (denoted by a red box in Figure 4.7). This module is similar to the Cable module explained in Section 3.2.2. However, Cable module only allows connection between components in the same subsystem. The Tline module can be modelled as an overhead transmission line or cable. Since an offshore network model is considered in this work, the Tline model represents a subsea cable model.

The cables are modelled as Bergeron models with RLC data parameters. Bergeron model is chosen to test the working of the network using travelling wave model. Moreover, as the 2 GW offshore network is developed from the single OWF model in Section 3.2.1, the same RLC cable parameters used in Section 3.2.2 are used in the Tline module for all the four pairs of cables.

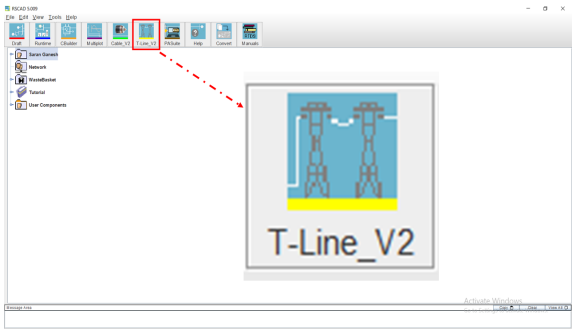

Figure 4.7: Tline module in RSCAD

In the Draft module, the cable model is added in the circuit using the unified Tline model shown in Figure 4.8 available in RSCAD power system library. The unified model consists of the following components:

- Calculation Block
- Sending End Terminal
- Receiving End Terminal

The detailed representation of the cable parameters in Tline module, and the representation of the cable model using the calculation block, sending end terminal and receiving end terminals in the Draft module is shown in Appendix D.6.

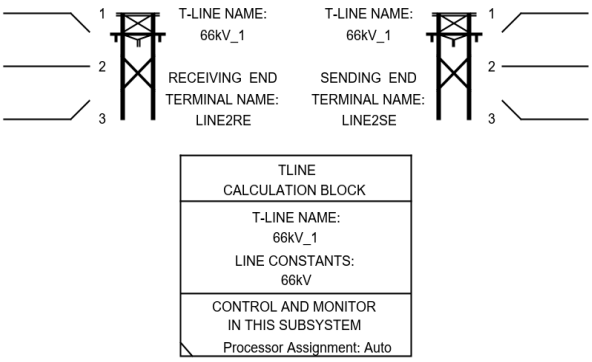

Figure 4.8: Tline configuration in Draft module in RSCAD

As the significant goal is to estimate the dynamic performance of the network under severe disturbances, a three-phase short circuit event in the middle of HVAC cable-1 is chosen. To perform a short circuit event in the middle of a 30 km long HVAC cable in RSCAD, two cable models of 15 km length are modelled and connected in series, and the three-phase fault logic available in RSCAD library is modelled in the middle of the two cables as shown in Figure 4.9. It must be noted that each cable model contains one set of sending and receiving end terminals. In order to connect two subsystems, sending end terminal from OWF is placed in subsystem-2, and its receiving end is placed in subsystem-1.

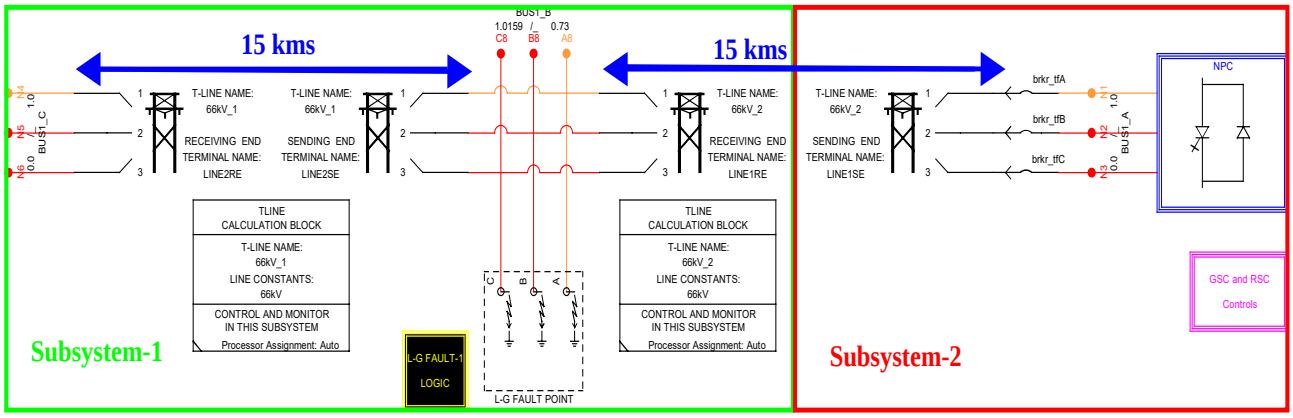

Figure 4.9: Representation of three-phase line to ground fault in the middle of HVAC cable-1 in RSCAD

4.3.3. Offshore Converter Stations

The offshore converter stations convert the HVAC offshore wind power to HVDC to transfer the power to the onshore system through HVDC links. The existing available HVDC links in the industry have a rated capacity of 1.4 GW. Examples for such projects are the NordLink cable connecting Norway and Denmark, NSN Link connecting Norway and the United Kingdom [51]. Moreover, the standard EMT models for MMCs available in CIGRE B4 DC Grid Test System [48] have a rated capacity of 1.2 GW. Therefore, with the currently available technology, two offshore converter stations are required for the transfer of 2 GW offshore wind power. From the description of MMC explained in Section 2.4, it can be understood that MMCs also involve PE components. Hence, similar to the OWF model, the average EMT model of MMC is also represented in a small time step block in RSCAD to represent fast switching events accurately. The average EMT model available in RSCAD consists of the MMC and interface transformer modelled in the small time step environment representing the offshore converter station. For this work, two small time step blocks are required for the representation of two offshore converter stations. Both the blocks are placed in subsystem-1. These two blocks must also be initialized with different time step to avoid conflict during initialization and thereby avoiding the time step overflow error during the start of simulation in the Runtime module. To evenly distribute the load on four cores, considering the core allocation for OWFs in Table 4.1, the cores for MMCs are allocated as shown in Table 4.2. The offshore converter station-1 consists of the interface transformer (IT-1) and MMC-1 whereas offshore converter station-2 consists of the interface transformers (IT-2a, IT-2b) and MMC-2.

Small time step block	Core assignment
MMC-1	3
MMC-2	2

Table 4.2: Core assignment of MMC models in subsystem-1

Interface Transformers

Interface transformers (also termed as converter transformers) are connected to the AC side of MMCs and depicted as IT-1 for offshore converter station-1 and IT-2a and IT-2b for offshore converter station-2 as shown in Figure 4.6. As explained in [36], these transformers entail the following main implications:

- Providing a reactance between the offshore network and the MMC.
- Preventing the flow of zero sequence currents between the offshore network and the MMC.

As mentioned in Section 4.3.3, in the available average EMT models in RSCAD library, the interface transformer is modelled with the MMC in a small time step environment in RSCAD. Considering a delta-wye type interface transformer and connecting MMC to the delta side of the transformer, allows for isolation of the zero sequence currents during faults. The available EMT models for offshore MMC stations from [48] are utilized for this work. These models are designed for 145 kV HVAC offshore network. Hence, to utilize the model for this work, the secondary side voltage of the transformer is changed from 145 kV to 66 kV. Additionally, there were modifications required to be made in the control structures of the MMC models to utilize it for the 66 kV HVAC network. These are explained in further sections of this chapter. There are mainly three interface transformers used in this work. The transformer (IT-1) is rated 66/380 kV, 1000 MVA in the offshore converter station-1. Two interface transformers in the offshore converter station-2 are rated 66/145 kV, 1000 MVA (IT-2a) and 145/380 kV, 1000 MVA (IT-2b) respectively. The need for two interface transformers in offshore converter station-2 is explained in the last section of this chapter.

Modular Multilevel Converters (MMCs)
As mentioned in Chapter 1, it is seen that Modular Multilevel Converters (MMCs) are the present converter topology preferred for VSC-HVDC transmission schemes due to their high efficiency and other advantages. They prove to be the state-of-the-art technology for HVDC transmission until today. The average EMT model of MMC in RSCAD has the option of modelling the MMC using half-bridge submodules or full-bridge submodules [52]. The voltage levels for HVDC offshore wind farm projects in Europe range from 300 kV to 640 kV DC voltage [51]. Hence, to continue with the latest trend, a voltage level of 640 kV DC is chosen for this work. Therefore, 320 submodules are required per arm to create a voltage of ± 320 kV for the positive and negative poles. Both the MMCs (MMC-1 and MMC-2) in the offshore converter stations are modelled for 640 kV DC.

4.3.4. HVDC Cables
The HVDC cables transfer the generated wind power from the offshore converter station to the onshore system. As mentioned in the above section, the voltage level chosen for HVDC transmission in this work is 640 kV DC. Therefore, each cable model must be suitable for ± 320 kV. The cable parameters available in [48] for ± 400 kV voltage are utilized in this work. The cable model is represented in frequency-dependent phase domain using the unified cable model block as explained previously in Section 3.2.2 [30]. The cables are modelled in subsystem-1 and are labelled as HVDC cable-1 and HVDC cable-2 for the connection from offshore converter station-1 and offshore converter station-2 to the onshore system respectively (Figure 4.6).

4.3.5. Onshore Equivalent Converter Stations
The connection between the offshore converter station and the onshore converter station follows a symmetrical monopole configuration, as shown in Figure 4.10(a) [13]. However, the DC part of the onshore converter stations are represented using an equivalent DC source for this work, as shown in Figure 4.10(b). This is done since the focus of the thesis is majorly on dynamic performance related to AC side of the network. Conventionally, the onshore converter stations provide DC voltage and reactive power control. Hence, the representation of a constant DC voltage source ensures the DC voltage control during the time of disturbances in the AC offshore network. The voltage of the DC sources are rated at 640 kV representing the HVDC transmission voltage. The equivalent representation of the symmetrical monopole configuration in RSCAD is shown in Appendix D.7.

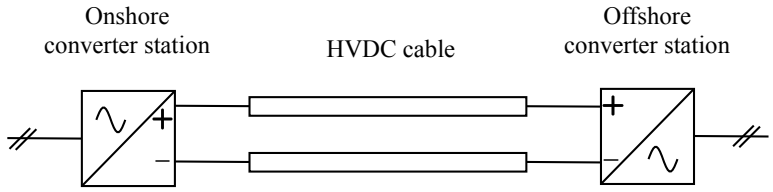

(a) Symmetrical monopole configuration [13]

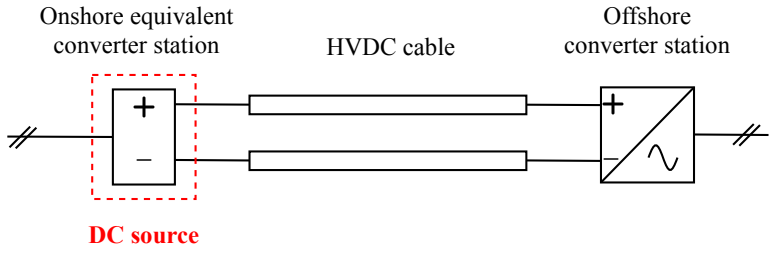

(b) Symmetrical monopole configuration by equivalent representation of DC side of onshore MMC station using a constant DC source

Figure 4.10: Symmetrical monopole configuration in HVDC network

4.4. Control Structures
This section explains the different control structures implemented and modifications required in the control scheme of converters for operation in the 66 kV HVAC network. The DVC inspired from [22] and implemented in Section 3.3.1 for Type-4 WG is extended for the 2 GW offshore network. There are mainly three control strategies used:

- DVC in the GSCs of the WGs used to represent aggregated OWFs
- Island mode control in MMC-1
- Non- island mode control in MMC-2

4.4.1. DVC

The control structure explained in Section 3.3.1 is implemented for all the four WGs. Since the same type of model is used for GSCs in all four WGs, the control loop parameters remain the same. The reactive and active control loop parameters are provided in Appendix D.1 and D.2 respectively.

4.4.2. Island Mode Control

It is highly necessary to use a control strategy in any of the MMCs which could provide the voltage and frequency reference for the MMC bus since it is connected to a weak network (OWF network). The reference voltage is created by the V/F control mode, which comes under the classification of the islanded mode of control for VSC [48]. For this study, MMC-1 is operated in the V/F control. A basic control strategy was developed according to the illustration provided in [43] and is shown in Figure 4.11. Since the voltage angle reference (θ), is generated by an independent Voltage Controlled Oscillator (VCO), this control is termed under island mode operation. Such an approach provides the grid forming behaviour for MMC-1 and is responsible for providing and absorbing power from the OWF network as and when required. The power flow is kept in balance during the steady state and transient condition with the help of this control [7].

The V/F control consists of a PI controller which has an input that takes in the difference between the measured voltage (V_{PCC}) and the reference PCC voltage (V_{PCC_ref}) in p.u. and provides the reference d-axis converter voltage (V_{PCC_d}) that is translated to abc frame (V_{abc_ref}) as shown in Figure 4.11. This makes V_{PCC_d} to be aligned with the grid voltage and the q-axis voltage (V_{PCC_q}) is set to zero. The parameters for the PI gains used for this control are referred from [48] and is specified in Appendix D.3.

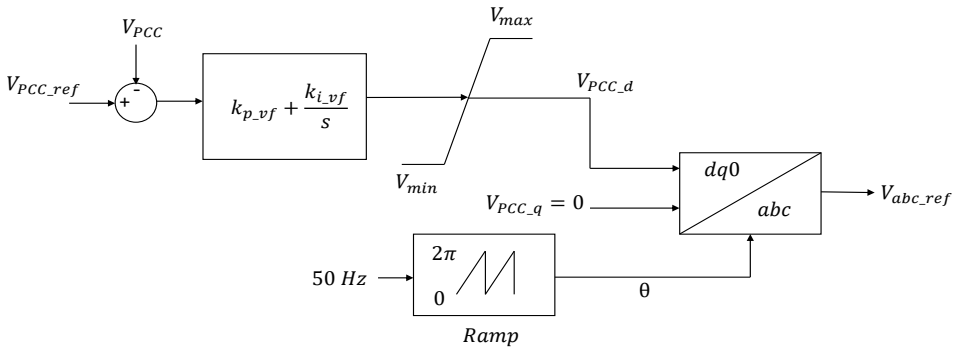

Figure 4.11: V/F control in MMC-1 [48]

4.4.3. Non- island Mode Control

This mode of operation is based on the conventional current control (grid following) approach, which consists of the outer control loop and the inner control loop. The outer loop consists of the d and q axes loops. The d-axis loop can provide control of DC voltage or active power and the q-axis loop can provide control of AC voltage or reactive power as depicted in Figure 4.12(a) and Figure 4.12(b) respectively. The outer control loop provides the respective current reference values as inputs for the inner current loops. MMC-2 is configured with this control for this work.

The parameters defined in this section are mathematically derived as given in [53]. The rotating dq frame provides a simplified control of the three-phase systems. As described in Section 2.3.2.4 and mentioned in Figure 2.9, the currents and voltages in the abc frame are transformed into dq frame using Clarke-Park transformation. As conventionally followed, the d-axis voltage is aligned with the grid voltage ($V_{PCC\_d\_2}$) at the HV bus of IT-2a interface transformer, and the q-axis is set to zero. This provides constant values for d and q components during steady state.

If active power is the priority in d-axis, active power control of MMC-2 is given by Equations 4.1 and 4.2.

$$P_{AC\_2} = V_{PCC\_d\_2} \times i_{d\_2} \tag{4.1}$$

$$i_{d\_ref\_2} = \frac{1}{V_{PCC\_d\_2}} \left(\frac{k_{i_P}}{s} \right) \left(P_{AC\_ref\_2} - P_{AC\_2} \right) \tag{4.2}$$

If DC voltage is the priority in d-axis, DC voltage control is provided by the following equation:

$$i_{d\_ref\_2} = C_{V_{DC\_2}}(s) \times \left(V_{DC\_ref\_2} - V_{DC\_2} \right) \tag{4.3}$$

where $C_{V_{DC\_2}}$ is the transfer function of the DC voltage control.

If reactive power is the priority in q-axis, reactive power control of MMC-2 is given by the following equations:

$$Q_{AC\_2} = -V_{PCC\_d\_2} \times i_{q\_2} \tag{4.4}$$

$$i_{q\_ref\_2} = -\frac{1}{V_{PCC\_d\_2}}\left(\frac{k_{i_Q}}{s}\right)\left(Q_{AC\_ref\_2} - Q_{AC\_2}\right) \tag{4.5}$$

The voltage difference at the equivalent reactance interface is calculated as following:

$$\Delta V_{PCC\_2} = V_{conv\_2} - V_{PCC\_2} \approx \frac{\omega(L_{trafo\_2} + L_{arm\_2}/2)Q_{AC\_2}}{V_{PCC\_2}} \tag{4.6}$$

where L_{trafo_2} is the interface transformer (IT-2b) leakage reactance and L_{arm_2} is the arm inductance in MMC-2.

Since the d-axis voltage is aligned with the grid voltage, inserting Equation 4.4 in Equation 4.6, the following equation is obtained:

$$\Delta V_{PCC\_2} \approx \omega(L_{trafo\_2} + L_{arm\_2}/2) \times i_{q\_2} \tag{4.7}$$

The control of AC voltage is obtained with the following equation:

$$i_{q\_ref\_2} = \left(\frac{k_{i_V}}{s}\right)\left(V_{PCC\_ref\_2} - V_{PCC\_2}\right) \tag{4.8}$$

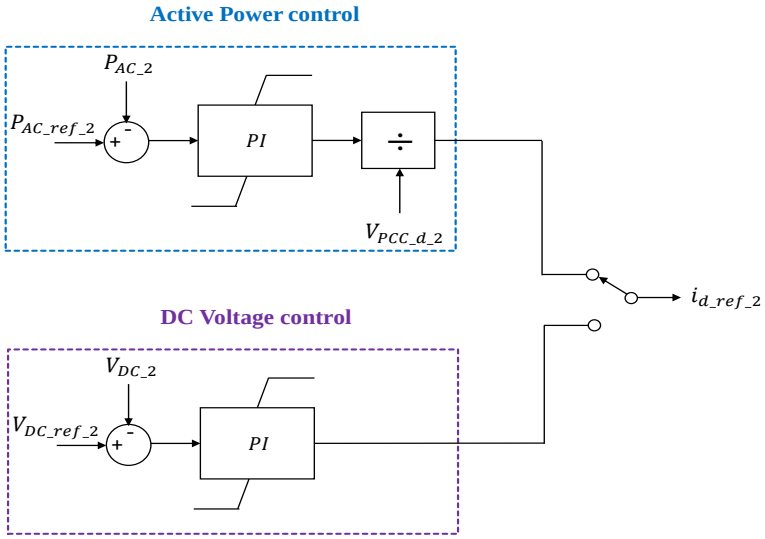

(a) Outer control loop representation for d-axis ($i_{d\_ref\_2}$)

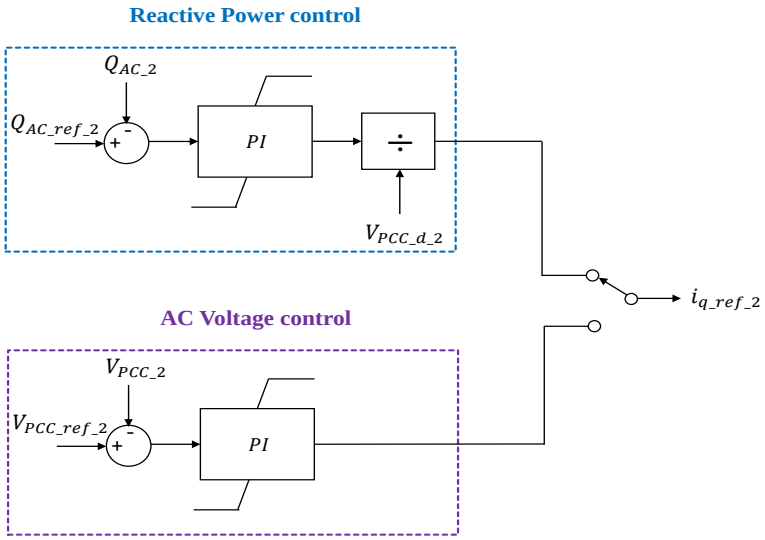

(b) Outer control loop representation for q-axis ($i_{q\_ref\_2}$)

Figure 4.12: Simplified structure of the outer loop control for MMC-2 [53]

The inner loop consists of PI controllers for d and q axis separately and provides a decoupled control action. The output from the inner loop control is then translated back to the abc frame using dq to abc frame transformation.

As the DC voltage in the HVDC link is maintained and controlled by the onshore equivalent MMC station represented by a constant DC source, the active power control is chosen as priority for d-axis for MMC-2 control. Similarly, as the AC voltage is controlled by the V/F control in MMC-1, reactive power control is chosen as priority chosen for q-axis for MMC-2. When active power is the chosen priority, $P_{AC\_ref\_2}$ represents the required amount of active power that must flow through offshore converter station-2 and must be defined externally by the user. However, the outer loop control available for the non-islanded mode in [48] is not suitable for parallel operation with V/F control. Hence, the outer loop is simplified, and the reference points ($i_{d\_ref\_2}$ and $i_{q\_ref\_2}$) for the inner loop are controlled directly by the user. This modification in outer loop and the power flow control in MMC-2 in RSCAD is detailed in Appendix C.2.1.

The inner control loop consists of PI controllers that play the major role in ensuring minimum steady state error. The inner control also contain the feed-forward term to compensate the cross coupling terms. The mathematical equations for the parameters of inner control loop are derived as provided in [53]. Applying Kirchoff's Voltage Law in Figure 4.13 and with the MMC representation in Figure 4.14, the equations are derived for offshore converter station-2 connected to the AC network. The assumptions involve, the direction of current is from the AC network to the MMC (the condition when offshore wind power is transferred from the offshore network to onshore system) and avoiding the star-point reactor:

$$\frac{V_{DC\_2}}{2} = v_{uj} + L_{arm\_2}\frac{di_{uj}}{dt} + R_{arm\_2}i_{uj} - L_{trafo\_2}\frac{di_j}{dt} - R_{trafo\_2}i_j + v_{PCC_j} \tag{4.9}$$

$$\frac{V_{DC\_2}}{2} = v_{lj} + L_{arm\_2}\frac{di_{lj}}{dt} + R_{arm\_2}i_{lj} + L_{trafo\_2}\frac{di_j}{dt} + R_{trafo\_2}i_j - v_{PCC_j} \tag{4.10}$$

where R_{trafo_2} is the interface transformer (IT-2b) resistance, R_{arm_2} is the arm resistance in MMC-2, v_{PCC_j} is the voltage at HV bus of IT-2a, j represents phases a, b and c. Upper arm and lower arm of MMC-2 are denoted by u and l respectively.

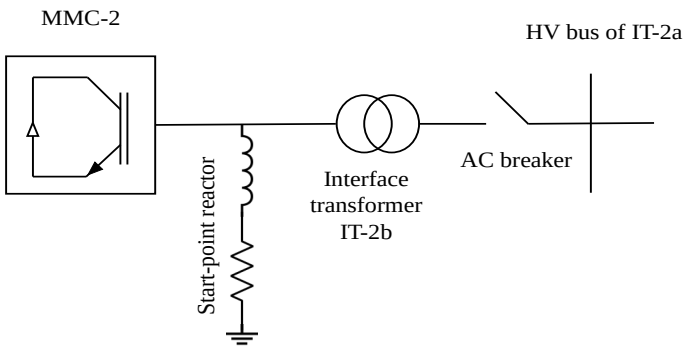

Figure 4.13: Representation of offshore converter station-2 connection to the AC offshore network [53]

The equations in dq frame can be represented as following:

$$V_{PCC\_d\_2} - V_{conv\_d\_2} = \left(\frac{L_{arm\_2}}{2} + L_{trafo\_2}\right)\frac{di_d}{dt} + \left(\frac{R_{arm\_2}}{2} + R_{trafo\_2}\right)i_d - \omega\left(\frac{L_{arm\_2}}{2} + L_{trafo\_2}\right)i_q \tag{4.11}$$

$$V_{PCC\_q\_2} - V_{conv\_q\_2} = \left(\frac{L_{arm\_2}}{2} + L_{trafo\_2}\right)\frac{di_q}{dt} + \left(\frac{R_{arm\_2}}{2} + R_{trafo\_2}\right)i_q + \omega\left(\frac{L_{arm\_2}}{2} + L_{trafo\_2}\right)i_d \tag{4.12}$$

The control loop is defined as follows:

$$V_{conv\_ref\_d\_2} = -\left(i_{d\_ref\_2} - i_d\right)C_{i_{ac}}(s) + V_{PCC\_d\_2} + \omega\left(\frac{L_{arm\_2}}{2} + L_{trafo\_2}\right)i_q \tag{4.13}$$

$$V_{conv\_ref\_q\_2} = -\left(i_{q\_ref\_2} - i_q\right)C_{i_{ac}}(s) + V_{PCC\_q\_2} + \omega\left(\frac{L_{arm\_2}}{2} - L_{trafo\_2}\right)i_d \tag{4.14}$$

where $C_{i_{ac}}(s)$ is the transfer function of the PI controller.

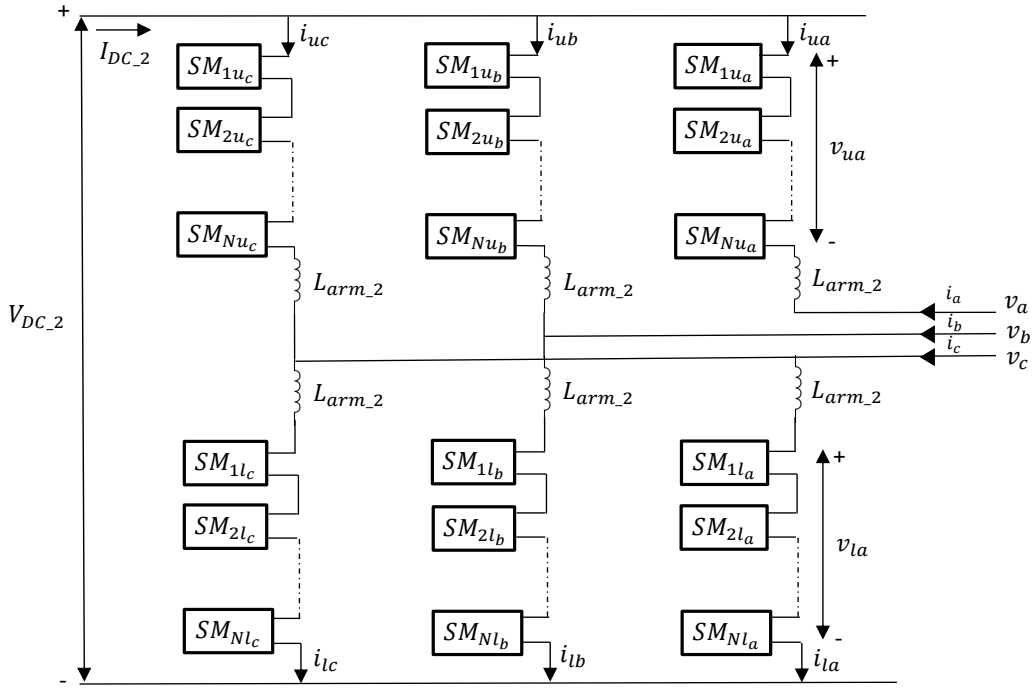

Figure 4.14: MMC-2 representation [53]

The inner control loop provides the control of reference voltages, as depicted in Figure 4.15, which are then used as inputs for the lower level control.

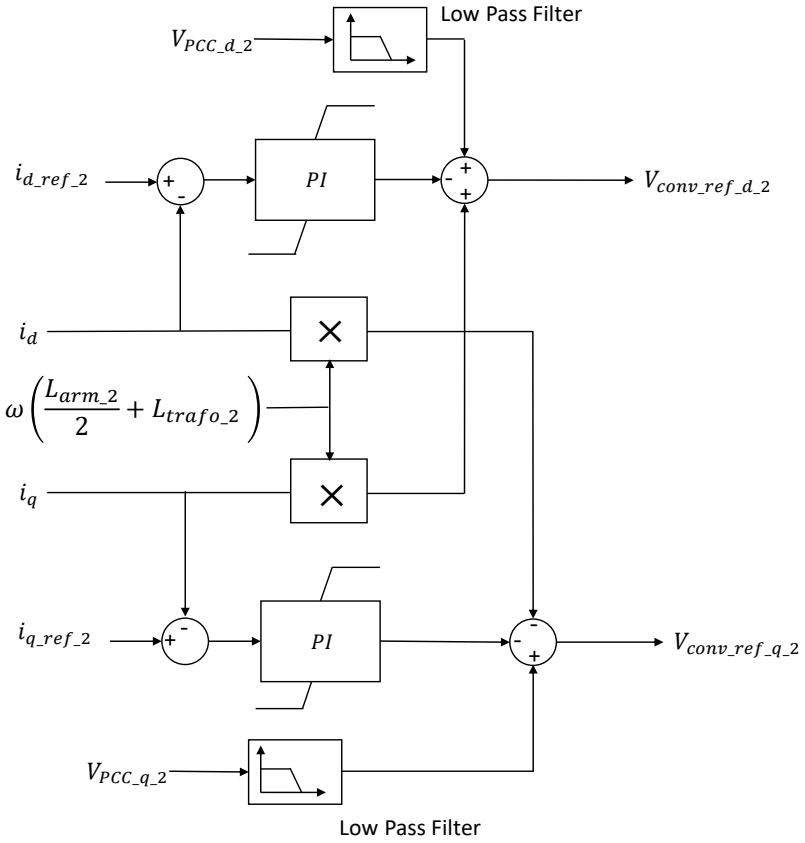

Figure 4.15: Inner loop control for MMC-2 [53]

The inner control loop model available in [48] is only suitable for a 145 kV HVAC network. This is why a second interface transformer (IT-2a) is used to convert the 66 kV HVAC voltage to 145 kV, as shown in Figure 4.6. To mitigate the effect of this transformer in terms of impedance, the leakage reactance and resistance of the transformer are kept

minimum (0.001 p.u.). However, it should be noted that this is a work around approach used in this work, and such a transformer with very low reactance is not practically used in a power system network. The non-island mode control in MMC-2 identifies the frequency and phase angle at the HV bus of the interface transformer (IT-2a) in Figure 4.6. The PLL in MMC-2 control performs this task and synchronizes with the measured grid voltage at the HV bus of IT-2a. The PI gains for the PLL were set based on parameter sensitivity analysis. The phase angle is generated by the PLL, which is used to transform it from abc to dq frame.

The lower level controls such as circulating current suppression control, modulation and third harmonic injection are available in the average EMT model of MMC controls in [48] and are used as such for this work in both MMC-1 and MMC-2. Further, the performance of the 2 GW offshore network is to be analyzed during steady state and dynamic conditions after incorporating the aforementioned control strategies.

5

Analysis of the Dynamic Performance of 2 GW, 66 kV HVAC Offshore Network

Connecting a large scale OWF network to an offshore-onshore HVDC link has always been a challenge. In this chapter, the operation scheme of the 2 GW offshore network presented in Chapter 4 is simulated and analyzed. Firstly, the initial conditions of the converters are defined, and then the stage-wise synchronization and operation of the network is explained. Later, the network is tested for short-term voltage stability and the power flow analysis for severe disturbances such as sudden disconnection of one OWF and a three-phase line to ground fault in the middle of a HVAC cable.

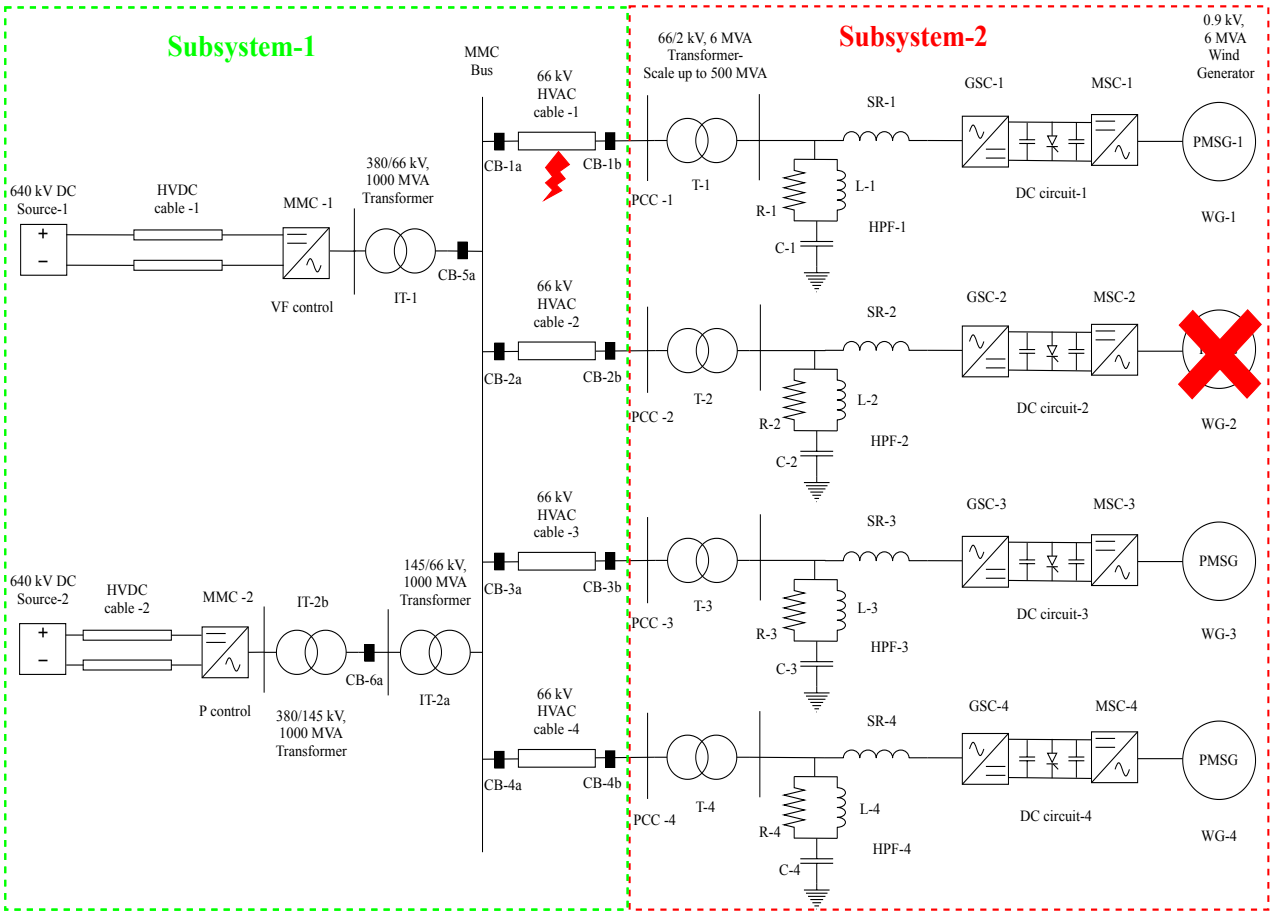

Figure 5.1: 66 kV HVAC offshore network connected to 2 x 1 GW HVDC links with offshore converter stations in RSCAD for two dynamic scenarios-
a) Disconnection of OWF-2 (represented by the cross symbol)
b) Three-phase line to ground fault in the middle of cable-1 (represented by the fault symbol)

5.1. General settings, Control modes and Pre-set conditions

The simulation time step for all the simulations is set to 50 μs. All plots are simulated for a span of 5 s. All the fault or switching events are timed to occur at 0.5 s of the simulation. The three-phase voltage and current graphs for all simulations are plotted for a shorter period (0.4 s to 1.3 s) to have a clearer view of the signals during the occurrence of an event. However, the voltage in p.u., active and reactive power graphs are plotted for the whole time (5 s) to analyze the voltage stability and power flow in the network during the simulation. In order to analyze the dynamic and steady state operation of the network, the controllers and set points need to be initialized before charging. They are set as follows:

- MMC-1:
  - Islanded mode operation (V/F control)
  - AC voltage control, V_{PCC_ref} = 1 p.u. (Reference AC voltage)
- MMC-2:
  - Non-islanded mode operation
  - Active power control, $I_{d\_ref\_2}$ = 0 (No power flow through MMC-2 in the initial conditions)
- Network:
  - Circuit breakers (CB-1a, CB-1b, CB-2a, CB-2b, CB-3a, CB-3b, CB-4a, CB-4b, CB-5a and CB-6a) in open condition

5.2. Synchronization of the Offshore Converter Stations

The AC side of MMCs is to be connected to simulate the synchronization scenario. Since the DC side is connected to DC sources, the charging of HVDC cables is not considered for this study. As mentioned in Section 4.4 in Chapter 4, MMC-1 works as grid forming (V/F control) and MMC-2 works as grid following (active power control). Once the simulation is started, the network is charged until the secondary side of the interface transformer, IT-1. The point of measurement of voltages, currents and powers for the offshore converter stations are at the LV side of IT-1 for converter station-1 and LV side of IT-2a for converter station-2. At the points of measurement, the voltage is the same as they are at the same potential (connected to MMC bus). Firstly, the circuit breaker, CB-5a is closed and the MMC bus is charged. The MMC bus voltage builds up to rated 66 kV [1] voltage on the AC as shown in Figure 5.2 and in terms of per unit to nearly 0.98 p.u. as shown in Figure 5.3. The currents at the measurement points for both the MMCs also increase and settles as shown in Figure 5.4(a) and 5.4(b). The current takes nearly 0.35 seconds to settle after the closing of the breaker due to selected PI parameters of the V/F control in MMC-1. Additionally, the transformer IT-2a is also charged in this process.

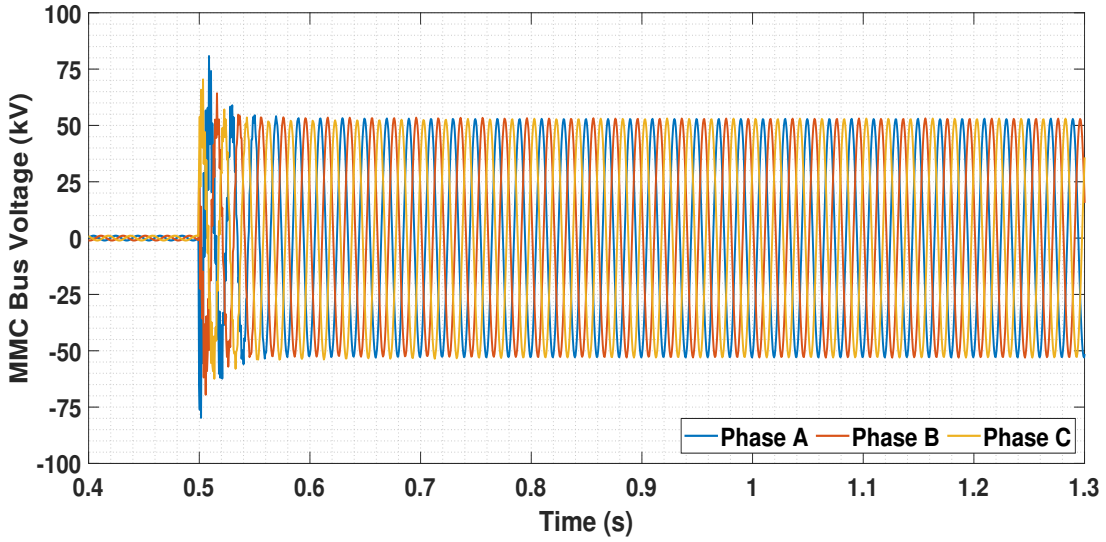

Figure 5.2: Voltages at MMC bus upon CB-5a closing operation

[1] (Phase peak voltage = $66 \times \frac{\sqrt{2}}{\sqrt{3}} = 53.88kV$)

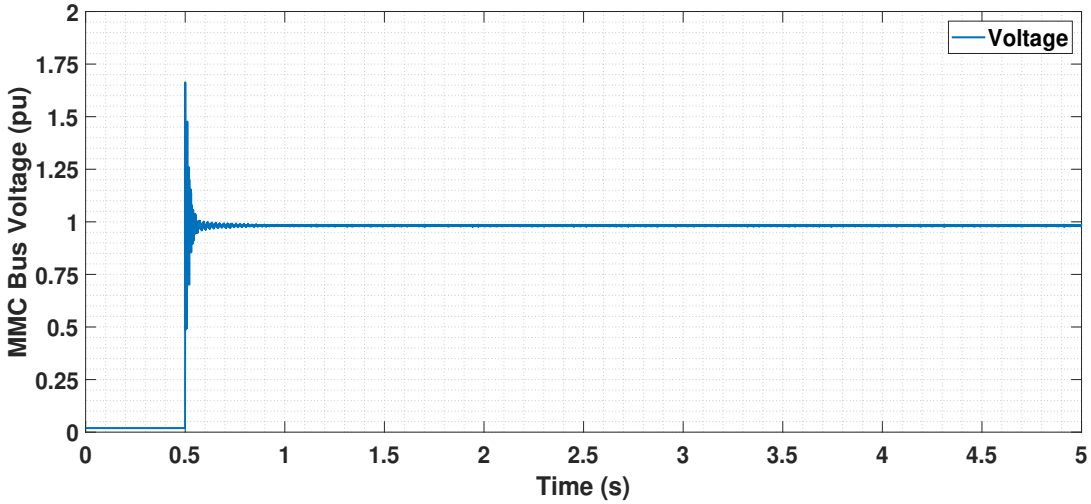

Figure 5.3: Voltage in p.u. at MMC bus upon CB-5a closing operation

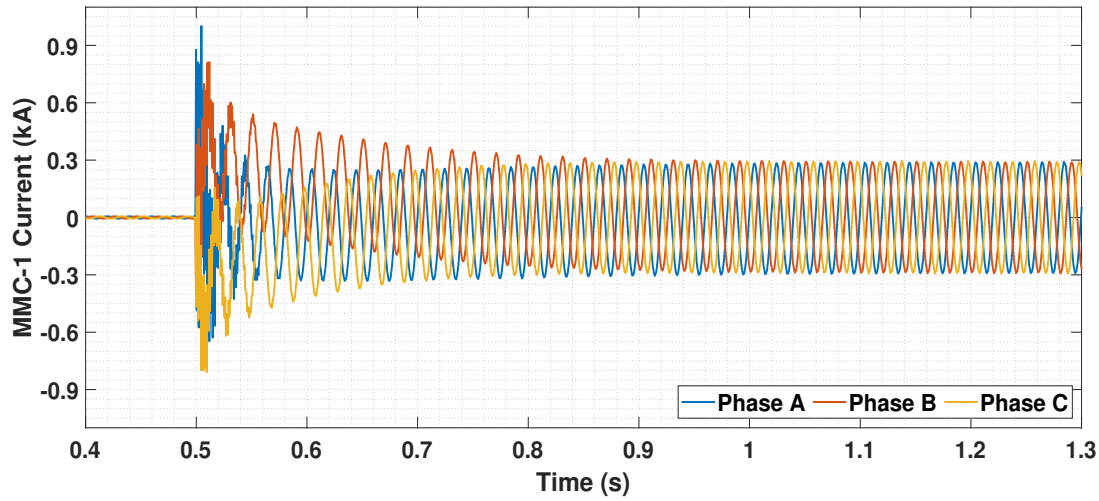

(a) Currents in MMC-1 bus

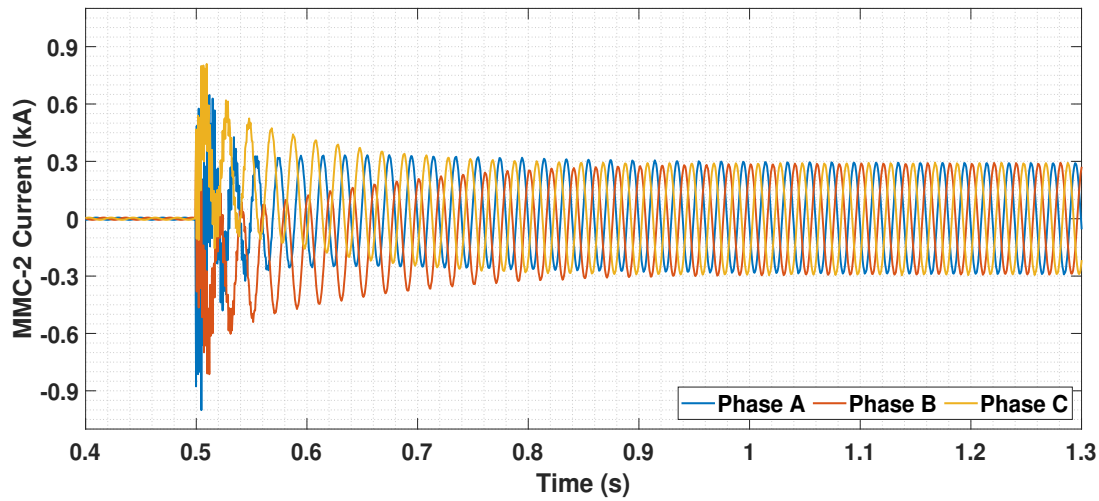

(b) Currents in MMC-2 bus

Figure 5.4: Currents in a) MMC-1 bus and b) MMC-2 bus upon CB-5a closing operation

The next step is to close the circuit breaker, CB-6a to connect MMC-2 to the network and hence synchronizing it with MMC-1. The voltage at the MMC bus remains the same after connecting MMC-2 as shown in Figure 5.5 and 5.6 since the voltage reference is provided and maintained by MMC-1. The currents also remain the same in both the MMCs after MMC-2 connection as seen in Figure 5.7(a) and 5.7(b). Now both the converter stations are synchronized and running.

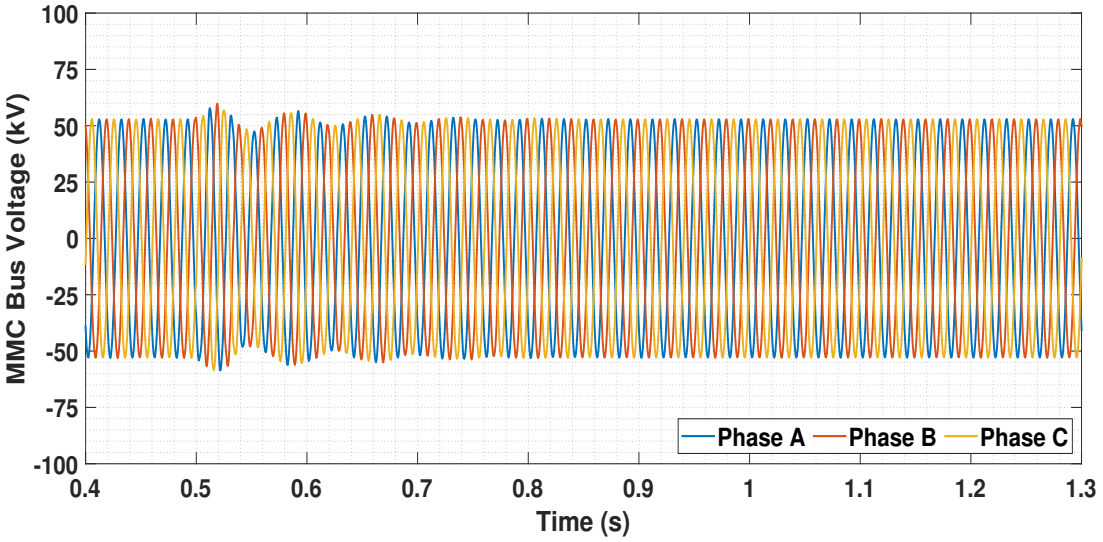

Figure 5.5: Voltages at MMC bus upon CB-6a closing operation

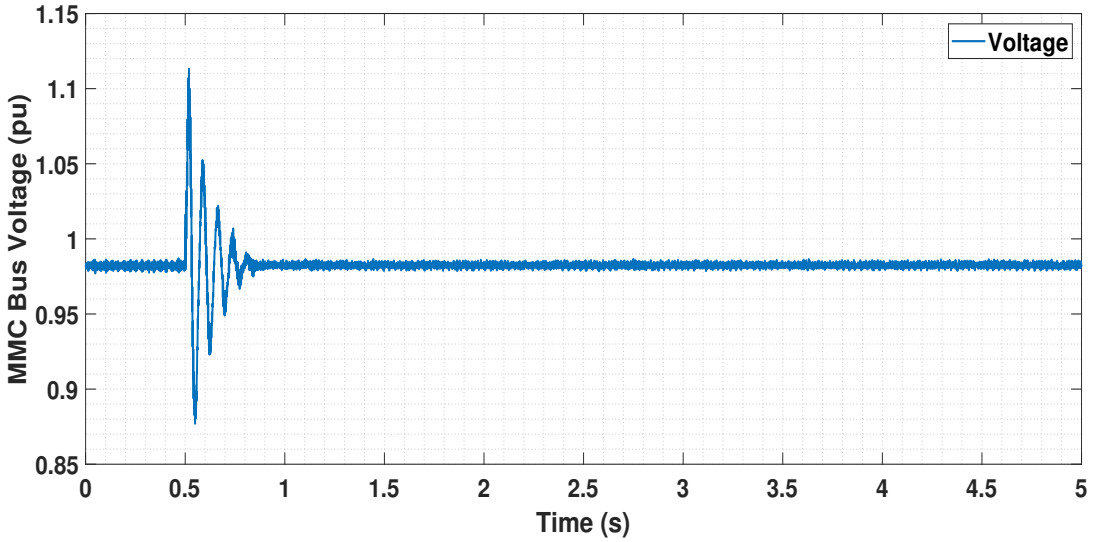

Figure 5.6: Voltage in p.u. at MMC bus upon CB-6a closing operation

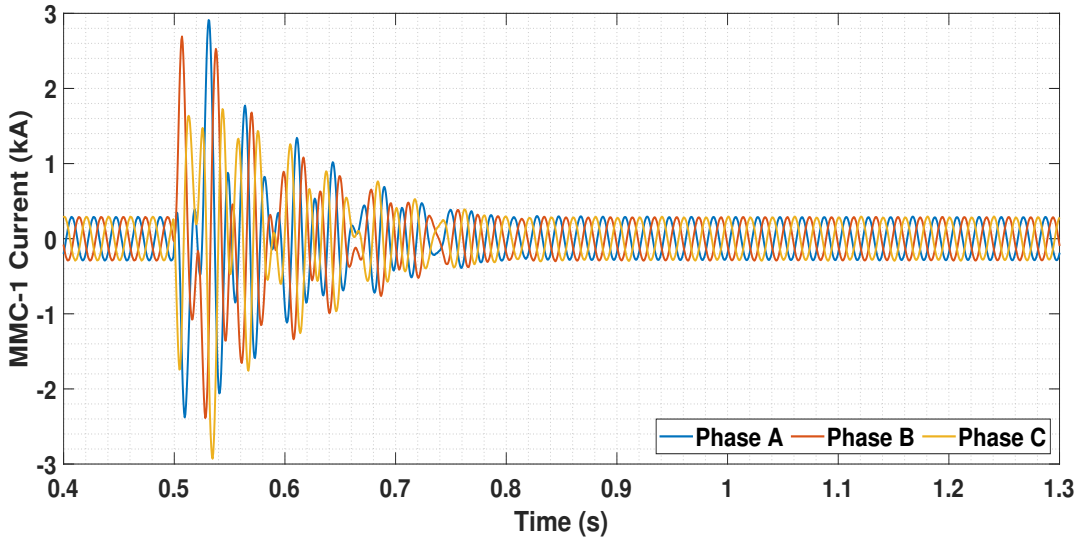

(a) Currents in MMC-1 bus

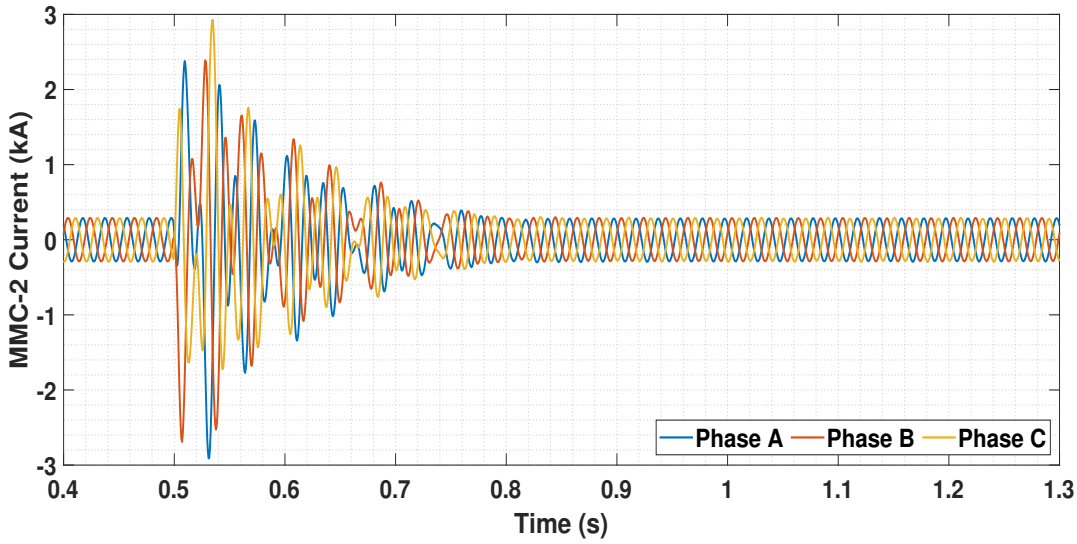

(b) Currents in MMC-2 bus

Figure 5.7: Currents in a) MMC-1 bus and b) MMC-2 bus upon CB-6a closing operation

5.3. Energization of the HVAC Cables and OWFs

The energization procedure of the AC network followed in this work involves charging of each HVAC cable and the corresponding OWF. Initially, cable-1 is charged and then OWF-1 is connected. The same is followed for the other OWFs as well. As mentioned in Section 4.3.1 in Chapter 4, each OWF has a maximum capacity of 500 MW that is represented by scaling up (by using the scaling factor function in RSCAD) of a WG model of 6 MW rated power. For the energization process, the OWFs are connected initially with lesser number of WG units of ~ 50 MW (8 × 6 MW = 48 MW) power to avoid a surge of voltage at PCC and to maintain the voltage within limits. Once stability is attained after connecting all the OWFs, the scaling in all OWFs is incremented. Since power only flows through MMC-1 until then, the increment can be until the maximum capacity of MMC-1, i.e. 1 GW.

The cable-1 gets energized when the CB-1a circuit breaker, as shown in Figure 5.1, is switched on. The voltage at MMC bus is increased and set to a value of nearly 1.05 p.u. as seen in Figure 5.8. MMC-1 provides the current for cable charging and the active power reference for the MMC-2 is not changed in this process. Hence, current flow in MMC-1 bus increases for cable-1 charging as shown in Figure 5.9(a) and the current flow in MMC-2 bus remains unchanged as shown in Figure 5.9(b). The disturbances observed during the switching operation at 0.5 seconds, before the currents stabilize to a particular value at 0.75 seconds, is due to the PI parameters chosen for the V/F control in MMC-1. Optimizing these parameters through small-signal stability analysis could achieve smoother results. The current in cable-1 upon CB-1a closing is depicted in Figure 5.10.

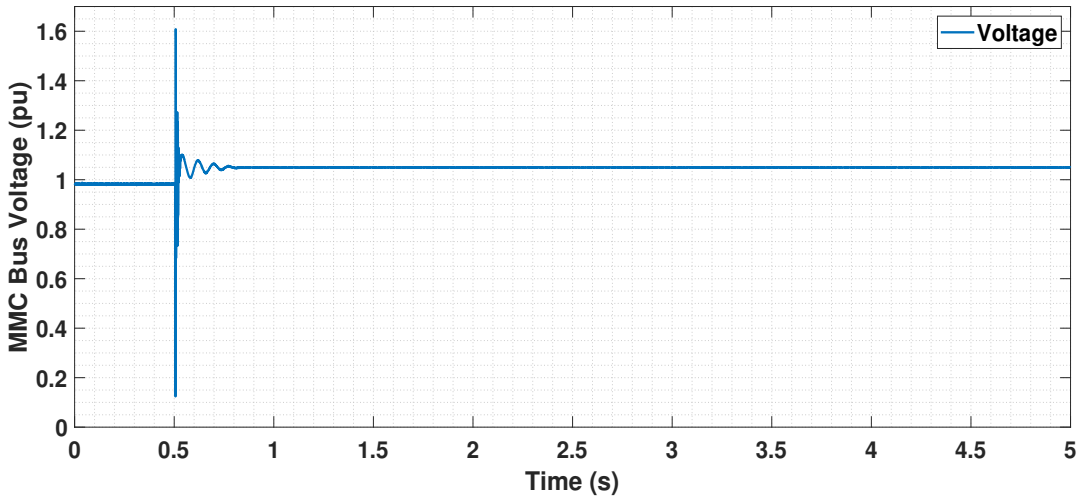

Figure 5.8: Voltage at MMC bus upon charging of cable-1

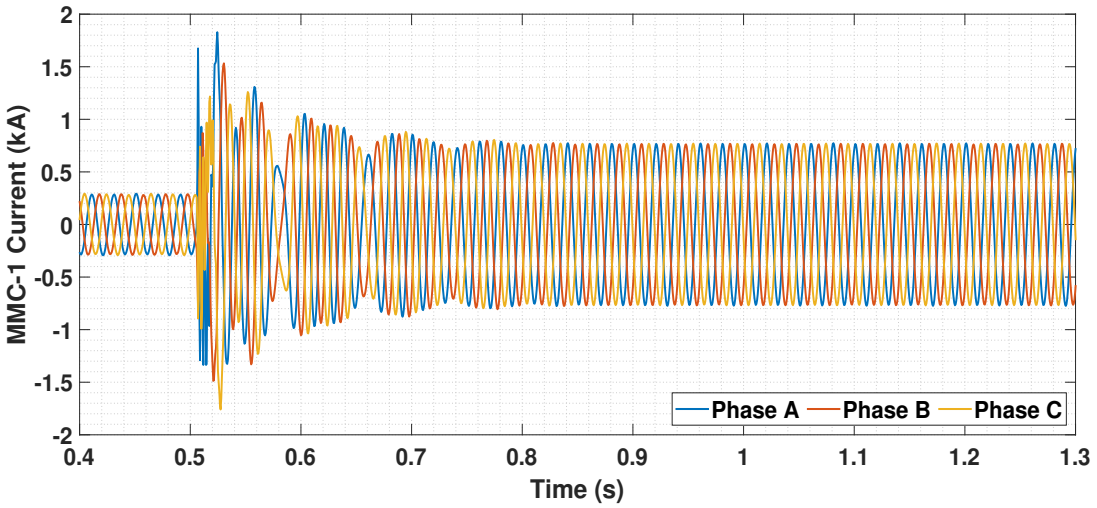

(a) Currents in MMC-1 bus

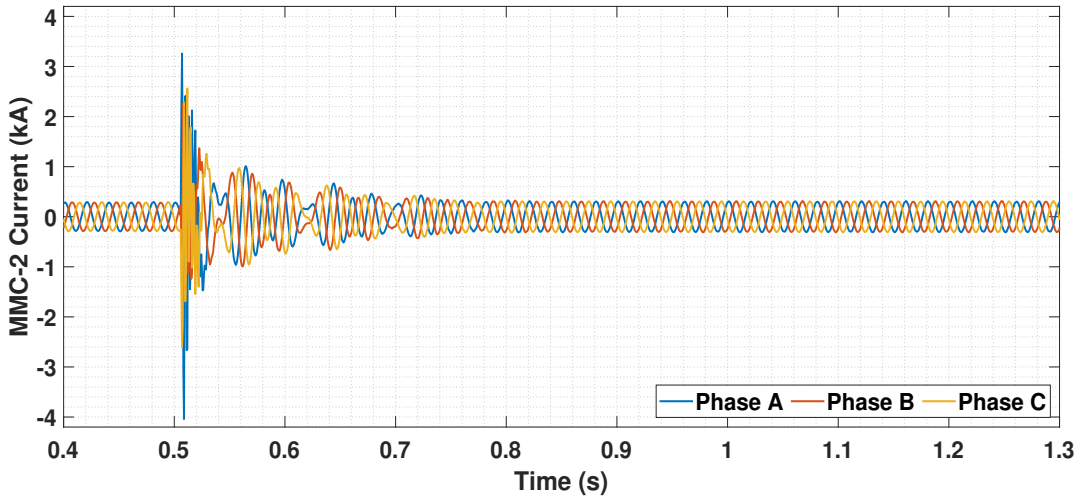

(b) Currents in MMC-2 bus

Figure 5.9: Currents in a) MMC-1 bus b) MMC-2 bus upon CB-1a closing operation for charging of cable-1

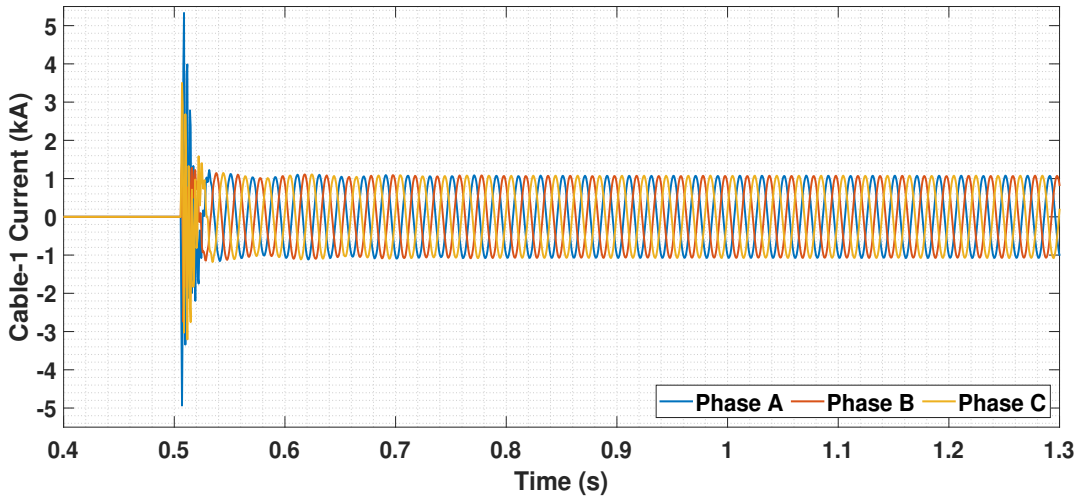

Figure 5.10: Currents in cable-1 upon CB-1a closing operation for charging of cable-1

After cable-1 has been charged, the breaker at the OWF-1 end (CB-1b) is switched on. OWF-1 gets connected to the network. As mentioned in Section 5.3, the OWF-1 is connected initially with less generation to keep the voltage at PCC-1 within limits. The initial high voltage at the PCC-1 before closing the breaker as seen in Figure 5.11 is due to the capacitance in the DC link. Once the breaker is closed, the voltage is maintained at nearly 1 p.u. as shown in Figure 5.11 and the currents in PCC-1 also increase as shown in Figure 5.12. The OWF starts generating 50 MW and this flows through MMC-1 as shown in Figure 5.13. In a similar way all the other OWFs are connected. All OWFs are connected with ~ 50 MW generation. A total power of ~ 200 MW through MMC-1 after connection of OWF-1, OWF-2, OWF-3 and OWF-4 is clearly depicted in Figure 5.13. There is no flow of active power in MMC-2 (Figure 5.14) since the rated capacity of 1 GW of MMC-1 is yet to be reached.

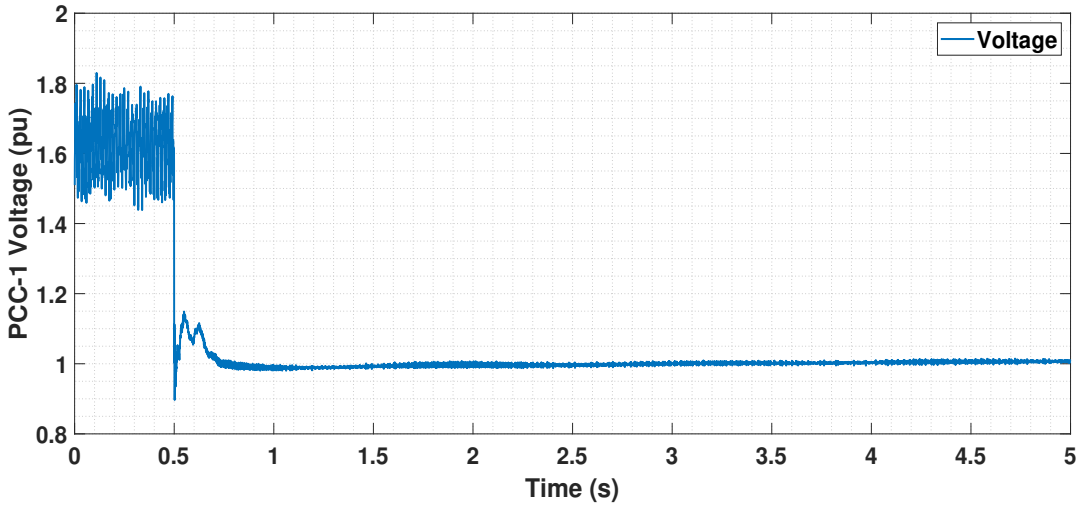

Figure 5.11: Voltage in p.u. at PCC-1 upon connecting OWF-1 with 50 MW generation to the network

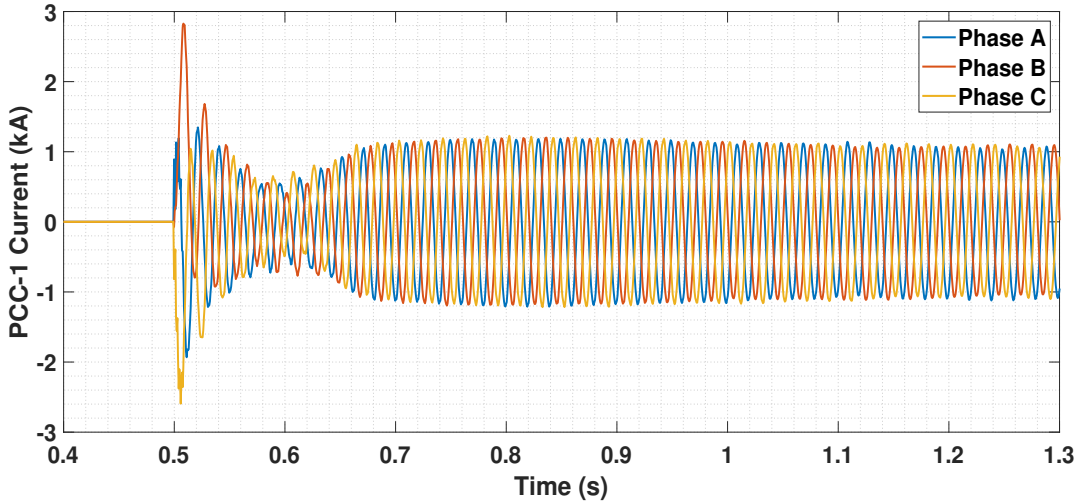

Figure 5.12: Currents in PCC-1 upon connecting OWF-1 with 50 MW generation to the network

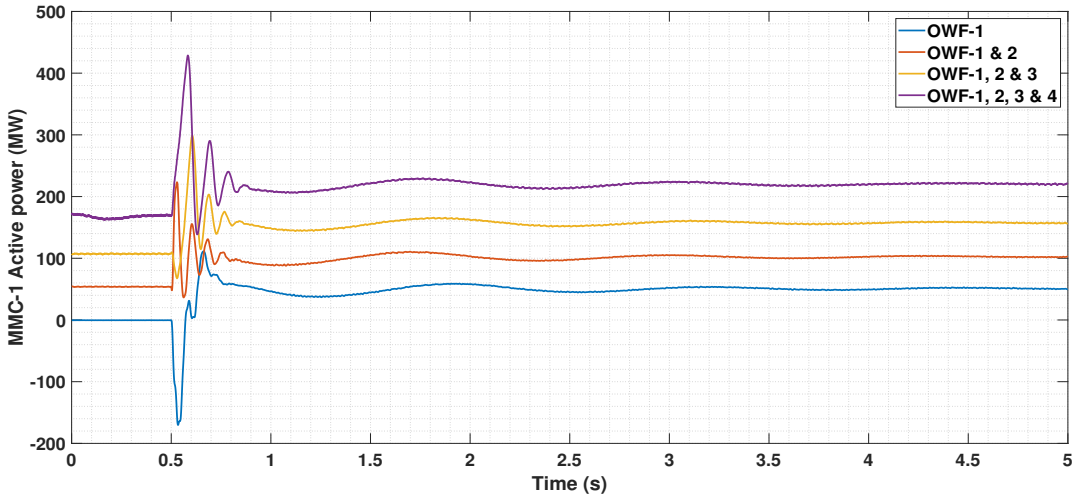

Figure 5.13: Active power in MMC-1 bus upon connecting all OWFs with 50 MW generation each

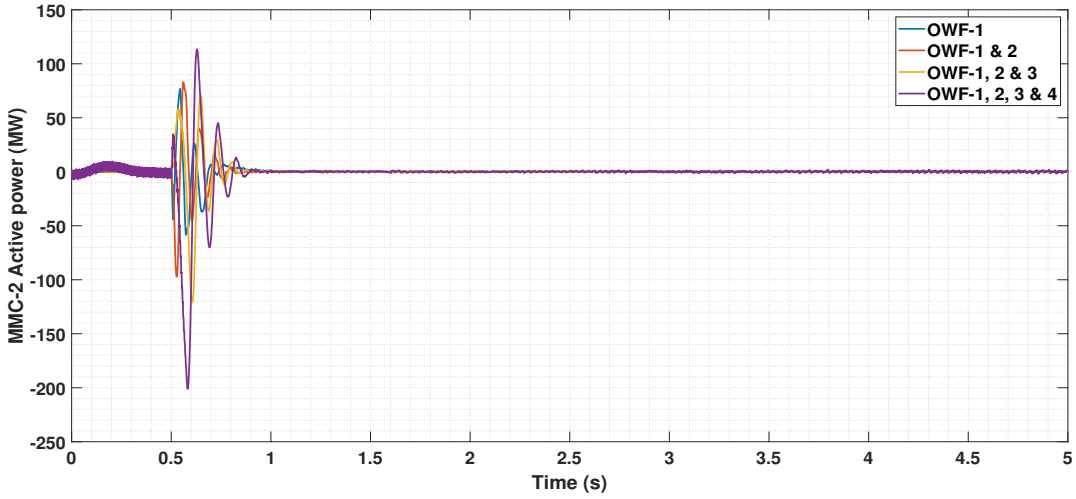

Figure 5.14: Active power in MMC-2 bus upon connecting all OWFs with 50 MW generation each

Once the system gets stabilized, the generation is increased in steps by increasing the number of parallel WG units. Such a procedure ensures the voltage to be within limits at all PCCs. The power flow to the MMC-2 is to be controlled in the next step. This is done by controlling the active power reference of MMC-2. For this study, OWFs are modelled to have the same scaling of power and hence generate the same amount of power. A step-by-step increment of ~ 50 MW in all OWF is done, and correspondingly the active power reference for MMC-2 is also increased. The procedure is detailed in Appendix C.3. Finally, the OWFs are made to generate ~ 500 MW each and the total of nearly 2 GW power is equally split between MMC-1 and MMC-2. Power losses are expected to occur during the transmission and, hence the active power flowing is nearly 960 MW in both MMCs as seen from the final steady state plots in Figure 5.15.

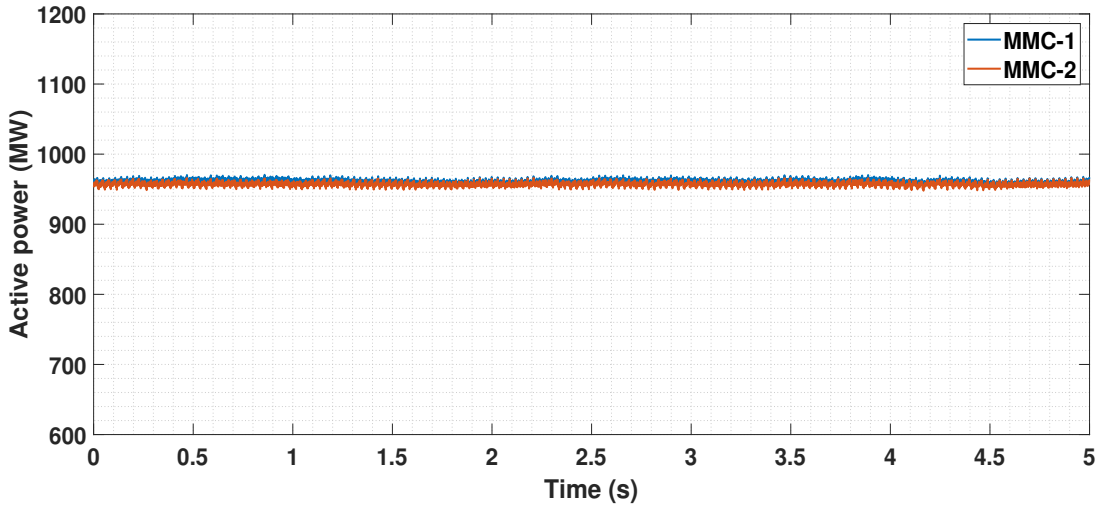

Figure 5.15: Active power in MMC-1 and MMC-2 buses upon connecting all OWFs with 500 MW generation each

From Figure 5.2 to 5.15, it can be said that, by viewing the respective voltages, currents and powers, the synchronization of both MMCs and the energization of the offshore AC grid is done successfully. The offshore AC grid converters and cables now operate at a voltage of 66 kV, the HVDC voltage is set to 640 kV and the total active power transmitted is nearly 2 GW in the network. Frequency of the system is stabilized at 50 Hz, and the power system is said to be operating in the steady state condition.

5.4. Dynamic Performance Analysis

Fault events and perturbations can occur in the grid, and the components in the system must be able to withstand these voltage surges and fault currents for a short duration of time. The performance of the network in terms of short-term voltage stability (fault occurring for a span of 6-10 cycles accounting for 120-200 ms) and power flow is analyzed. The coordination among different controllers available in the network is studied during severe perturbations in the network as described below.

5.4.1. Disconnection of One OWF

The first event is a sudden disconnection of one OWF. OWF-2 is permanently disconnected from the circuit by opening the breaker, CB-2a connected towards the OWF-2 cable end at 0.5 s. Once the breaker is open, the generation of ~ 500 MW is lost, and the power flow is reduced through MMC-1, as shown in Figure 5.16. This is because MMC-1 is the one in grid forming control (provides power balance in the network) and also the active power reference of MMC-2 is unchanged. In the post-fault period, the active power flow through MMC-2 is seen to be higher than the pre-fault period. Reason for this can be justified from the increase in voltage at the OWF side shown in the following section. MMC-2 is seen to be operating with the maximum rated capacity of 1 GW in this condition. The decrease in generation in MMC-1 can also be viewed from the currents flowing in MMC-1 as witnessed in Figure 5.17(a) whereas the currents remain the same in MMC-2 as seen from the current in Figure 5.17(b).

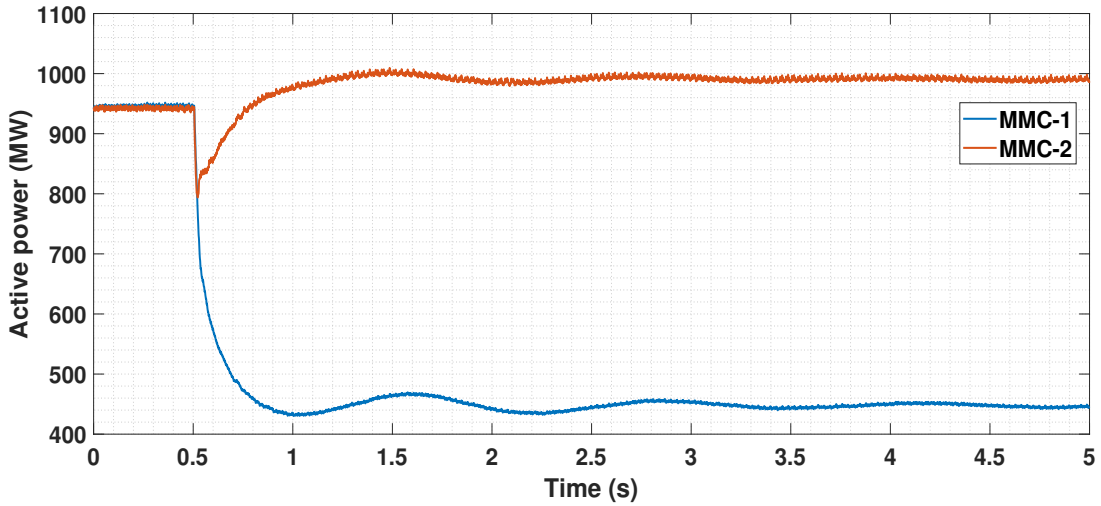

Figure 5.16: Active power in MMC-1 and MMC-2 buses upon OWF-2 disconnection event

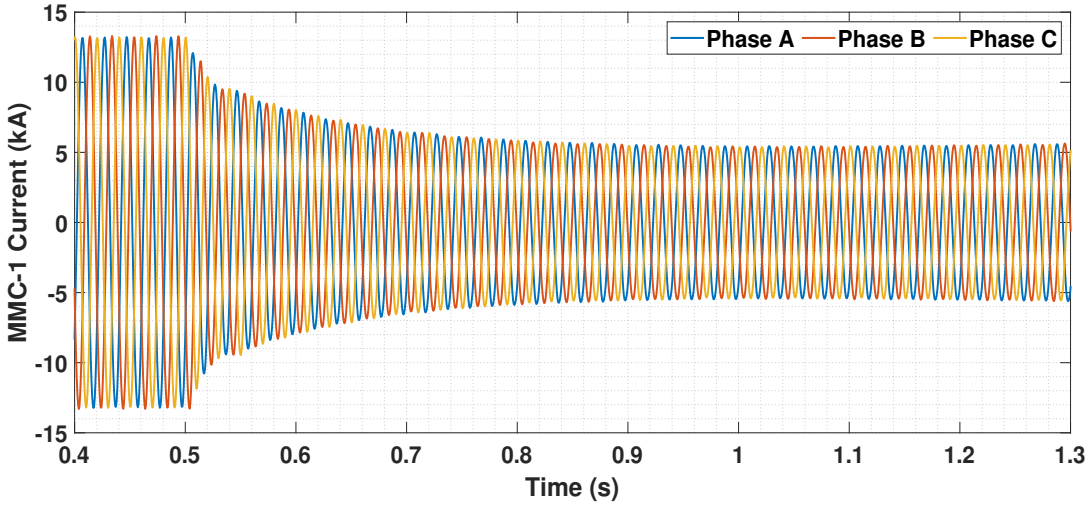

(a) Currents in MMC-1 bus

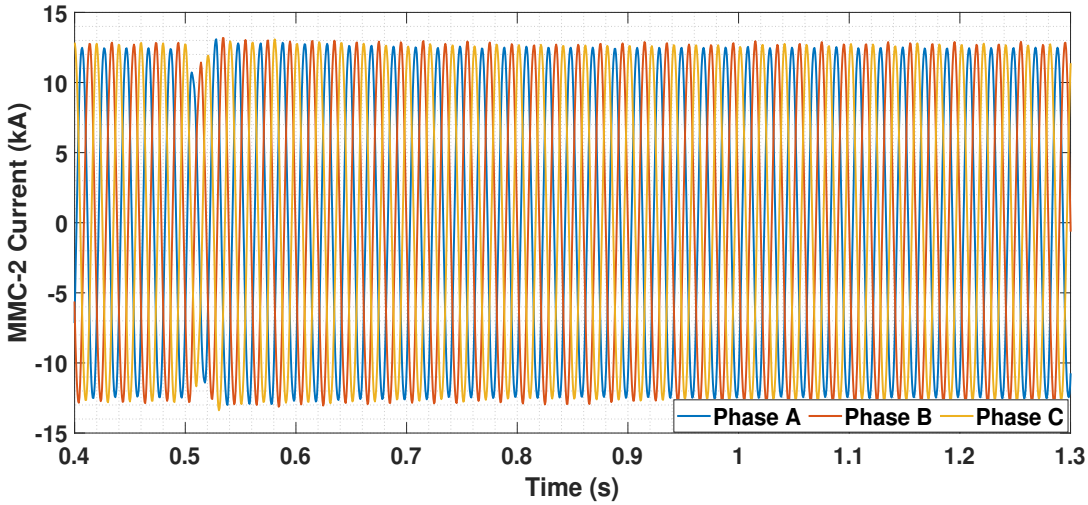

(b) Currents in MMC-2 bus

Figure 5.17: Currents in a) MMC-1 bus and b) MMC-2 bus upon OWF-2 disconnection event

In the OWFs side, the voltage at PCC-2 goes beyond bounds and is in the condition as before energizing. This can be observed from the voltage in p.u. graph in Figure 5.18b). During the disconnection of OWF-2, there occurs a drop in voltage at PCC-1, 3 and 4 as seen from the voltage graphs in Figure 5.18a), c) and d). This happens since they are all connected to a common bus (MMC bus). Moreover, in the post-fault period, voltages at PCC-1, 3 and 4 are stabilized and settle to a higher value (nearly 1.08 p.u.) than the pre-fault voltage to compensate for the loss of OWF-2. This is due to the fast local voltage control in the DVC of the WGs. But the currents at these OWFs remain the same since the scaling factor for each OWF is still 83 (83 × 6 MW = 498 MW). This can be viewed from the current measured at PCC-1 in Figure 5.19. Similar is the case for PCC-3 and PCC-4 and the graphs are shown in Appendix C.4.1. As voltage increases and current remains the same, the active power generated from the OWF- 1, 3 and 4 increases and therefore the power flowing through MMC-2 also increases.

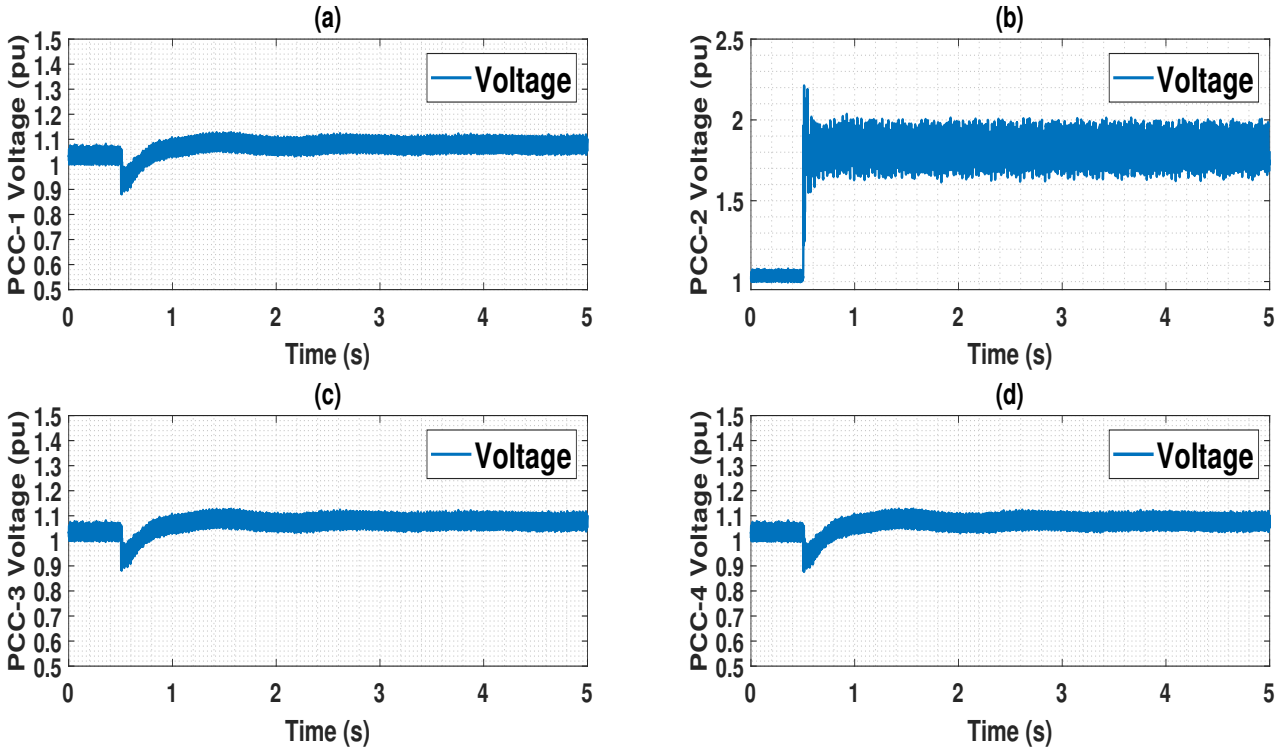

Figure 5.18: Voltage in p.u. at a) PCC-1, b) PCC-2, c) PCC-3 and d) PCC-4 upon OWF-2 disconnection event

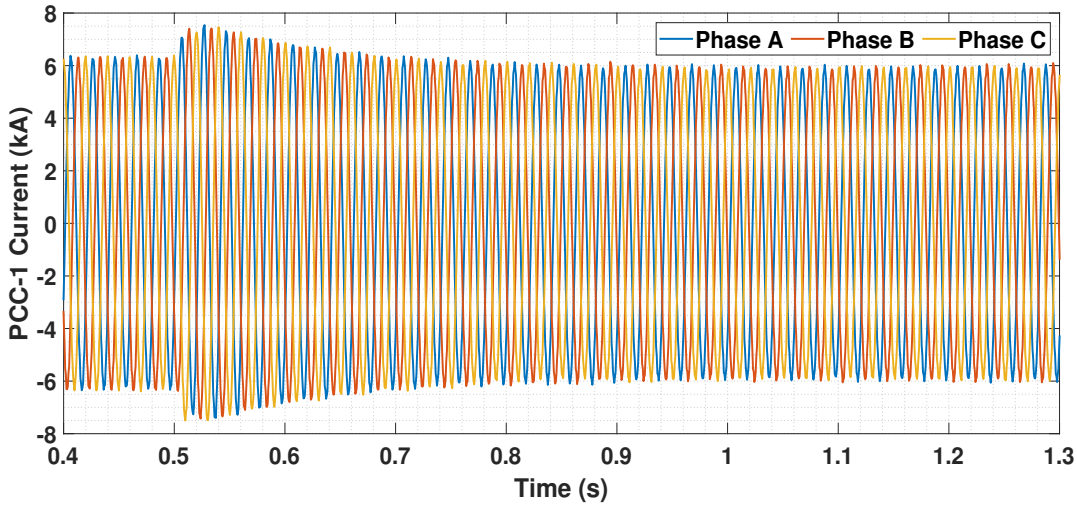

Figure 5.19: Currents at PCC-1 upon OWF-2 disconnection event

5.4.2. Three-phase Line to Ground Fault

Before the application of three-phase line to ground fault, a logic to operate the circuit breaker (CB-1a) at the cable-1 end is developed as shown in Figure 5.20. This logic is inspired from the "Fault Control" model [2] available in RSCAD. For the fault, the line to ground fault component available in RSCAD library is used [30].

Circuit Breaker Operation Logic

The logic is developed for the operation of the circuit breaker CB-1a in Figure 5.1 by detecting overcurrent. The signal 'SWD2A' is the signal for operating CB-1a. Initially, the breaker is closed during the energizing process using the switch 'CabMMC_side'. Once the system is fully operational after connecting all the four OWFs and achieving 2 GW power in the network, the 'Activ' switch in Figure 5.20 is turned on. This is done to provide the switching operation of CB-1a by comparing the RMS current (I_{rms}) and the maximum phase current (I_{phase_max})[3] at CB-1a. The system is still in steady state condition. Once the fault is applied, when I_{rms} becomes greater than I_{phase_max}, the SR flip flop detects the change and holds a value of zero for the signal 'SWD2A'. This action causes the breaker CB-1a to open. The delay block before the signal 'SWD2A' provides time delay for the operation of circuit breaker after the fault has been detected.

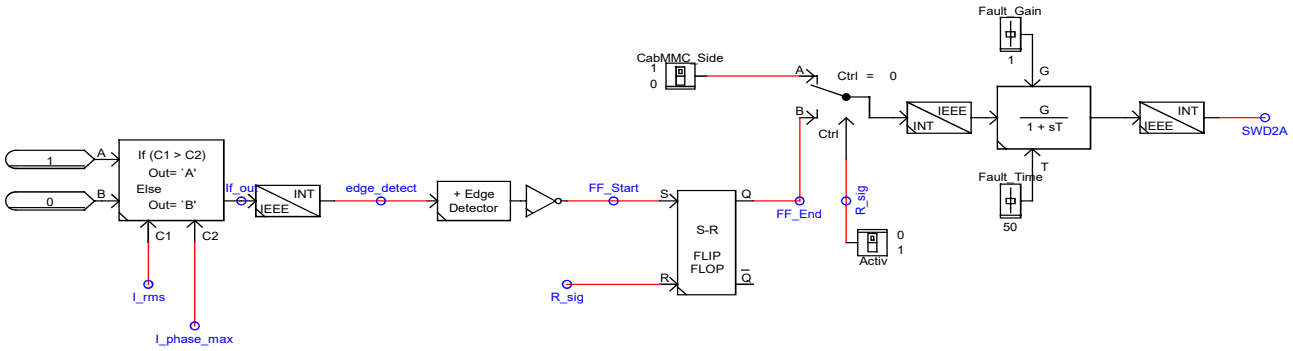

Figure 5.20: Circuit breaker operation logic

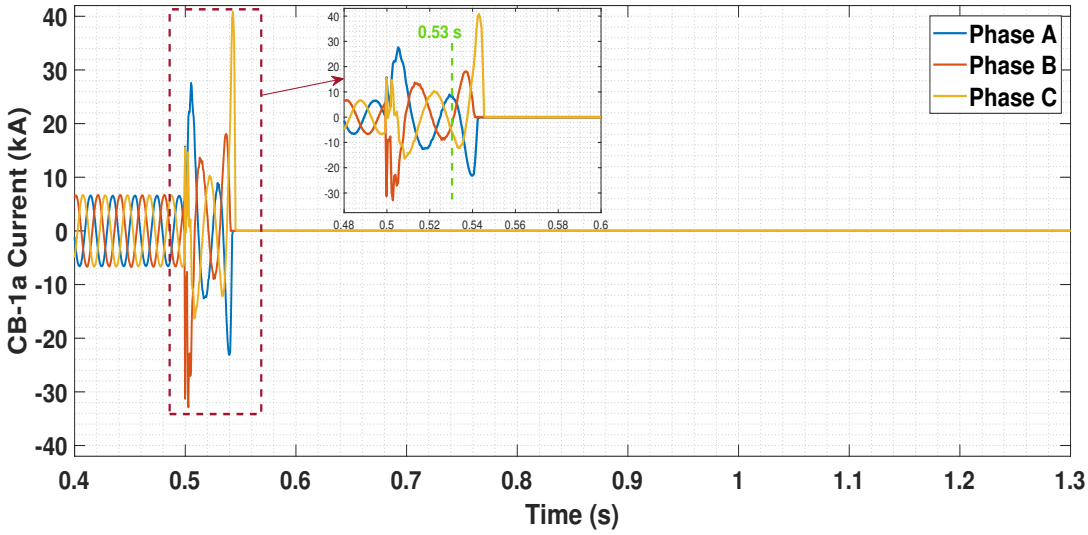

Figure 5.21: Currents in circuit breaker (CB-1a) upon three-phase line to ground fault in the middle of cable-1

In order to analyze the short-term voltage stability of the system, a permanent three-phase line to ground fault is applied in the middle of HVAC cable-1. The response of the network is recorded, and the plots for voltages, currents, active and reactive powers are depicted from Figure 5.21 to Figure 5.30 for the event. During the time of the fault, the RMS current exceeds the maximum phase current and the logic developed detects this overcurrent at CB-1a. This

[2] Tutorial » SAMPLES » Mainstep » Fault Control

[3] I_{phase_max} = 10 % above I_{phase} = 1.1 × I_{phase}

$$I_{phase} = \frac{Apparent\ power\ in\ single-phase}{Line\ to\ neutral\ voltage}$$

leads to the opening of breaker CB-1a according to the logic explained in the previous paragraph. The overcurrent is detected at 0.53 s of the simulation from the developed logic. A short delay of nearly 12 ms is provided to open the breaker after the fault has been detected similar to a practical scenario (Figure 5.21). After the circuit breaker is opened, OWF-1 is isolated from the network and total power provided to the onshore system is reduced. The total power in the pre-fault period is nearly 2 GW, and after the fault, the total power is reduced to nearly 1500 MW. Similar to the disconnection of one OWF discussed earlier in Section 5.4.1, the power flow is reduced through MMC-1 as shown by the blue line in Figure 5.22. It is also worthy of mentioning that the network is stable by viewing the stable voltage in the post-fault period in MMC bus, as shown in Figure 5.23.

Increase in active power in MMC-2 after the fault has been cleared (as seen from the red line in Figure 5.22) can be explained by viewing the current profiles in the OWFs detailed in the following paragraph. A major observation can be viewed from the profile of transients during the fault in the currents of both the MMCs in Figure 5.24(a) and 5.24(b). The initial rise in current till 0.53 s is due to the occurrence of the three-phase fault. The breaker is opened at 0.542 s. The profile of currents at nearly 0.59 s are complementary in both MMCs, i.e. the currents are decreasing in MMC-1 and increasing in MMC-2. This is due to the difference in control strategies in MMC-1 (V/F control) and MMC-2 (active power control).

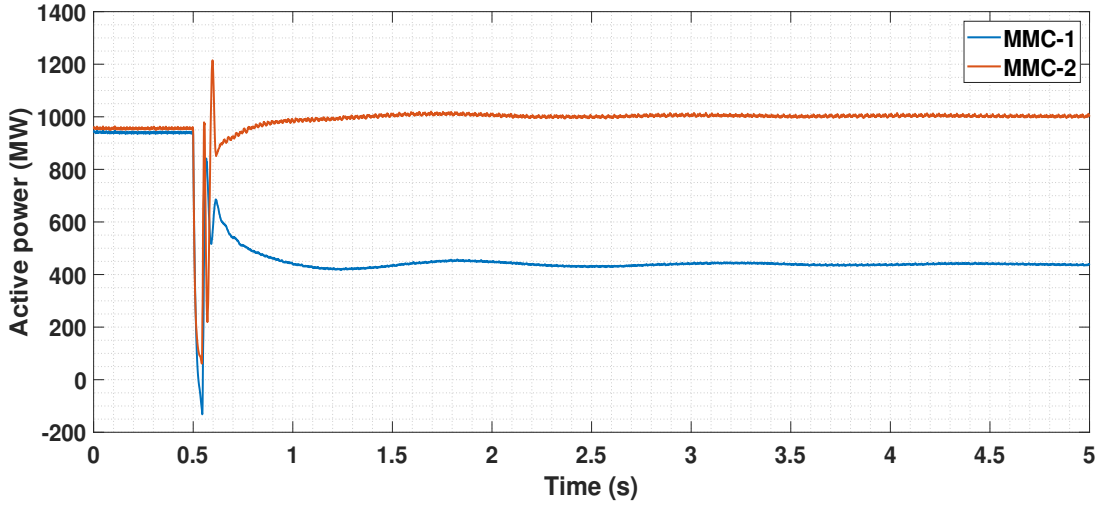

Figure 5.22: Active power in MMC-1 bus and MMC-2 bus upon three-phase line to ground fault in the middle of cable-1

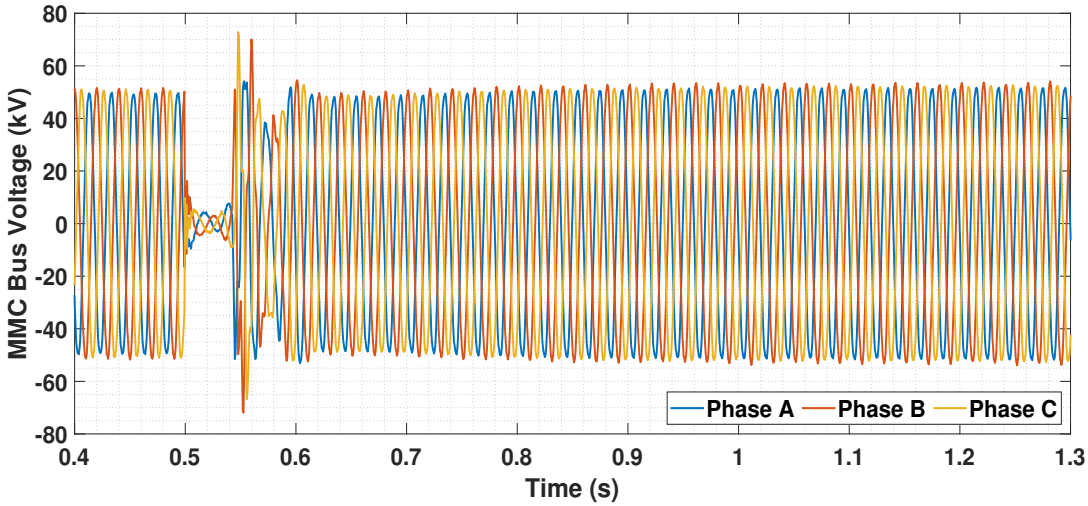

Figure 5.23: Voltages at MMC bus upon three-phase line to ground fault in the middle of cable-1

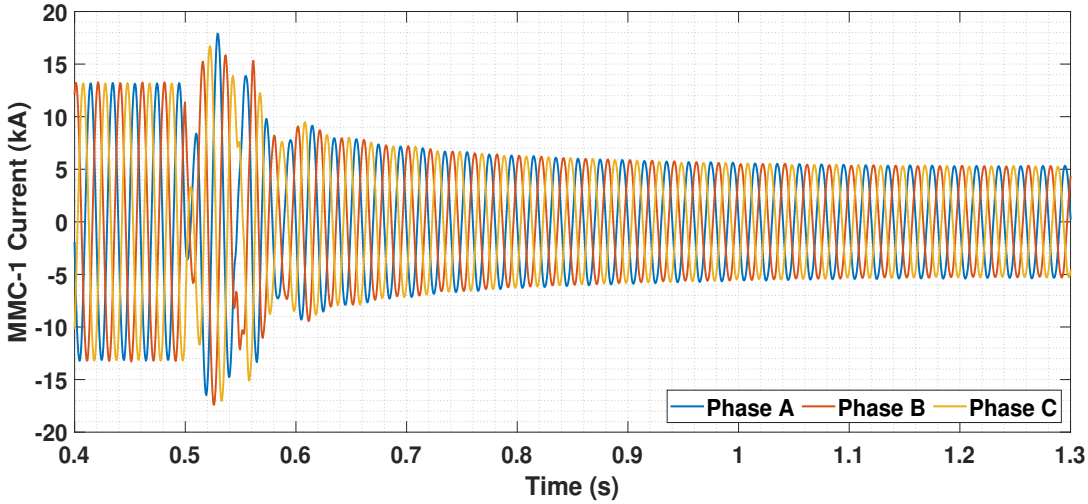

(a) Currents in MMC-1 bus

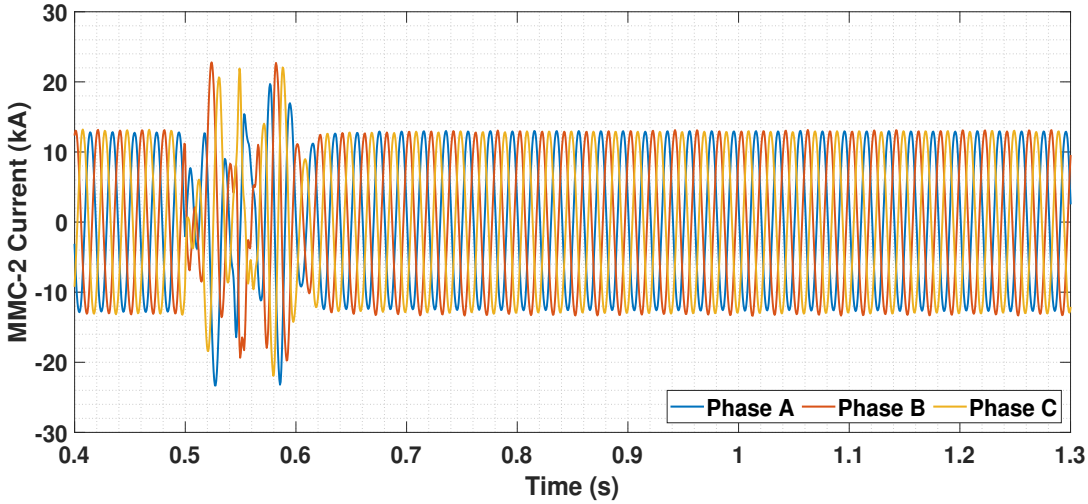

(b) Currents in MMC-2 bus

Figure 5.24: Currents in a) MMC-1 bus and b) MMC-2 bus upon three-phase line to ground fault in the middle of cable-1

Analyzing at the OWFs side of the network, the DVC is modelled to provide rated reactive current to flow to the fault location by controlling the voltage of the GSC, as explained in Section 3.3.1. From the voltage in p.u. plot in Figure 5.25 and the three-phase voltage plot in Figure 5.26, it can be seen that the voltage at the PCC-1 drops and remains low throughout the fault period. During the time of fault in cable-1 and after CB-1a is opened, the voltage angle and magnitude at PCC-1 goes to zero. The PLL in GSC-1 is synchronized with the AC voltage at PCC-1. The voltage magnitude at GSC-1 remains non-zero, and the voltage angle is zero during the time of fault as the PLL follows the angular reference at PCC-1. Therefore, due to higher voltage magnitude at GSC-1 than at PCC-1, reactive power will flow from GSC-1 to PCC-1, and since the voltage angle is zero at GSC-1 and PCC-1, active power transmitted is zero during the time of the fault. This is performed in DVC by controlling the d-axis reference voltage of GSC-1 and thereby indirectly controlling the current coming out of the GSC-1 to PCC-1. The current limitation algorithm implemented in the DVC in Section 3.3.1.3, limits the output current to the rating of the converter and hence rated reactive current flows from the GSC-1 as seen in Figure 5.27.

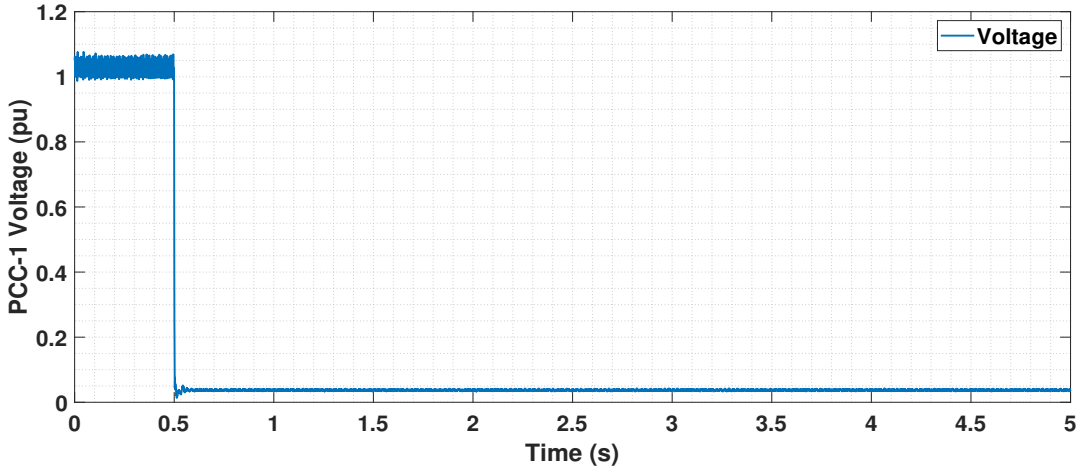

Figure 5.25: Voltage in p.u. at PCC-1 upon three-phase line to ground fault in the middle of cable-1

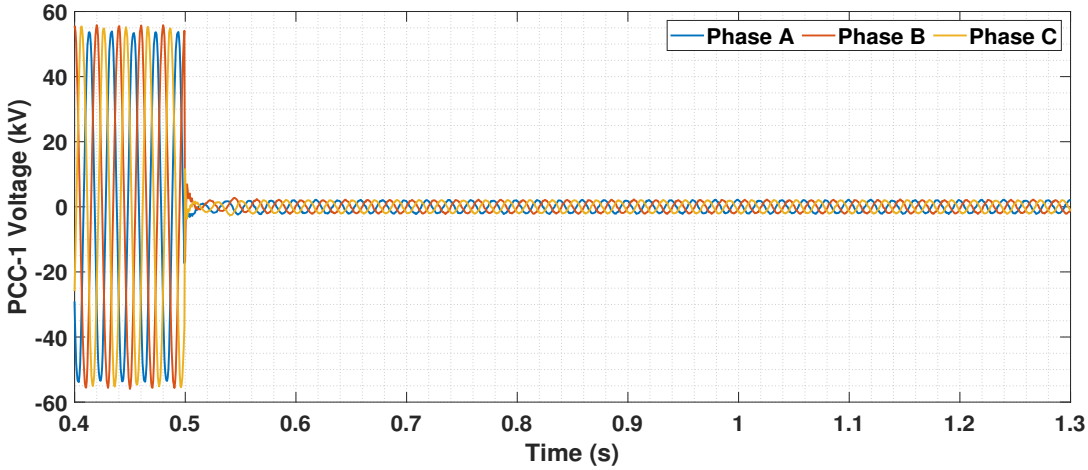

Figure 5.26: Voltages at PCC-1 upon three-phase line to ground fault in the middle of cable-1

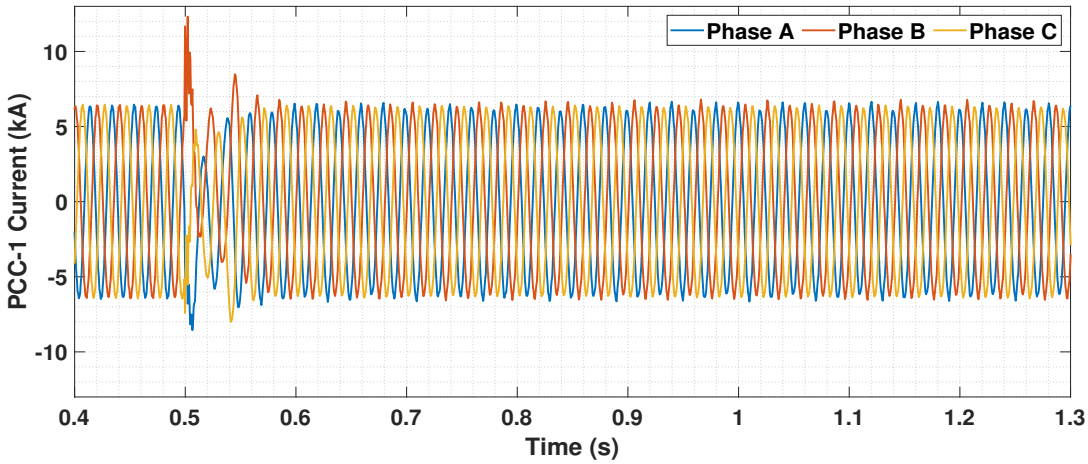

Figure 5.27: Currents in PCC-1 upon three-phase line to ground fault in the middle of cable-1

Voltages at PCC-2, 3 and 4 have transients during the time of fault and are then stabilized to a slightly higher value than the pre-fault state to compensate for the loss of OWF-1. This is due to the fast local voltage control in DVC as

seen for the case of disconnection of one OWF. The post-fault voltage value is within the tolerance limit (±10 %), and this can be viewed from the graphs in Figure 5.28. An important observation in the voltage graphs of OWFs-2, 3 and 4 is the occurrence of spikes right after the circuit breaker CB-1a is opened, as can be seen in Figure 5.28. There can be two reasons for such a phenomenon to occur. The first is that after the circuit breaker CB-1a is opened, reactive current injection still takes place (at 0.59 s in Figure 5.29 for PCC-2) and this causes the voltage at the corresponding PCC also to rise. Such a rise in voltage is not applicable in real-world OWFs and is, therefore, a drawback due to the OWF modelling. These spikes can be ignored as they do not represent the performance of the real hardware. The second reason could be due to two control strategies that provide the voltage reference in the network. It is seen that during the steady state and post-fault condition, the V/F control is dominant and provides the voltage reference in the network. However, during the time of the fault, DVC in all OWFs take the role of providing the voltage reference in the corresponding PCCs as seen in PCC-1 during the time of three-phase line to ground fault in cable-1. The sudden change back to the steady state condition after the fault is released could lead to discrepancies between the V/F mode and the DVC. The conflict between these control strategies occur as to which control strategy provides the voltage reference right after the circuit breaker is open and hence this causes a spike in voltage at the PCCs.

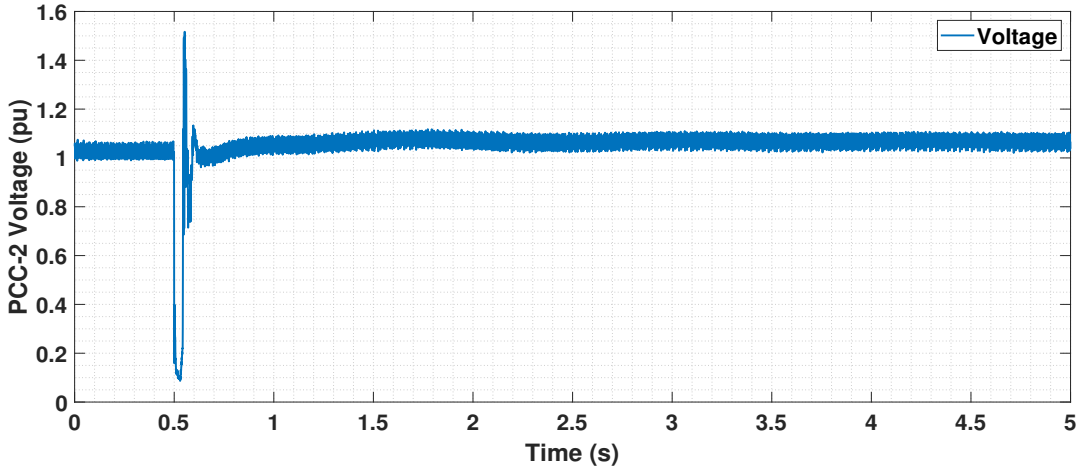

Figure 5.28: Voltage in p.u. at PCC-2 upon three-phase line to ground fault in the middle of cable-1

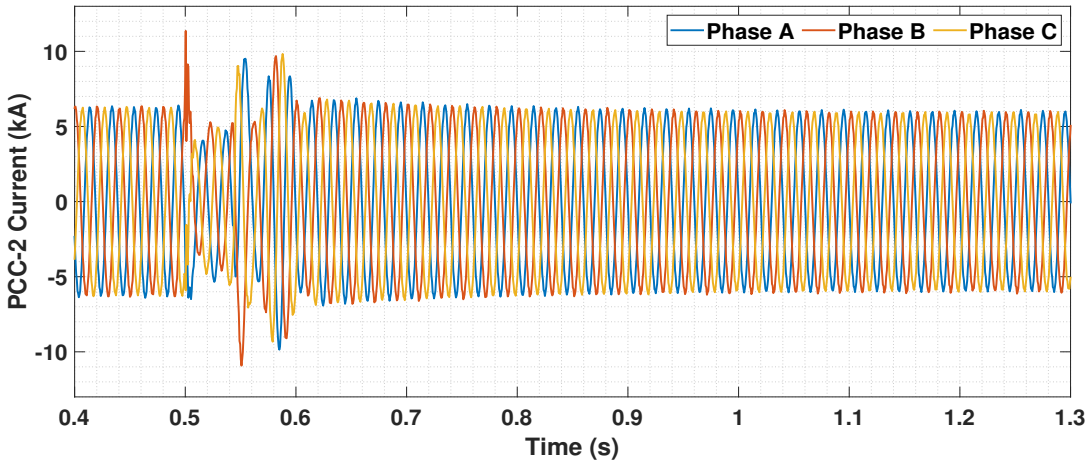

Figure 5.29: Currents in PCC-2 upon three-phase line to ground fault in the middle of cable-1

The currents from the OWFs-2, 3 and 4 are the same in the post-fault region as the pre-fault condition (Figure 5.29 for PCC-2) since the scaling factor for each OWF is still the same. DVC control in these OWFs operate during the time of fault and limit the currents by controlling the voltages at corresponding PCCs. Due to the increase in voltage in the post-fault period at the PCCs-2, 3 and 4, the active power generated also will be higher from the OWFs-2, 3 and 4 and it is reflected in the increase in active power in MMC-2 as shown in Figure 5.22. Another important observation is in the profile of transients in currents in PCCs-2, 3 and 4 following the occurrence of the fault. As shown in Figure 5.29

for PCC-2, the current is limited from 0.5 to 0.54 s during the time of fault. After the breaker has been operated at 0.542 s, the profile of currents (from 0.55 s to 0.6 s) is similar to that of the MMC-2 (Figure 5.24(b)). This is due to the re-synchronization to the grid by the PLL in MMC-2 control and the PLL in DVC of WG-2, 3 and 4.

In practice, if a three-phase fault occurs in a subsea cable, it is difficult that the fault clears on its own and would require human interference. During such critical islanding situations, the DVC allows rated reactive current to flow to the fault location by controlling the GSC voltage and thereby protecting the converters in the OWF from high over-currents. Based on the reference grid codes mentioned in [12], during steady state operation, the active current must be the priority, and during the time of the fault, the priority must be changed to reactive current. The major takeaway from this chapter is that the DVC follows the reactive current injection requirement during the time of the fault, as shown from the currents in PCC-1 in Figure 5.30 even while working in coordination with other controls in the network. Current is limited to the rated current of the converter by the current limitation algorithm in DVC without the requirement of any external controls.

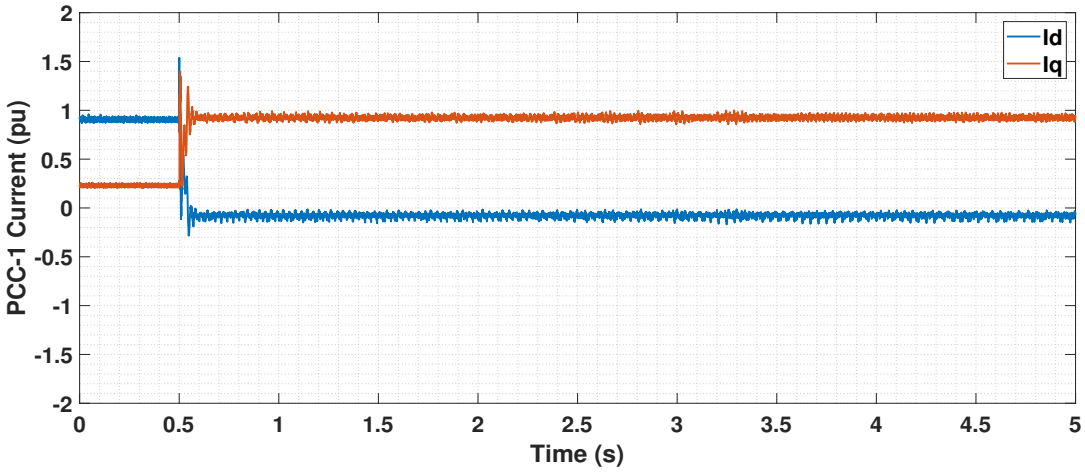

Figure 5.30: Currents in d and q axes in PCC-1 upon three-phase line to ground fault in the middle of cable-1

6

Conclusions and Future Scope

This chapter provides a concise description of the achieved results in the previous chapters, answers to the formulated research questions in Chapter 1, and the future scope of this thesis is presented at the end.

6.1. Summary

The thesis tackles the research problems identified in Chapter 1 related to the need for large scale offshore networks with the available technology and provides solutions to mitigate technical challenges related to voltage and frequency control while developing large scale offshore networks.

From literature, it is seen that the current state-of-the-art technology, MMC-HVDC transmission, for transferring offshore wind power is limited to a maximum capacity of 1.2 GW [8]. Hence, a configuration for a large scale offshore network (greater than or equal to 2 GW) with the available technology is currently lacking. It is expected that the upcoming OWF projects will be utilizing 66 kV HVAC transmission from OWFs to the offshore converter station due to their significant advantages over the conventional combination of 33 kV and 145 kV [11]. Moreover, the technical challenges related to voltage and frequency control in islanding of OWFs is not full filled in real-time application and lacks the major requirement of reactive current injection by the WGs during dynamic conditions [25].

This thesis adopts the latest trend in technology, and it overcomes the above mentioned research gaps by achieving the overall goal of developing a generic digital twin model of 2 GW, 66 kV HVAC offshore network in RSCAD and performing analysis on the dynamics of voltage and power at various locations in the network. The digital twin model developed in this thesis adopts a modified hybrid configuration with two MMCs working in parallel and connecting four OWFs to the onshore system. The layout adopted for the 2 GW offshore network is achieved by modifying the layout of the hub-and-spoke principle in [46]. Additionally, the technical challenges faced while using conventional current control strategies in WGs related to voltage and frequency control, are mitigated by implementing a new control strategy, DVC, in all the four WGs in RSCAD for real-time application.

To achieve the overall goal, initially, the DVC is implemented for real-time application in RSCAD for one OWF connected to a 66 kV HVAC network. The large scale 2 GW offshore network is developed by modularly connecting four of the aforementioned single OWFs in parallel. The 2 GW offshore wind power is transferred to the onshore network through two parallel connected MMCs. The key features of the model include- all the WGs are equipped with DVC, one MMC working in V/F control and the other working in active power control. Such a model is unique because it incorporates a hybrid layout that allows for the coordination of the above mentioned strategies during steady state and dynamic conditions in the network.

Few significant results of the model include the achievement of short-term voltage stability in the network during severe dynamic scenarios. The requirement of reactive current injection by WGs during islanding is fulfilled by performing three-phase fault analysis. These results confirm the stable operation of the network under severe dynamic scenarios, and the corresponding network model can be utilized for further advancements on the size of the offshore network.

6.2. Answers to Research Questions

Research Question 1 : How effective is the DVC when implemented in an EMT average model of Type-4 WG connected to a 66 kV equivalent HVAC system in RSCAD?

As the upcoming projects are expected to have 66 kV HVAC transmission from OWFs to the offshore converter station, the DVC in GSC of Type-4 WG connected to an infinite grid, is modelled for a 66 kV HVAC offshore network in RSCAD. The performance of DVC is tested for the most severe disturbance, i.e. the three-phase line to ground fault. The three-phase line to ground fault is implemented in the middle of the 66 kV HVAC cable. On viewing the voltage profile at the PCC following the fault, it is observed that DVC provides stable operation in terms of short-term voltage stability. This is due to the fast control action of the local voltage control in the reactive power loop of the DVC to support the PCC voltage during the time of the fault. In terms of reactive current injection, the DVC provides active current priority during steady state conditions and reactive current priority during the time of the fault, which is an important requirement by most of the grid codes. The effect of damping during the time of fault is controlled by the washout filters in the active and reactive power control loops. A parameter sensitivity analysis is performed for the washout filters to assess the effectiveness of damping.

Research Question 2 : What insights can be attained by the EMT average model of Type-4 WG with DVC in 66 kV network in RSCAD in comparison with a similar system modelled with a simplified Type-4 WG configuration with DVC in DIgSILENT PowerFactory?

The performance of the implemented DVC in a average model of Type-4 WG in RSCAD for a 66 kV HVAC network is compared with the benchmark DVC for a simplified Type-4 WG model in PowerFactory for a similar 66 kV HVAC network. The comparison is made in terms of short-term voltage stability and reactive current injection following a three-phase line to ground fault in the network. A three-phase line to ground fault in the middle of the HVAC cable is simulated in both the models in EMT platform. The voltage, active and reactive current profiles are compared and found to have good correspondence following the three-phase line to ground fault. This shows the validation of the DVC implemented in the average model of the Type-4 WG for a 66 kV HVAC offshore network in RSCAD. Moreover, it is observed that the model developed in RSCAD has slight transients in the active and reactive currents throughout the simulation. This is due to the detailed model representation of GSC in RSCAD when compared to the simplified model in PowerFactory. These results show that the RSCAD model provides a better detailed representation of the real-world operation of the implemented DVC and can be used as a reference model. The way DVC is modelled to provide voltage support during the time of fault in 66 kV HVAC network are in line with the results from previous studies, in which DVC is implemented for a 33 kV HVAC network as explained in [21].

Research Question 3 : How can Type-4 WGs with implemented DVC work in coordination with offshore MMCs within a multi-gigawatt offshore transmission network?

Due to the urging need to move for large scale offshore networks with the currently available technology, a modified hybrid layout is implemented for the development of a 2 GW offshore network. The layout contains the connection of four OWFs connected to a common bus to which two MMCs working in parallel are connected. To tackle the technical challenges related to voltage and frequency control in offshore islanded networks, all four OWFs are modelled with the implemented DVC. This is done by modularly connecting the single OWF model with implemented DVC developed in Chapter 3. To provide the voltage reference during steady state operation, it is proposed that one of the MMCs (MMC-1) is operated in V/F control and to continue the flow of power in the network constantly, it is proposed that MMC-2 is operated in active power control. The coordination between the V/F control in MMC-1, active power control in MMC-2 and the DVC in OWFs provide a synchronized operation during the steady state and dynamic conditions in the network. One of the highly severe conditions tested is the disconnection of one OWF. OWF-2 is considered for this event. In such a situation, it is observed that the network remains stable following the disconnection and the power flowing through MMC-1 reduces as it is working in V/F control, i.e. capable of providing and absorbing power. Another highly severe event tested is the three-phase line to ground fault in one of the HVAC cables. A circuit breaker logic is modelled to isolate OWF-1 from the network when the fault occurs in HVAC cable-1. It is observed that the operation of the entire network remains stable during the pre-fault condition where active current is injected or can be termed as active power is generated by all the OWFs. During the time of fault in HVAC cable-1, circuit breaker at the end of the cable is opened upon detection of overcurrent and thereby, islanding OWF-1. The fast local voltage control in DVC in OWF-1 provides voltage support during the time of the fault, and due to the grid conditions, the reactive current is injected by OWF-1 to the fault location. The currents are limited to the rating of the GSC by the employed current limitation technique. Hence, it can be concluded that the V/F control provides the voltage reference during the pre-fault and post fault condition for the network and DVC provides voltage reference at the corresponding PCC when the OWF is islanded.

Research Question 4 : How effectively do Type-4 WGs with implemented DVC perform when connected in an offshore network for parallel operation?

The four OWFs with implemented DVC are connected to a common MMC bus in the 2 GW offshore network. This makes the OWFs to be working in a parallel configuration. The voltage and current profiles at the PCCs of all the OWFs are similar in the steady state since all the four OWFs are modelled and simulated by considering the same wind speed profile (generating an equal amount of power). During the highly severe conditions such as the disconnection of OWF-1, it is observed that the power generated from other OWFs connected to the network compensate equally for the loss of the disconnected OWF-1 by providing a slightly higher voltage at the corresponding PCCs. This is done equally by the local voltage control in the corresponding DVC to support for the voltage drop, due to the assumption of having similar parameters in all DVC. Additionally, in the event of a three-phase fault in HVAC-1 cable, there occurs a drop in voltages in other PCCs as well since they are connected to a common bus. However, voltages at the PCCs are recovered in the post fault condition and stabilized by the corresponding fast voltage control in DVC to equal values due to the similar settings in the control loops. Therefore, it can be concluded that each OWF contributes equally to maintain the power balance in the network during steady state and dynamic conditions.

6.3. Recommendations for Future Work

Having successfully achieved the defined goals for this thesis and based on the studies performed, the author provides recommendations in the following section:

- The availability of additional NovaCor processor at TU Delft could be fully utilized to scale up the model to a capacity of 4 GW by accordingly connecting WGs and MMCs in a modular approach. The practical scenario of multi-terminal AC network can be implemented, and the performance of the WGs with DVC can be analyzed.
- The present model of DVC is applicable for three-phase fault analysis. Analysis can be extended for single-phase faults that are more common to occur in the real scenario by developing a negative sequence control loop for the DVC.
- Various other network topologies can be researched on and tested with the implemented DVC to investigate the cost-benefit feature for the industry experts.
- The integration of the onshore converter station to the offshore network by removing the DC sources from the present model can be accomplished, and extensive fault analysis can be performed in the MMC-HVDC network.
- The practicality of the controller can be tested by performing Hardware In Loop testing of the implemented DVC in a properly set-up test bench.
- The developed 2 GW generic model can be incorporated with other control strategies suggested in Section 1.2 for WGs, and studies related to the interoperability of these controllers and coordination with MMC control strategies can be performed.

Appendices

A

WG model Utilized in RSCAD and PowerFactory

A.1. RSCAD model

The Type-4 WG model is utilized for this thesis work, and the complete implementation of the model is described in this section.

The PMSG modelled in the small time step block, consists of the parameters shown in Figure A.1. The PMSG component majorly operates in two modes: Speed or Lock mode (LCKFR = 0) ; Torque or Free mode (LCKFR = 1). As the name suggests, a control signal directly controls the speed of the machine in speed mode, and a control signal directly controls the torque of the machine in torque mode.

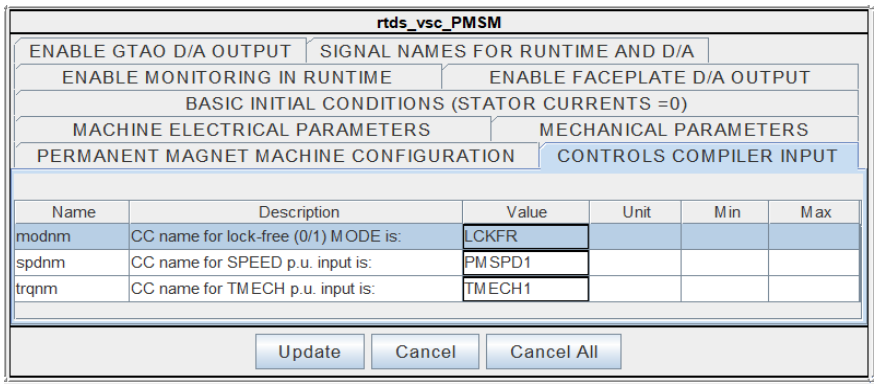

Figure A.1: PMSG data

The major three blocks that represent the control system of Type-4 WG are:

- Aerodynamic model
- Machine Side Converter model
- Grid Side Converter model

A.1.1. Aerodynamic model

The aerodynamic block consists mainly of the wind turbine data and the coefficient data i.e. is the $C_p(\lambda,\beta)$ parameters, as shown in Figures A.3(a) and A.3(b). The parameters used are for a 6 MVA rated WG model. The detailed configuration of the aforementioned parameters is described in "WTG50R3.pdf" in the Samples folder in RSCAD. The aerodynamic model consists of the two mass representation model of WG shown in Figure A.4, and the pitch angle control is shown in Figure A.5.

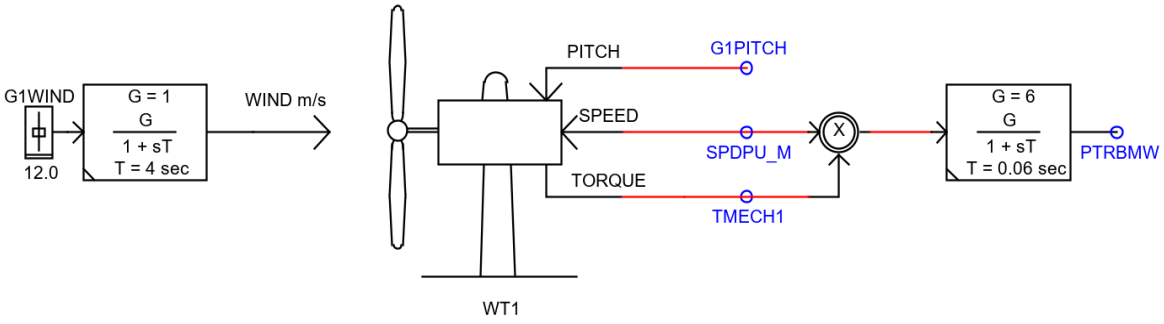

Figure A.2: Aerodynamic model

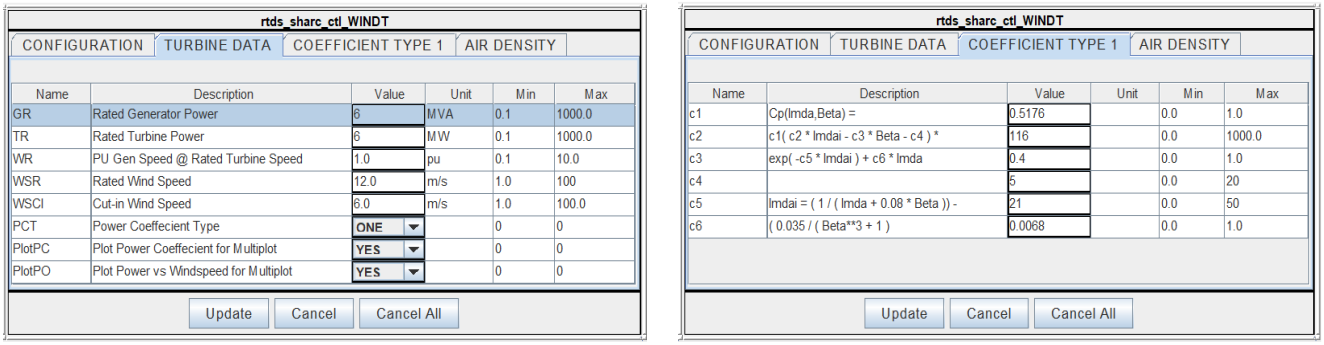

(a) Turbine data

(b) Coefficient data

Figure A.3: Aerodynamic model data

The inputs for the two-mass model are the mechanical torque from the aerodynamic model and the electrical torque from PMSG. The output is the change in rotor speed ($SPDPU\_M$) and the generator speed ($SPDPU$). The two-mass model represents the non-linear nature of the wind turbine aerodynamics. To protect the turbines from damage due to high wind speeds, the pitch control mechanism is adapted. The maximum speed is controlled through the limits of the $G1MXPSD$ parameter. When the speed goes beyond the limit, a pitch angle ($G1PITCH$) is calculated, and this is provided as input to the aerodynamic model to compute a new speed.

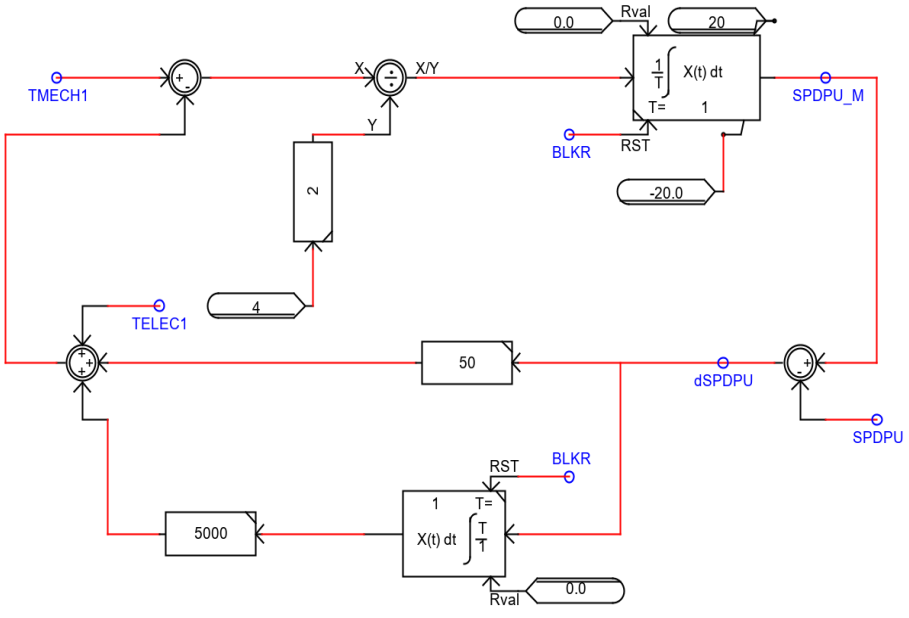

Figure A.4: Two-mass model

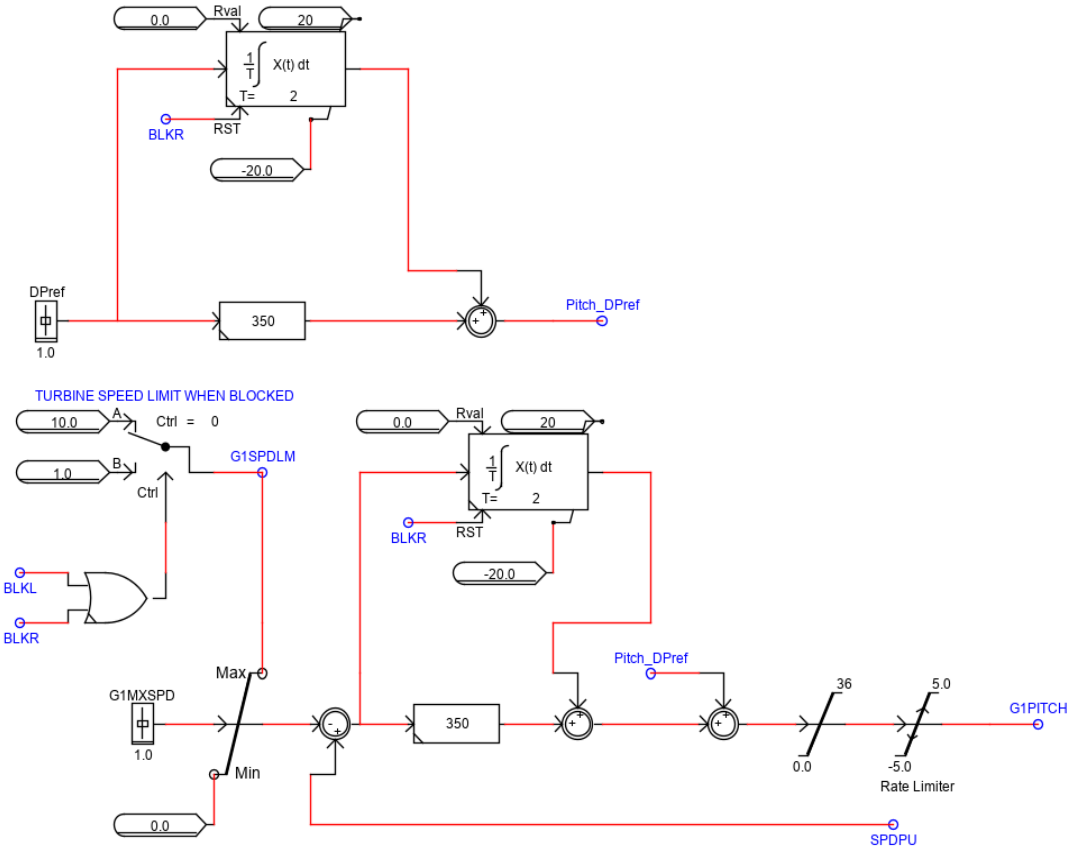

Figure A.5: Pitch angle control

A.1.2. Machine Side Converter model

The overall MSC control is depicted, as shown in Figure A.7. A three-level VSC is used for operation as MSC in this model. The conventional vector current control utilized in the MSC control. As required for PI control operation, the abc signals are transformed to the dq frame using the rotor angle measurement for alignment and synchronizing with the dq reference frame. The MSC control consists of two inner fast control loops using PI controllers that regulate the converter currents during all conditions, i.e. steady-state and dynamic scenarios. The reference values for the inner control loop is provided by the outer control loop. By measurement of active power of the WG, a MPPT control is used to output an optimum speed reference ($WMOPTPU$) as shown in Figure A.6. The error difference from the optimum speed reference and the rotor speed is regulated through an outer PI control loop. The modulation index for the MSC control is same as GSC control and is given by Equation 3.16.

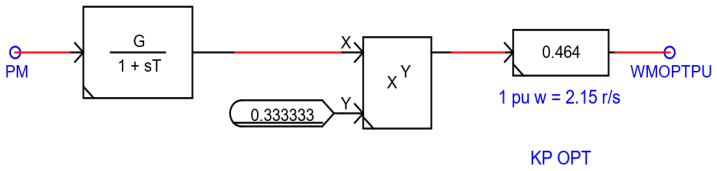

Figure A.6: MPPT controller

The gating for the MSC control utilizes PWM and the inputs for the triangular wave repeater in terms of point and slope, in the small time step environment are defined as shown in Figure A.8. However, the rated frequency of the PMSG is chosen to be 3.77 Hz, and the frequency of the carrier wave is 31 times this frequency. Hence the slope of the triangular signal is double the carrier frequency which is then sent to the small time step block.

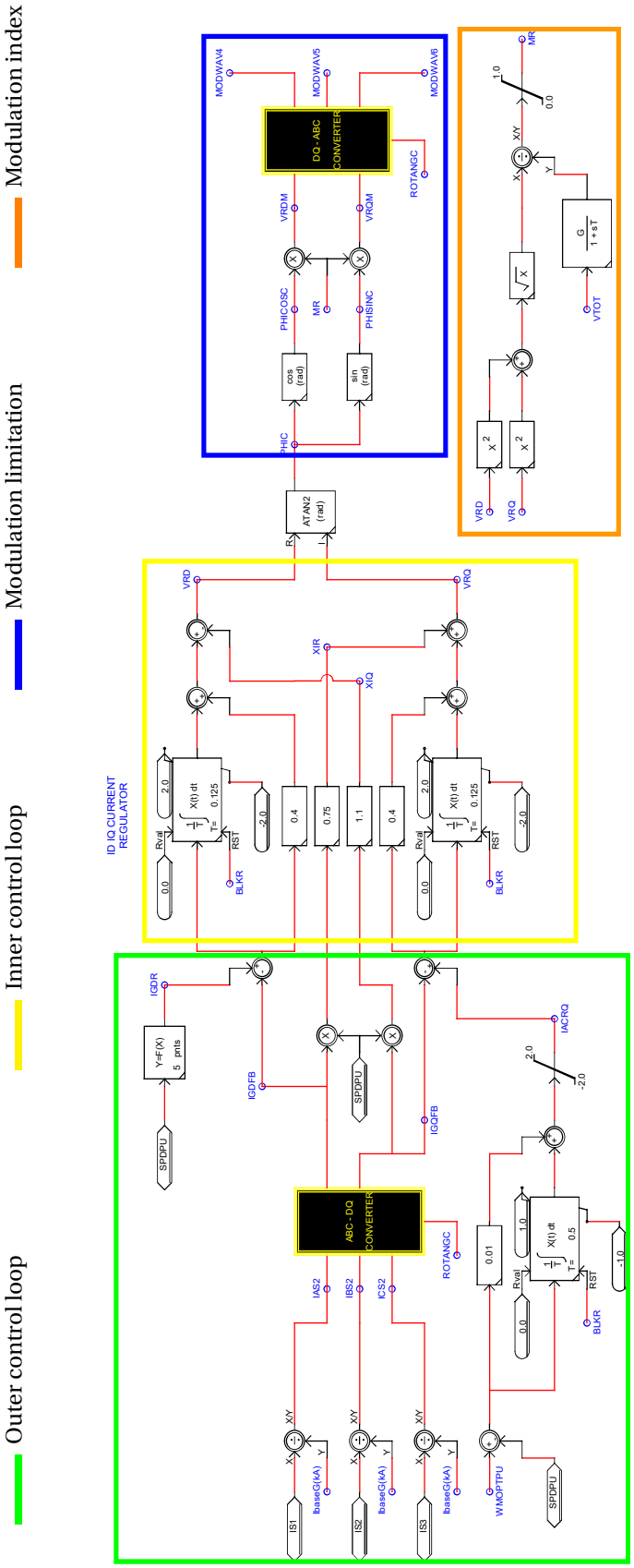

Figure A.7: MSC control

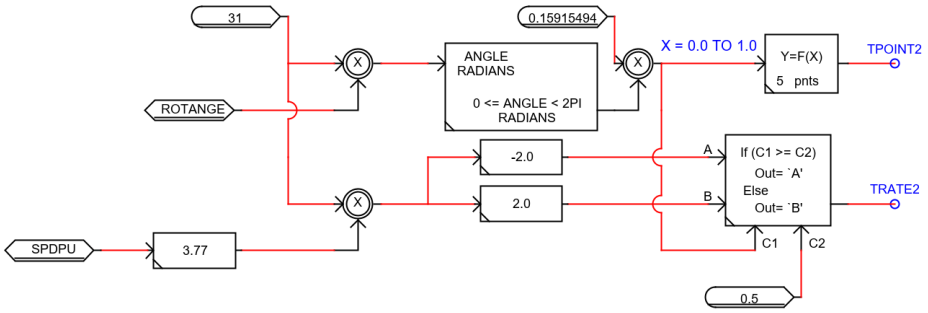

Figure A.8: Triangular wave inputs

The triangular wave repeater and the firing pulse generator blocks are placed in the small time step environment, as shown in Figure A.9. As the name suggests, the triangular wave repeater creates the triangular-carrier wave taking the points and slope as input and provides the carrier wave to the firing pulse generator. Each VSC have dedicated firing pulse generator which takes the carrier wave input from the triangular wave repeater (e.g. TWAVE6) and the modulation signal from the large-time step block controls (e.g. MODWAV6). Depending on the comparison of these signals, the switching of the valves takes place. The firing signal to be sent to the VSC leg are named for example FPOUT6. The number denomination for the three-phases of MSC are 4,5 and 6 respectively in this model.

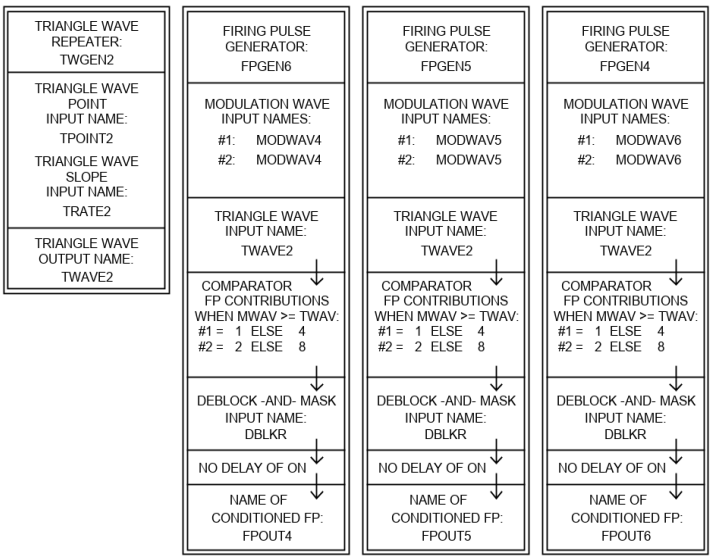

Figure A.9: Triangular wave repeater and Firing pulse generator for MSC

There exists a DC link in between the MSC and the GSC consisting of capacitor banks on either end and a chopper circuit in between. The voltage in the upper and lower capacitive branches in the MSC side is depicted as $V3$ and $V4$. Voltages in the branch at the GSC side are $V1$ and $V2$. The voltages $V1$ and $V2$ sum up to V_{DC_ref} in the outer control loop for the GSC as explained in Section 3.3.1.2. Hence, the control of d-axis voltage is associated with the control of active power, and this task is accomplished by regulating the DC voltage. The voltage across the DC link is maintained constant during steady state conditions. During the time of disturbance in the network, the chopper circuit gets activated and holds the DC voltage within the limit. The chopper gets activated when the DC voltage $(V1 + V2)$ goes above 1.05 p.u. as shown in Figure A.10. The chopper also utilizes PWM for gating and the signals involved are a 50 Hz carrier signal and, the difference between the maximum voltage limit (1.05 p.u. in this case) and the measured DC voltage as the modulating signal. The triangular wave repeater block and the firing pulse generator block for the chopper is also placed in the small time step block and is shown in Figure A.11(b). The firing pulse output is provided to the circuit valve shown in Figure A.11(a).

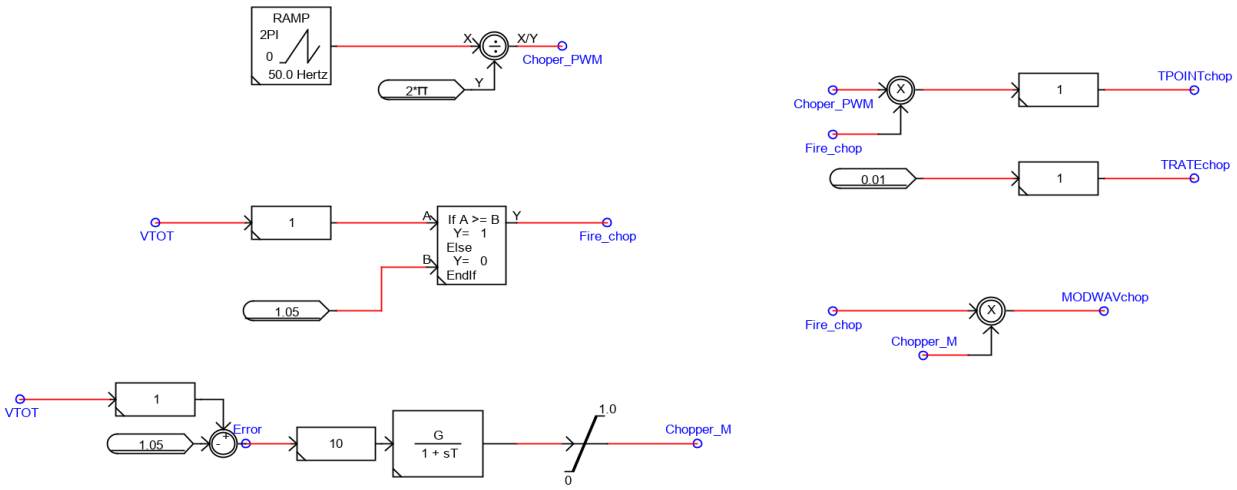

Figure A.10: Chopper activation control

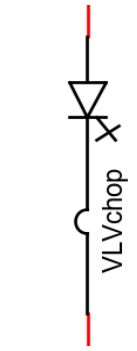

(a) Chopper circuit valve

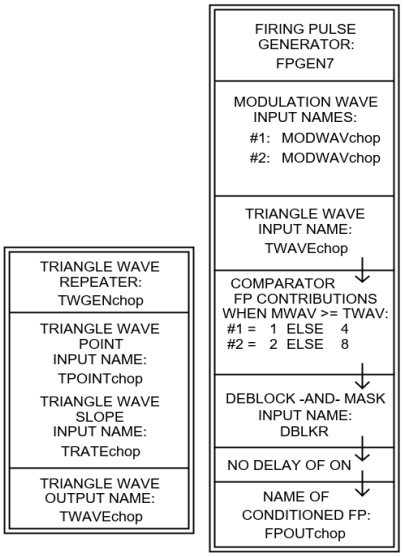

(b) Triangular wave repeater and Firing pulse generator for DC circuit

Figure A.11: Chopper circuit in small time step block

A.1.3. Grid Side Converter model

GSC also uses a three-level VSC similar to the MSC. The GSC also uses PWM technique for gating, and the points and slope for the triangular wave are created by the PLL as shown in Figure A.12. The PLL block plays a significant role in the entire network as it computes the phase angle of the space vector that defines the synchronization of the rotating dq frame with the abc frame. The input for the PLL is the three-phase voltage at the PCC, and the angle is defined such that the d-axis aligns with the grid voltage and q-axis voltage is zero. This is done to achieve decoupled control of the two axes. Thereby, d-axis provides control of active power, and q-axis provides control of reactive power. The proportional and integral gains need to be defined in the PLL block. The influence of these parameters in a grid dominated with PE is an ongoing topic of research.

The slope and points for the triangular wave repeater are also generated in Figure A.12. The frequency of the carrier wave is chosen to be 19 times the nominal frequency (19*50 Hz). Therefore, the points would be 2*19*50 Hz if x = 0 and -2*19*50 Hz if x = 1. The angle is also multiplied by 19 and is between 0 and 2π, hence has to be divided by 2π to achieve points between 0 and 1. The triangular wave repeater and the firing pulse generator for the GSC are similar to that of the MSC and are shown in Figure A.13. The numbers denominated for the three-phases of GSC are 1,2 and 3 respectively.

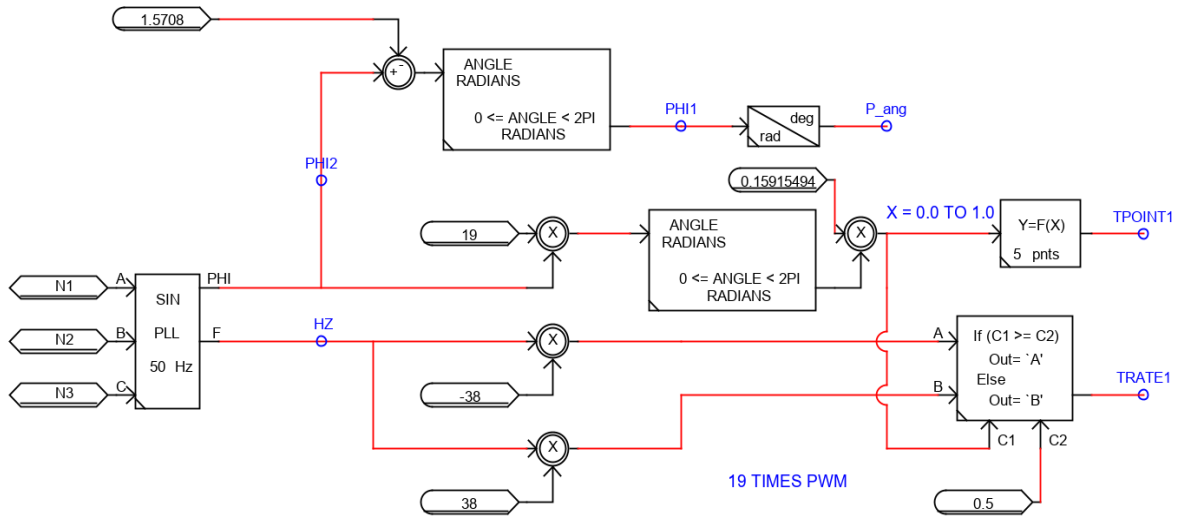

Figure A.12: PLL circuit, points and slope for triangular wave generation

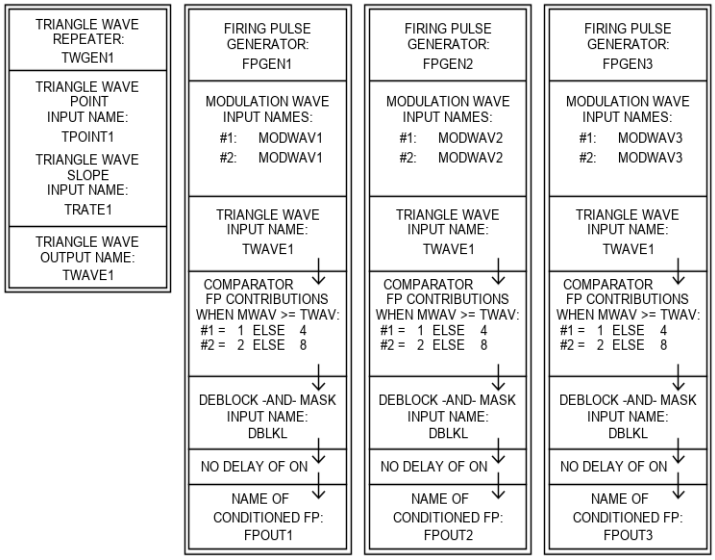

Figure A.13: Triangular wave repeater and Firing pulse generator for GSC

The GSC control block has the abc to dq transformation and vice versa, of PCC voltages and currents, measurement of PCC voltage in p.u. and the measurement of DC voltage in p.u., as shown in Figure A.14. The generation of the gating pulses are similar to the MSC control. The outer and inner control loop structure of the implemented DVC is illustrated in Figure A.15.

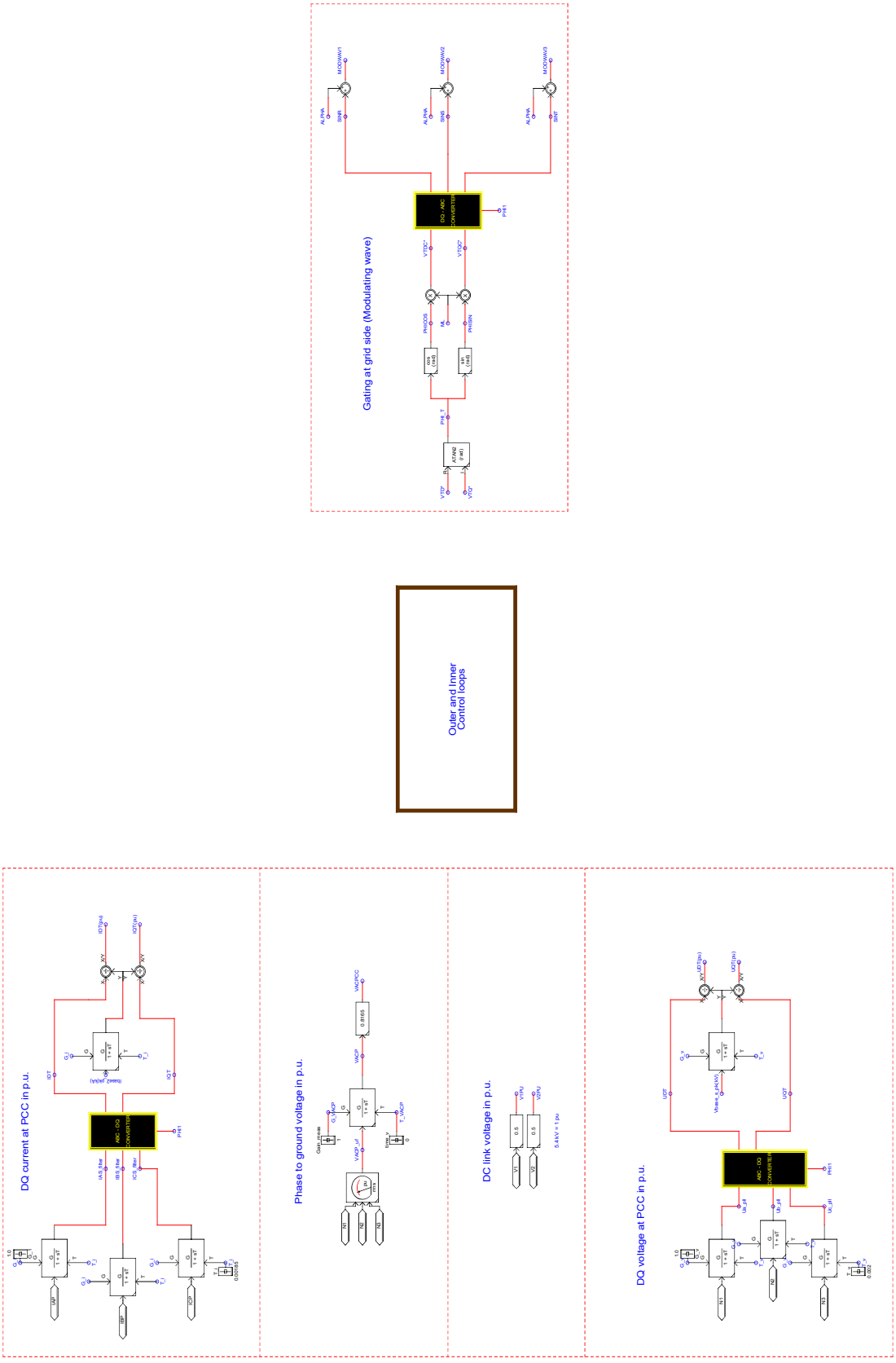

Figure A.14: GSC control

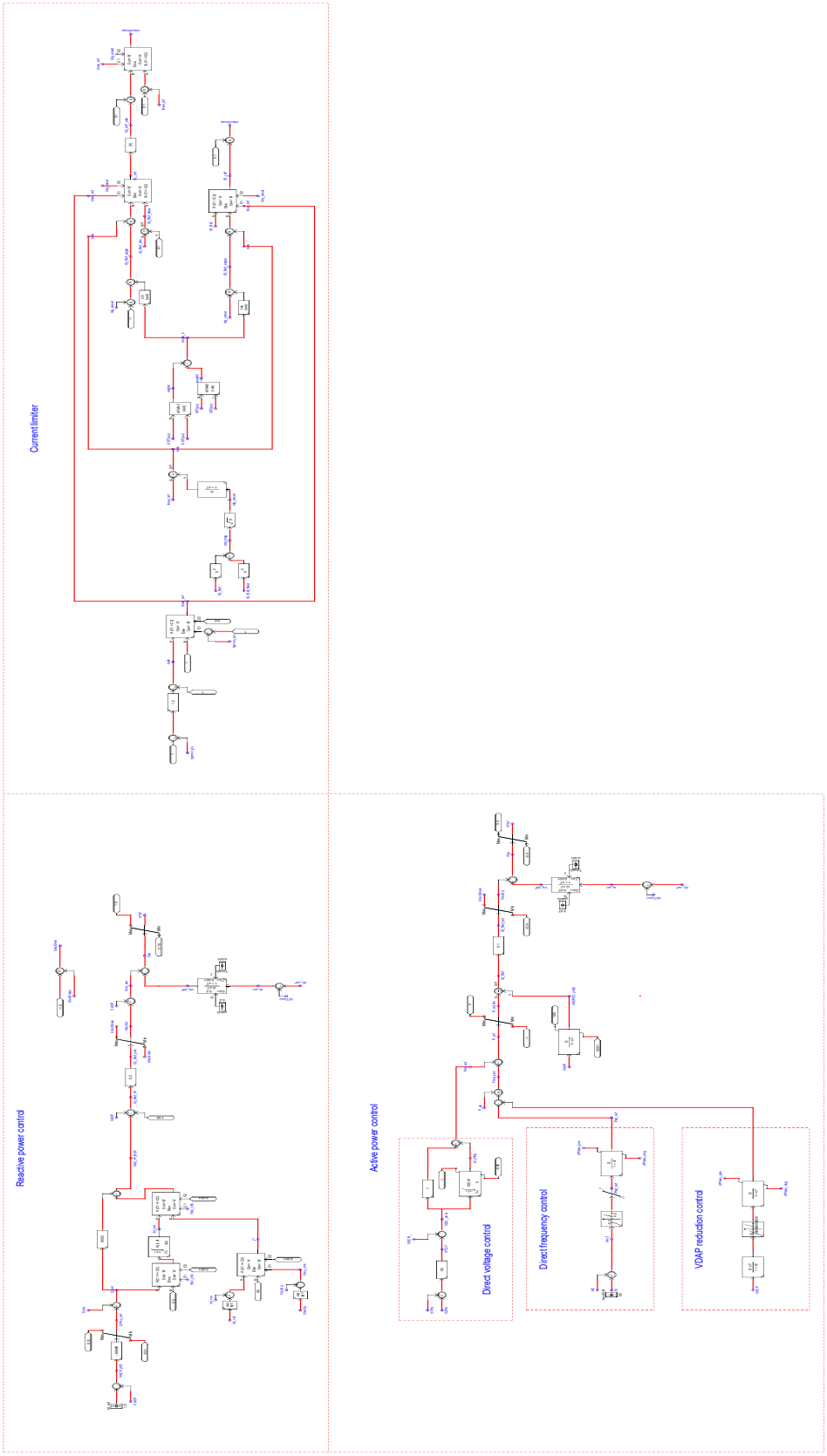

Figure A.15: DVC representation in RSCAD

A.2. PowerFactory model

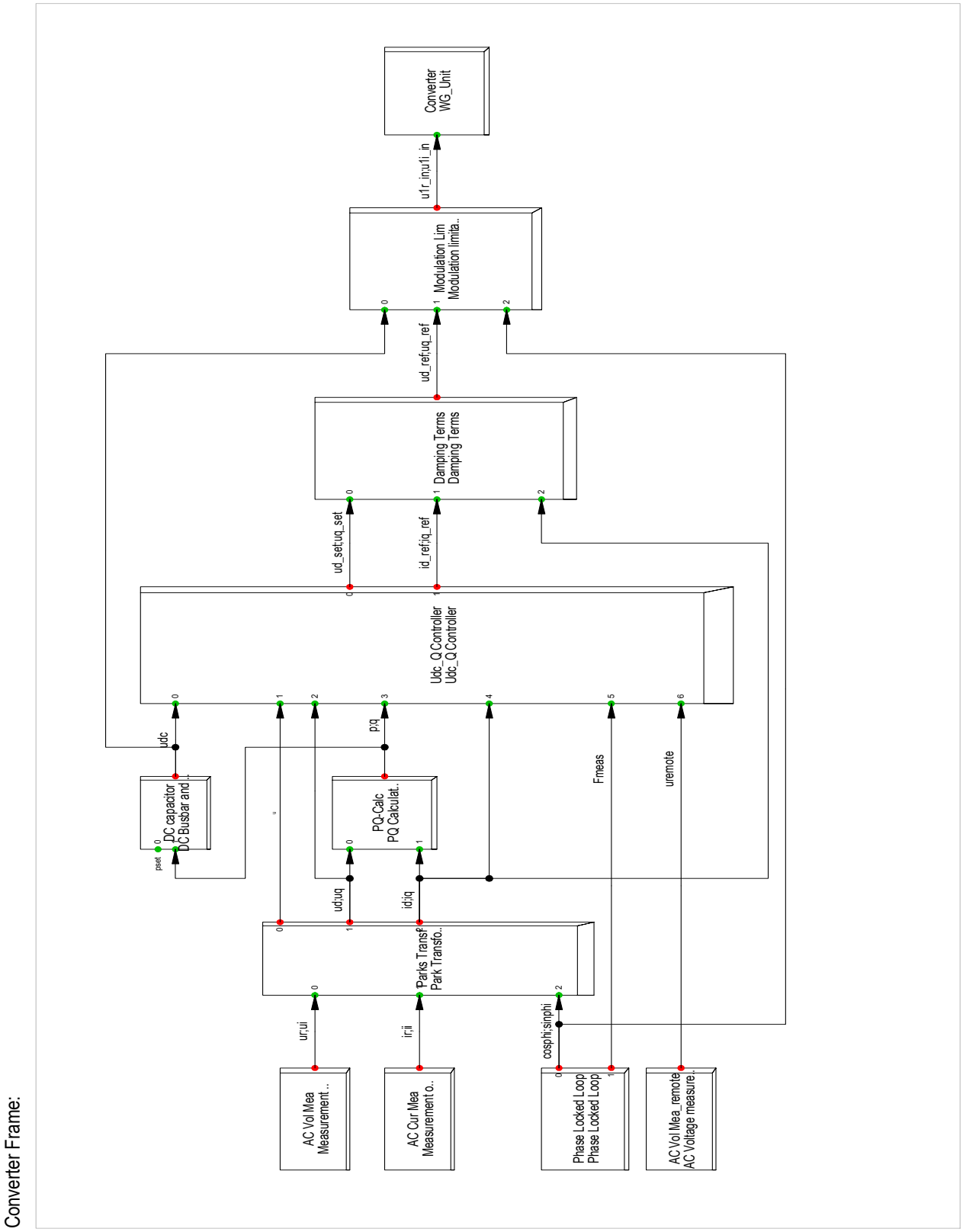

Figure A.16: FSC representation in PowerFactory [38]

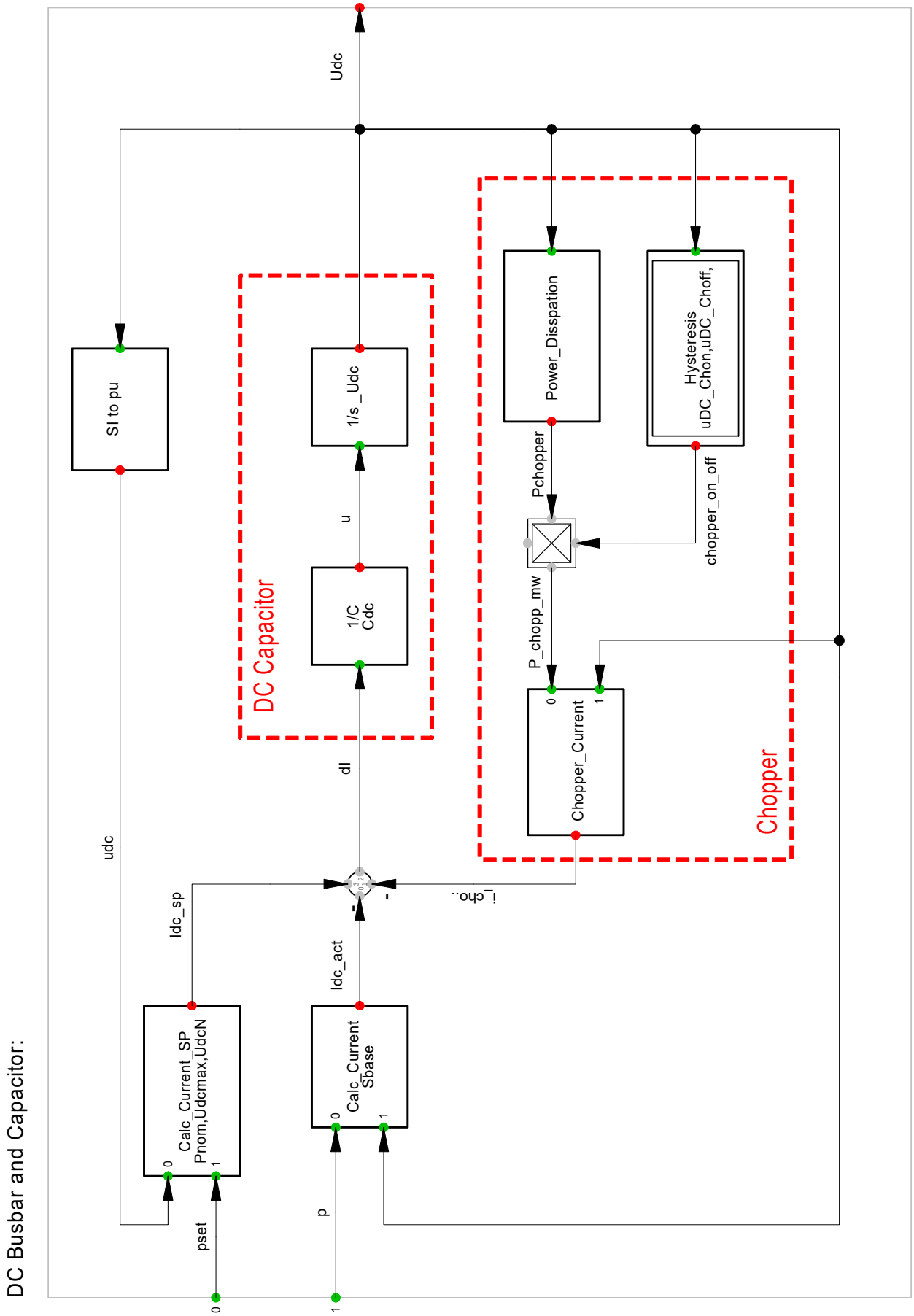

Figure A.17: DC bus representation in PowerFactory [38]

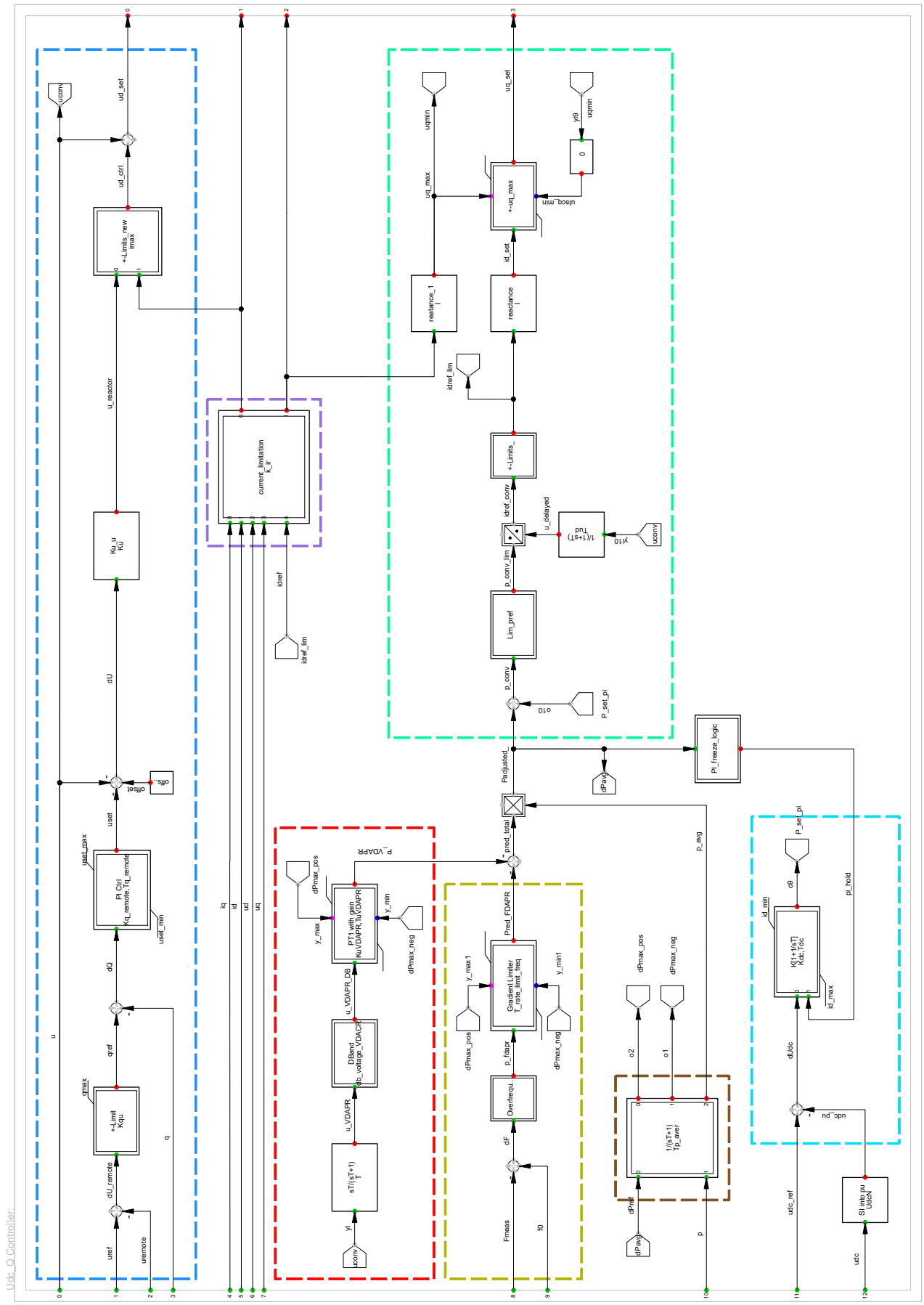

Figure A.18: DVC representation in PowerFactory [38]

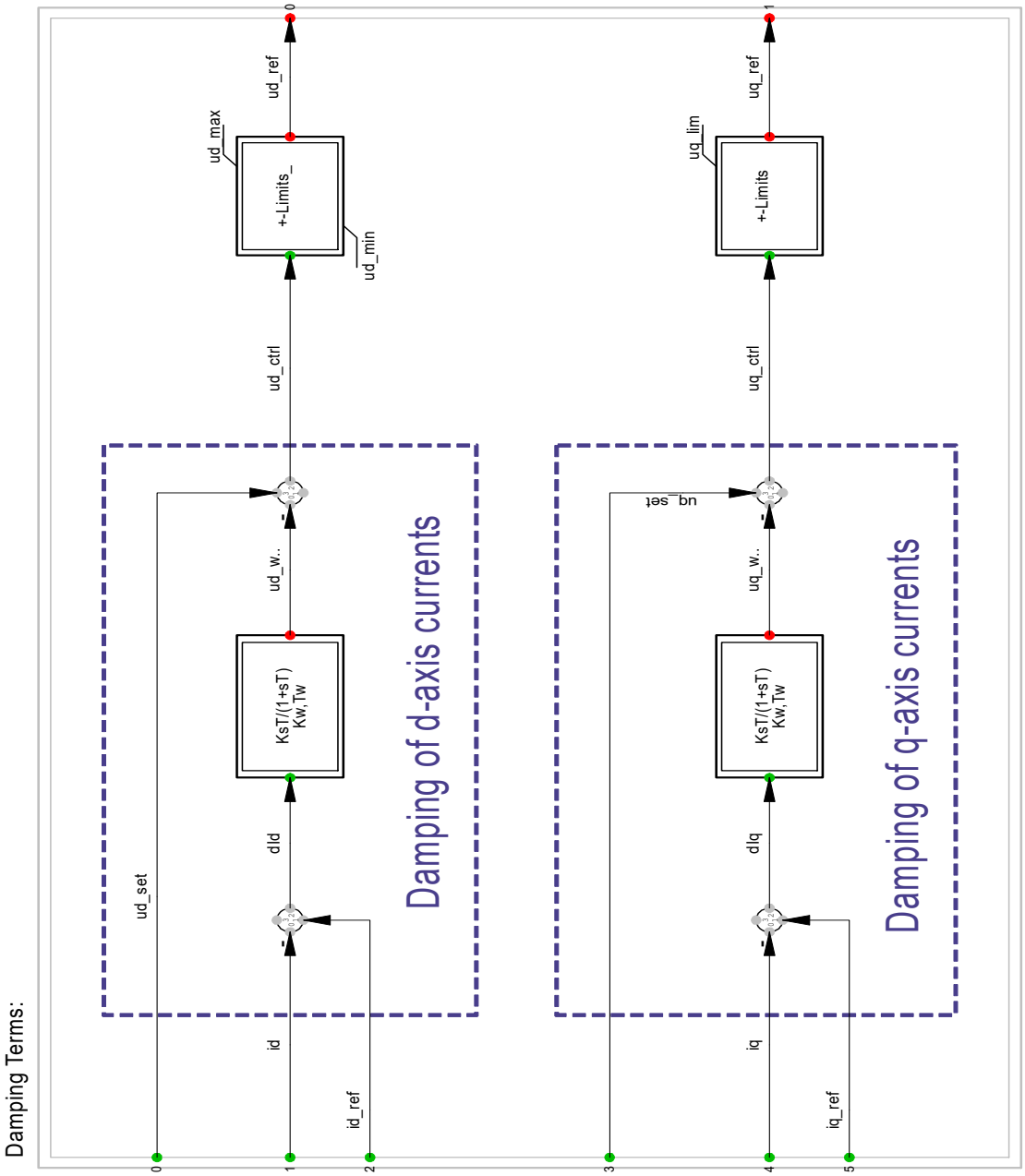

Figure A.19: Washout filter representation in PowerFactory [38]

B

66 kV Network Representation in RSCAD and PowerFactory

B.1. Single OWF 66 kV network, Draft module in RSCAD

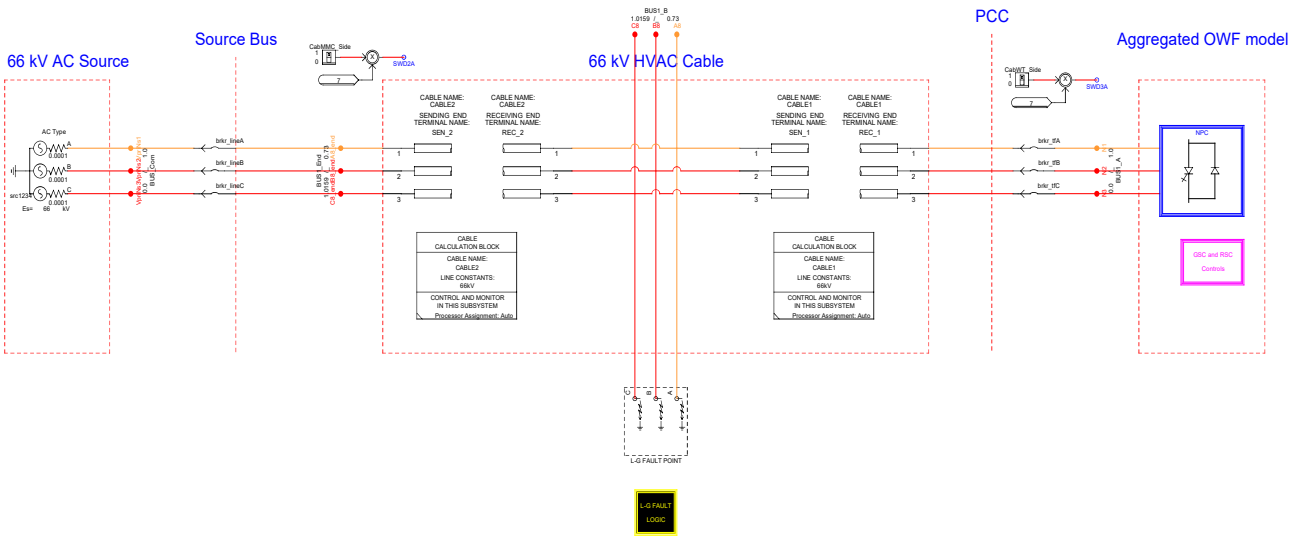

Figure B.1: 66 kV HVAC test system representation in Draft module in RSCAD

B.2. Single OWF 66 kV network, Runtime module in RSCAD

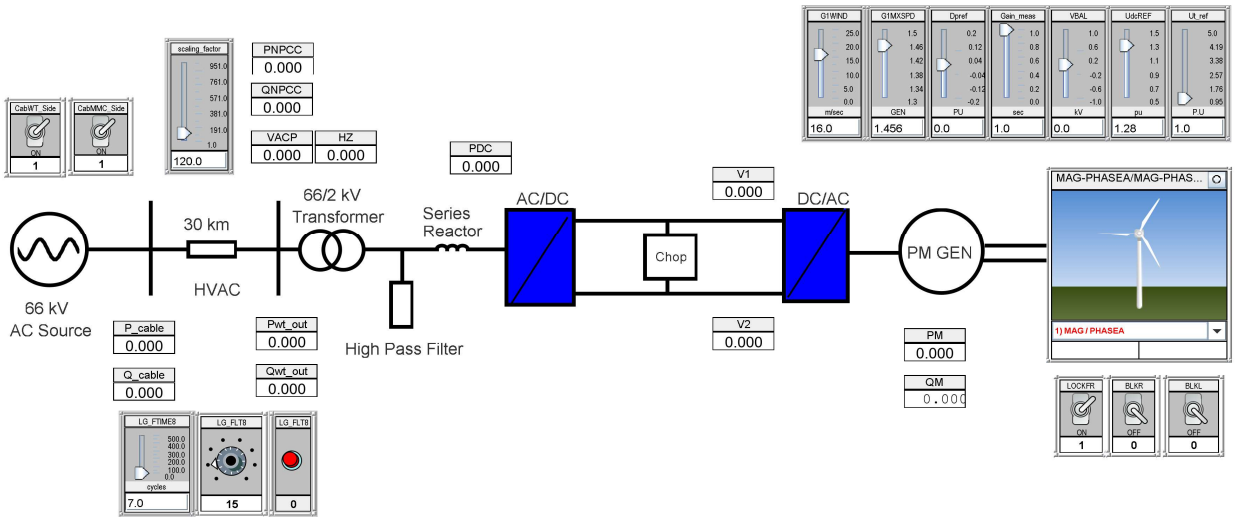

Figure B.2: 66 kV HVAC test system representation in Runtime module in RSCAD

B.3. Single OWF 66 kV network in PowerFactory

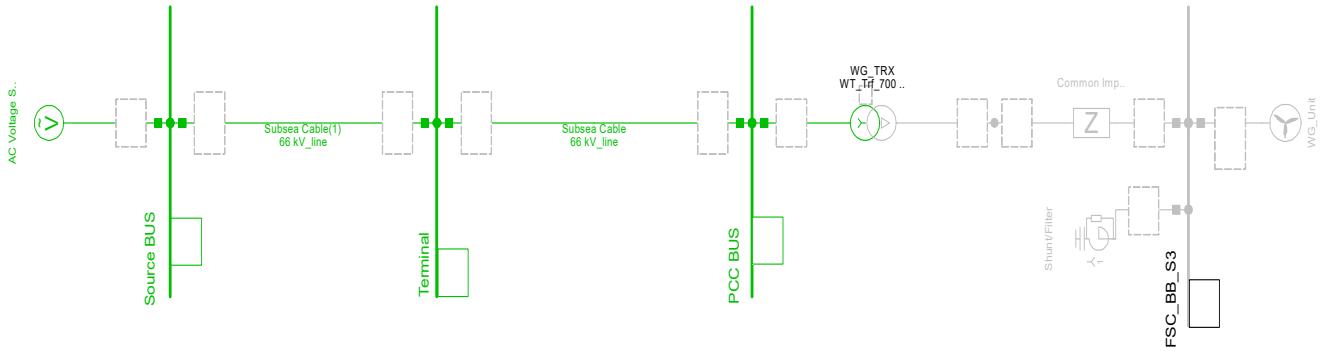

Figure B.3: 66 kV HVAC test system representation in PowerFactory

B.4. Additional graphs

B.4.1. Three-phase line to ground fault

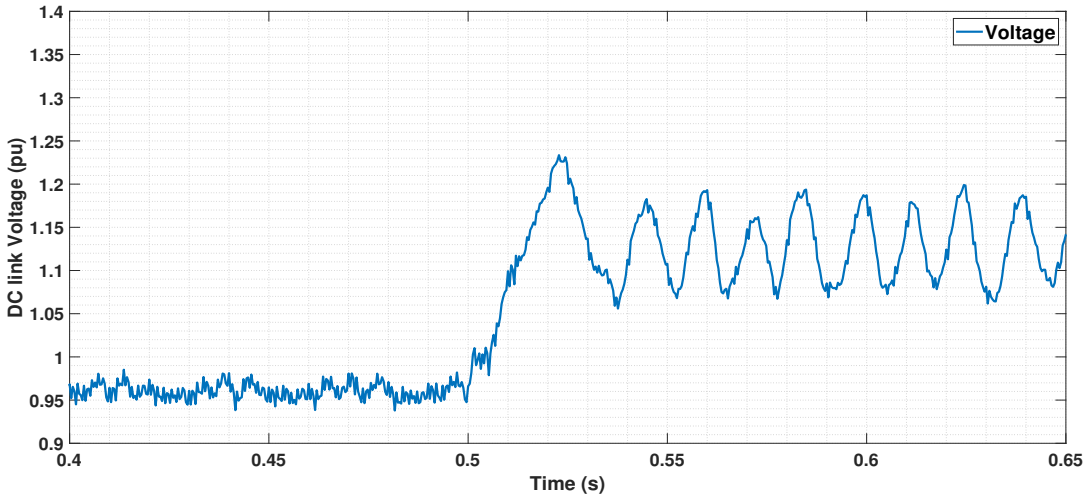

Figure B.4: Voltages at DC link upon three-phase line to ground fault in the middle of cable in RSCAD

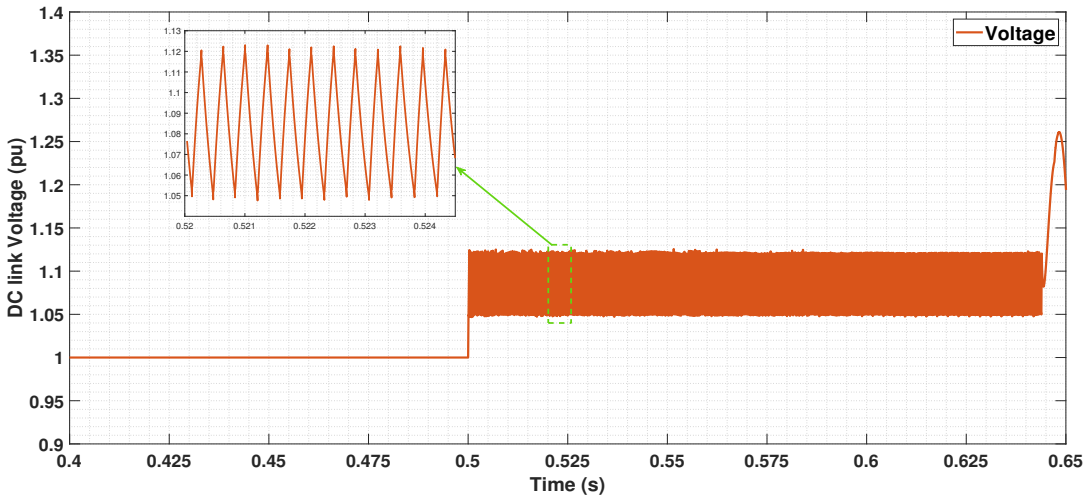

Figure B.5: Voltages at DC link upon three-phase line to ground fault in the middle of cable in PowerFactory

During the time of fault, the DC link voltage increases as seen in the Figures B.4 and B.5. The chopper gets activated when the voltage goes above 1.05 p.u. in both the models. However, switching of the chopper depends on the time delay of the signal given to the triangular wave repeater in the RSCAD model. Whereas, the hysteresis block shown in Figure A.17 determines the activation of the chopper in the PowerFactory model.

C

2 GW Network Representation in RSCAD

C.1. MMCs and HVAC cables in Draft module

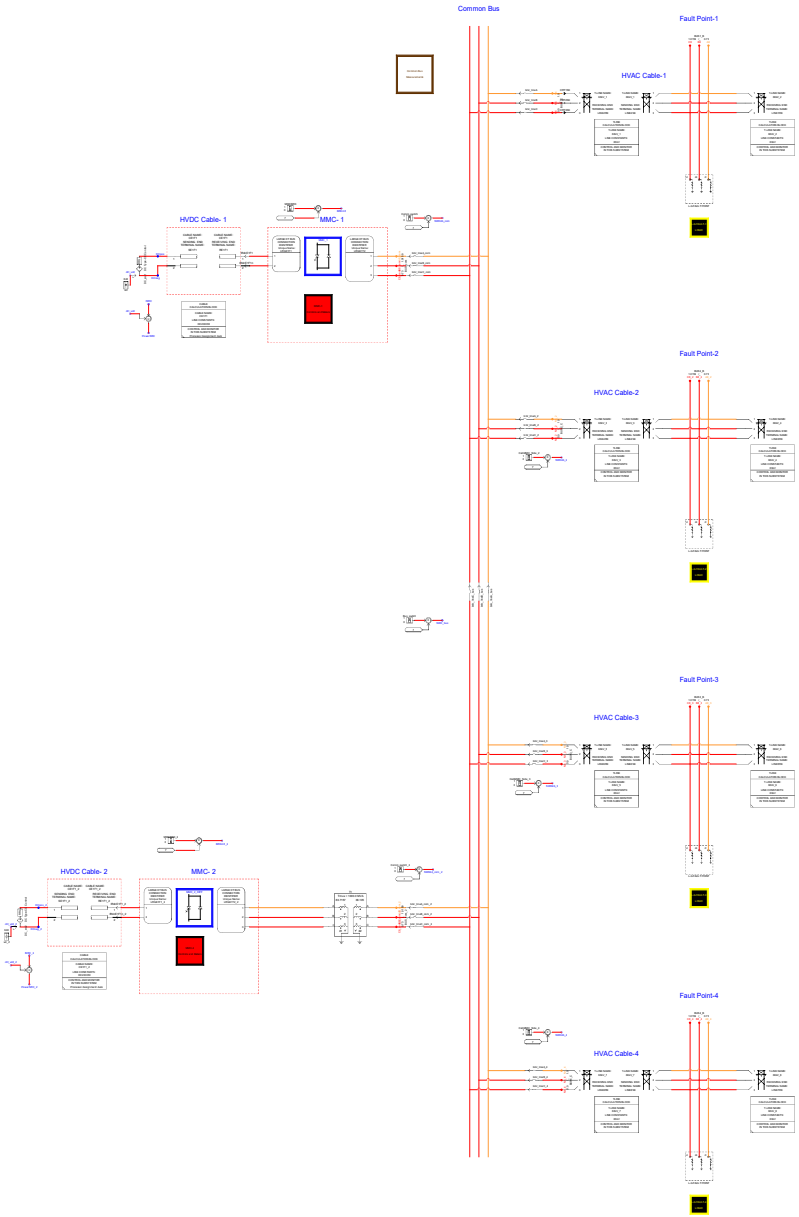

Figure C.1: Subsystem-1: 66 kV HVAC cables connected to offshore converter stations in Draft module in RSCAD

C.2. OWFs in Draft module

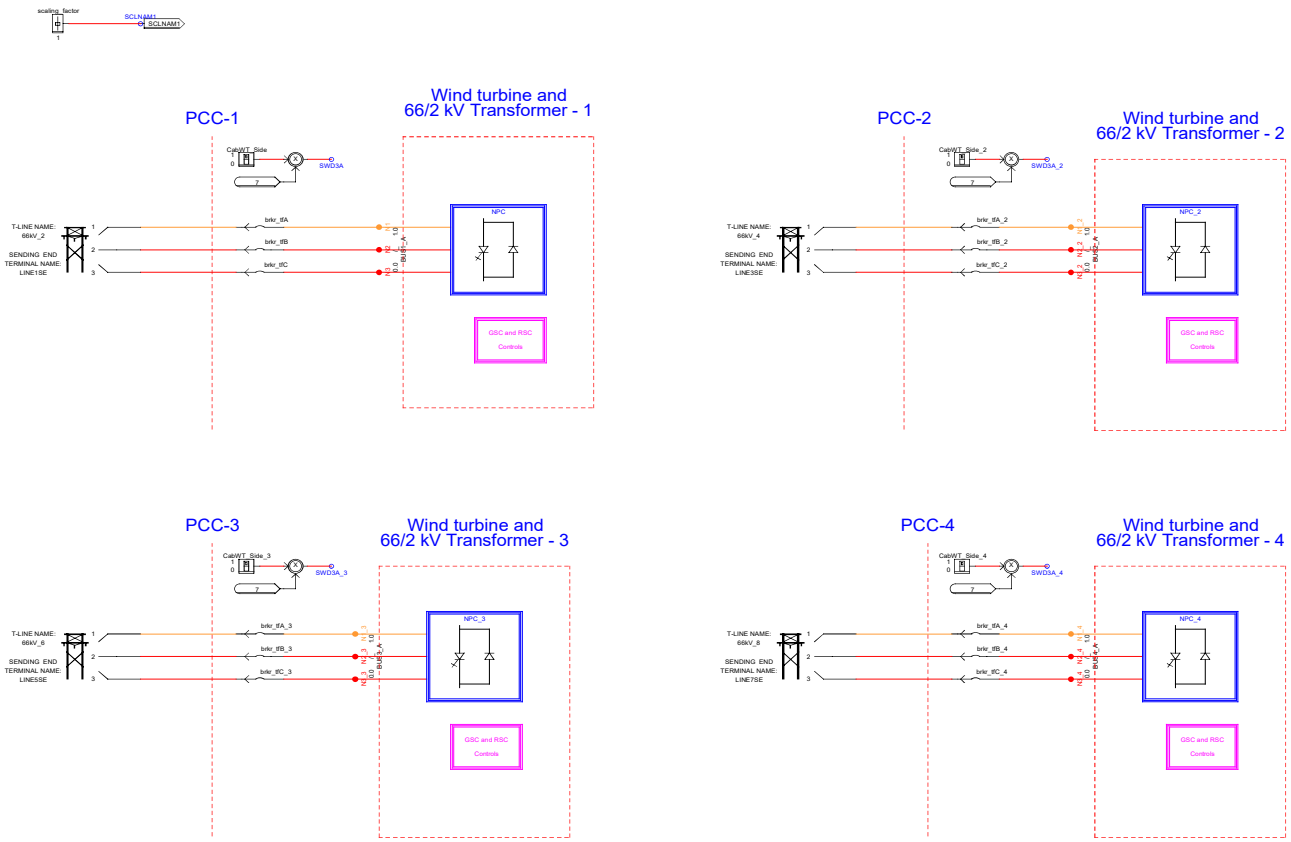

Figure C.2: Subsystem-2: OWFs connected to HVAC cables in Draft module in RSCAD

C.2.1. Modification in Outer Loop Control

In order to simplify the system, the active power loop output variable which is the active power reference (idref2) is made to be controlled by the user using a slider (ID_ref_control) in Runtime file directly as shown in Figure C.3. This allows the user to control the amount of active power flowing through the MMC-2 bus. The 'ID_ref_control' value is varied from 0 to a maximum of 0.4. There is no flow of power in MMC-2 when 'ID_ref_control' = 0. The maximum power flow is achieved when 'ID_ref_control' = 0.4.

The RMS current (I_rms) is calculated at the breaker (CB-1a) and is compared with the maximum current (I_phase_max) which is 10% above the phase current as given in Equation C.2. When 'I_rms' current exceeds 'I_phase_max', 'idref2' is set to zero for that duration. Once, 'I_rms' becomes less than 'I_phase_max', the control is given back to 'ID_ref_control' slider in Runtime module, as shown in Figure C.3. This allows power to flow in MMC-2 after the breaker CB-1a has been operated.

$$I_{phase} = \frac{S_{single\_phase}}{V_{LN}} \tag{C.1}$$

$$I_{phase\_max} = 1.1 * I_{phase} \tag{C.2}$$

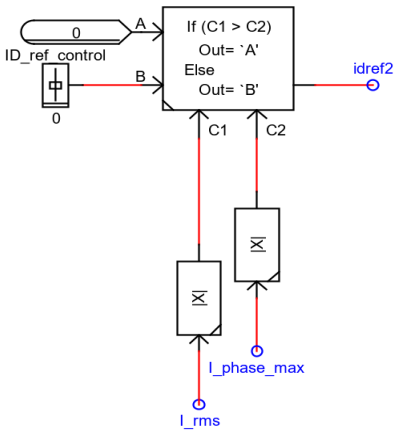

Figure C.3: Idref2 control logic

C.3. Steps for operation of the model in Runtime module

Scaling factor is set to 10 before simulation. ID_ref_control is also set to 0 before starting the simulation.

C.3.1. Energization of the network

- Compile the Draft file "WT4_MMC2_Draft.dft" and ensure there are no errors.
- Open the Runtime file "WT4_MMC2_Draft.sib".
- Switch on the 'MMCBRK' switch to charge the MMC bus.

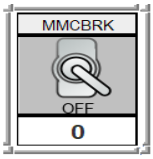

Figure C.4: MMCBRK switch

- Switch on the 'MMCBRK_2' switch to connect MMC-2 to the network.

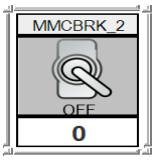

Figure C.5: MMCBRK_2 switch

- Switch on the 'CabMMC_Side' breaker switch to charge Cable-1. Then switch on 'CabWT_Side' breaker switch to connect OWF-1 to the network.

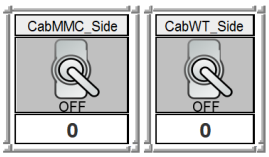

Figure C.6: CabMMC_Side and CabWT_Side switches

- Switch on the 'CabMMC_Side_2' breaker switch to charge Cable-2. Then switch on 'CabWT_Side_2' breaker switch to connect OWF-2 to the network.

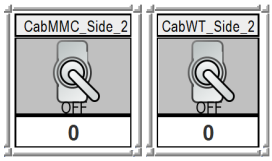

Figure C.7: CabMMC_Side_2 and CabWT_Side_2 switches

- Switch on the 'CabMMC_Side_3' breaker switch to charge Cable-3. Then switch on 'CabWT_Side_3' breaker switch to connect OWF-3 to the network.

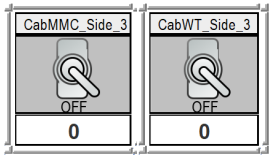

Figure C.8: CabMMC_Side_3 and CabWT_Side_3 switches

- Switch on the 'CabMMC_Side_4' breaker switch to charge Cable-4. Then switch on 'CabWT_Side_4' breaker switch to connect OWF-4 to the network.

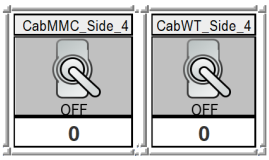

Figure C.9: CabMMC_Side_4 and CabWT_Side_4 switches

After the final step, nearly 200 MW active power flows through MMC-1 and there is no power flow in MMC-2.

C.3.2. Full generation from OWFs and power flow in MMC-1 and MMC-2

- Increase scaling_factor from 10 to 40.
- Change ID_ref_control from 0 to 0.2.
- Increase scaling_factor from 40 to 60.
- Change ID_ref_control from 0.2 to 0.3.
- Increase scaling_factor from 60 to 80.
- Change ID_ref_control from 0.3 to 0.38.
- Increase scaling_factor from 80 to 90.
- Change ID_ref_control from 0.38 to 0.4.
- Finally, increase scaling_factor from 90 to 92.

A total of nearly 2 GW power flows in the network after the above steps. 1 GW through MMC-1 and 1 GW through MMC-2.

ID_ref_control	Power through MMC-2
0	0 MW
0.2	475 MW
0.4	950 MW

Table C.1: Power flow control in MMC-2

C.3.3. Disconnection of One OWF

OWF-2 is chosen for this thesis.

- Open the breaker switch 'CabMMC_Side_2' to disconnect OWF-2.
- The above test can also be performed on other OWFs as well by opening 'CabMMC_Side' for OWF-1, 'CabMMC_Side_3' for OWF-3 and 'CabMMC_Side_4' for OWF-4 respectively.

C.3.4. Three-phase line to ground fault

The control logic in Figure C.3 and the breaker logic in Section 5.20 is modelled for HVAC cable-1 for this work.
First, the steps C.3.1 and C.3.2 must be performed to achieved 2 GW power transmission.

- Switch on the 'Activ' switch to change control of circuit breaker CB-1a from 'CabMMC_Side' switch to the logic explained in Section 5.4.2.1. The network still operates in steady state in this condition.
- Apply the fault by clicking the 'LG_FLT8' button (red in colour).

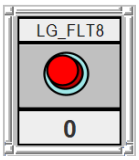

Figure C.10: Fault button

C.4. Additional graphs

C.4.1. Disconnection of OWF-2

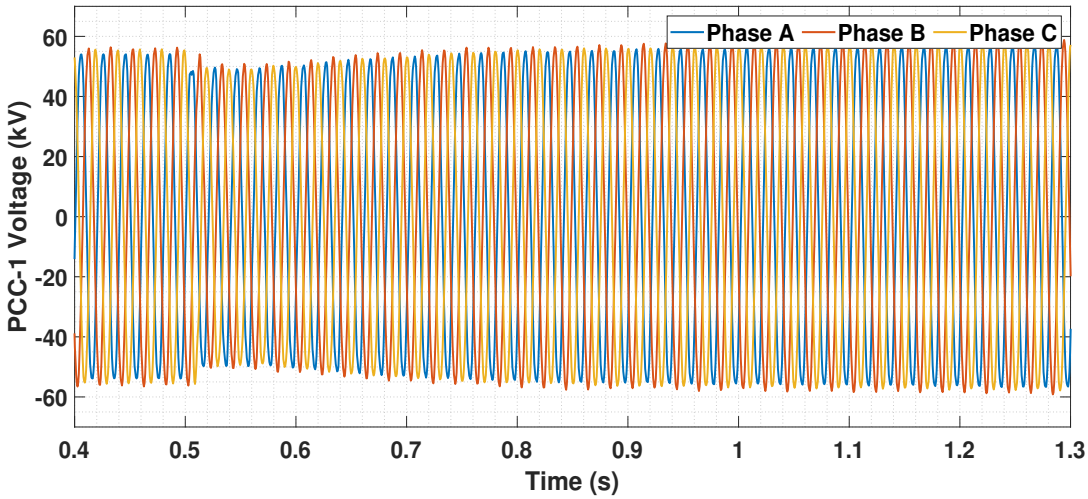

Figure C.11: Voltages at PCC-1 upon OWF-2 disconnection event

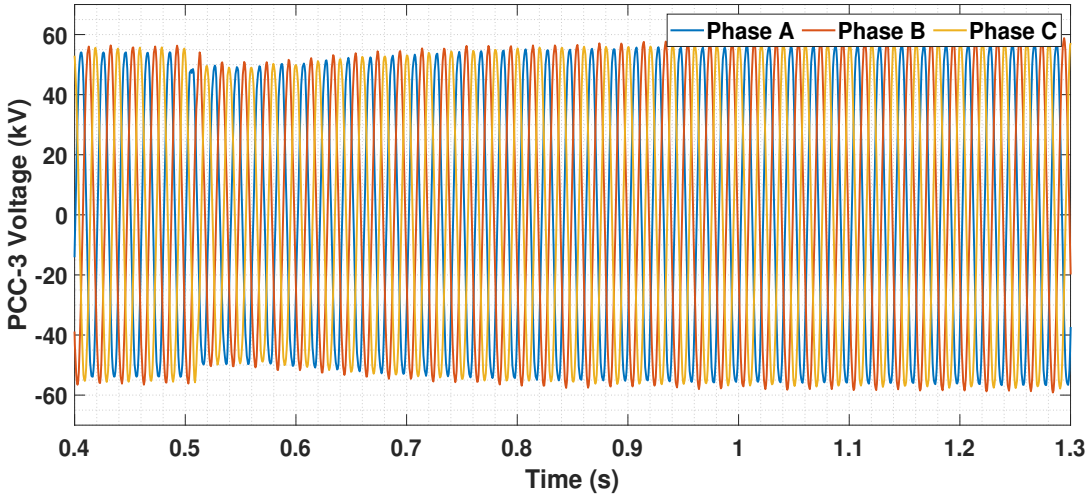

Figure C.12: Voltages at PCC-3 upon OWF-2 disconnection event

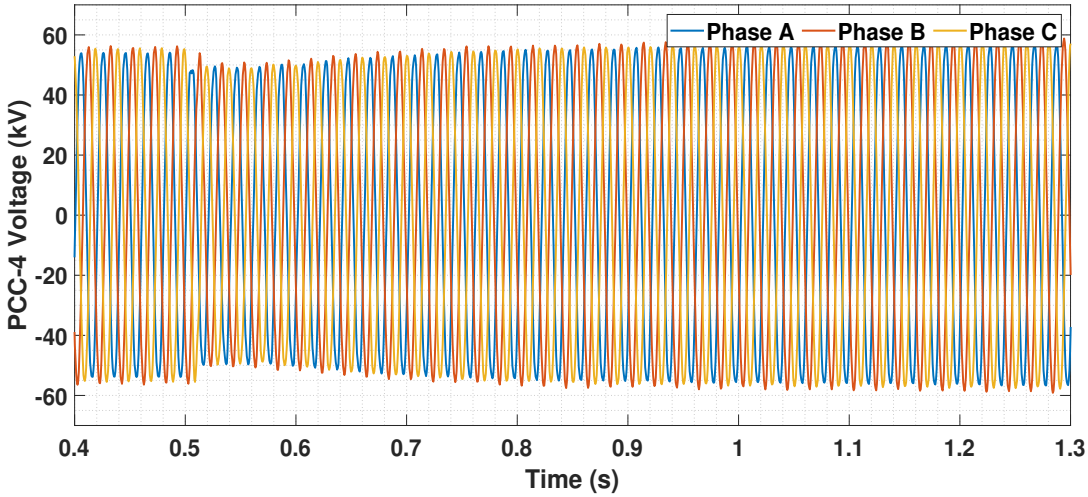

Figure C.13: Voltages at PCC-4 upon OWF-2 disconnection event

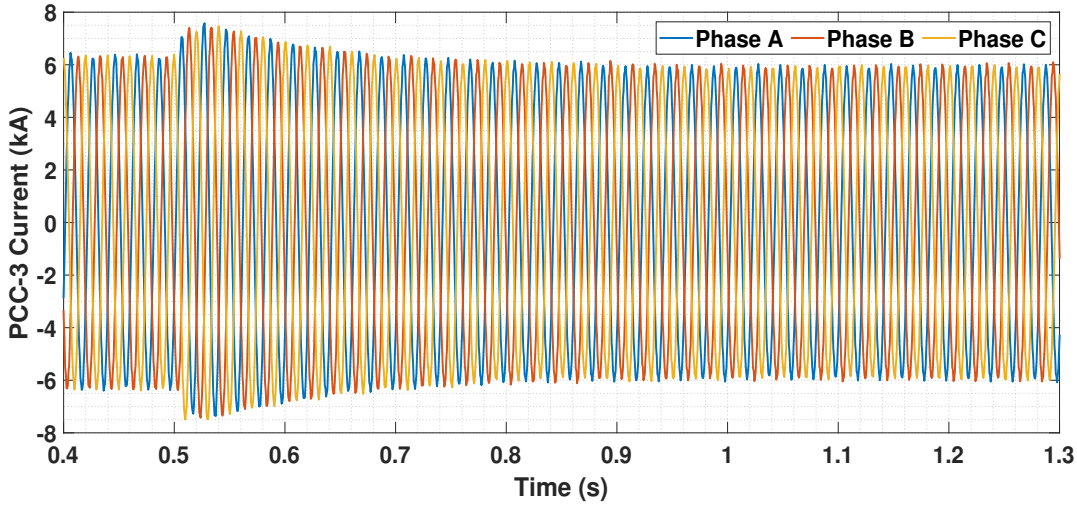

Figure C.14: Currents in PCC-3 upon OWF-2 disconnection event

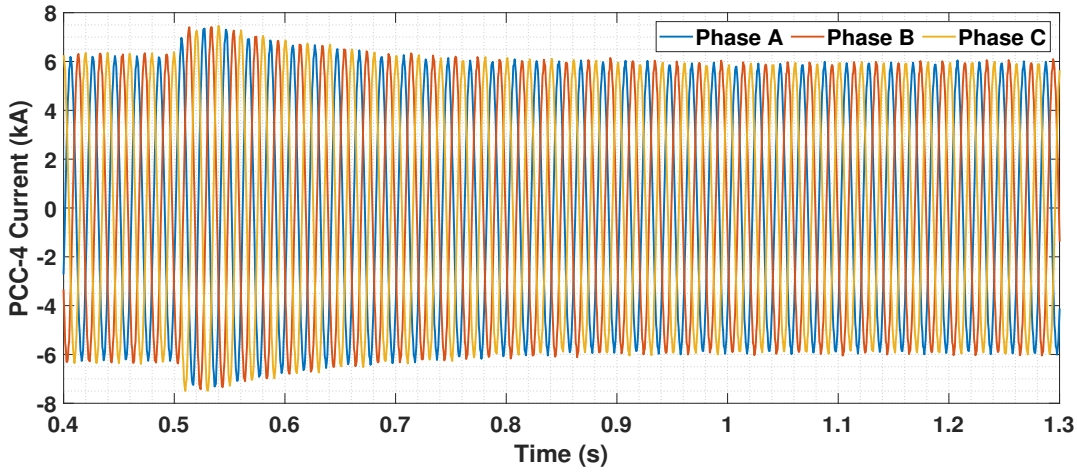

Figure C.15: Currents in PCC-4 upon OWF-2 disconnection event

C.4.2. Three-phase fault line to ground fault

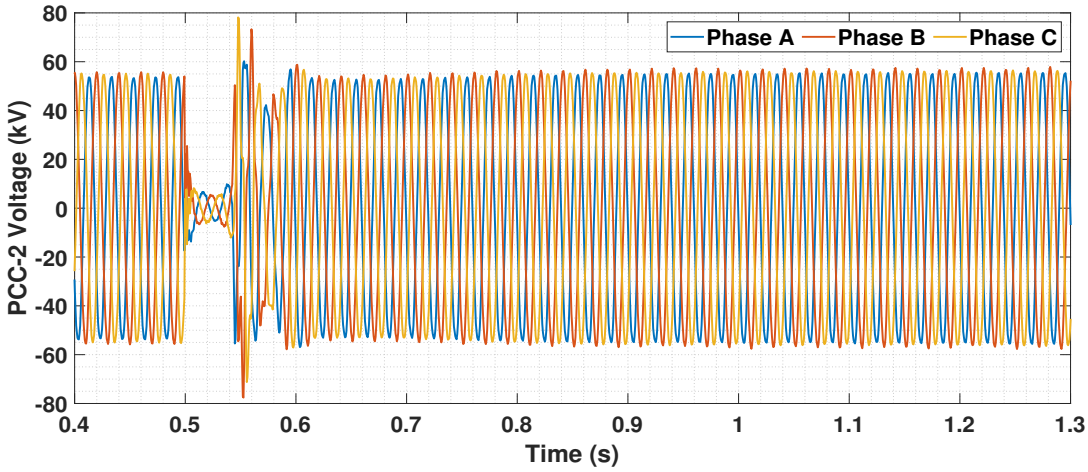

Figure C.16: Voltages at PCC-2 upon three-phase line to ground fault in the middle of cable-1

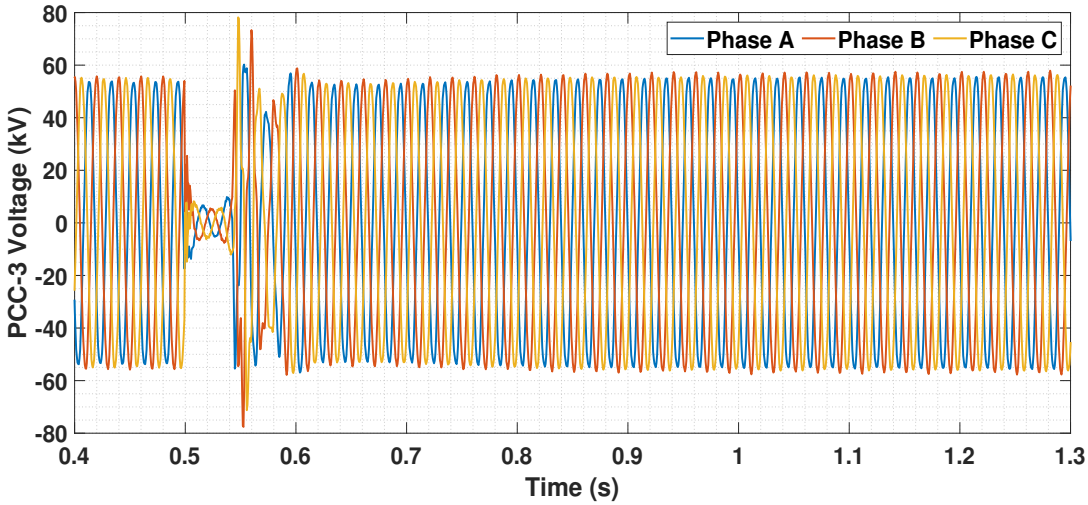

Figure C.17: Voltages at PCC-3 upon three-phase line to ground fault in the middle of cable-1

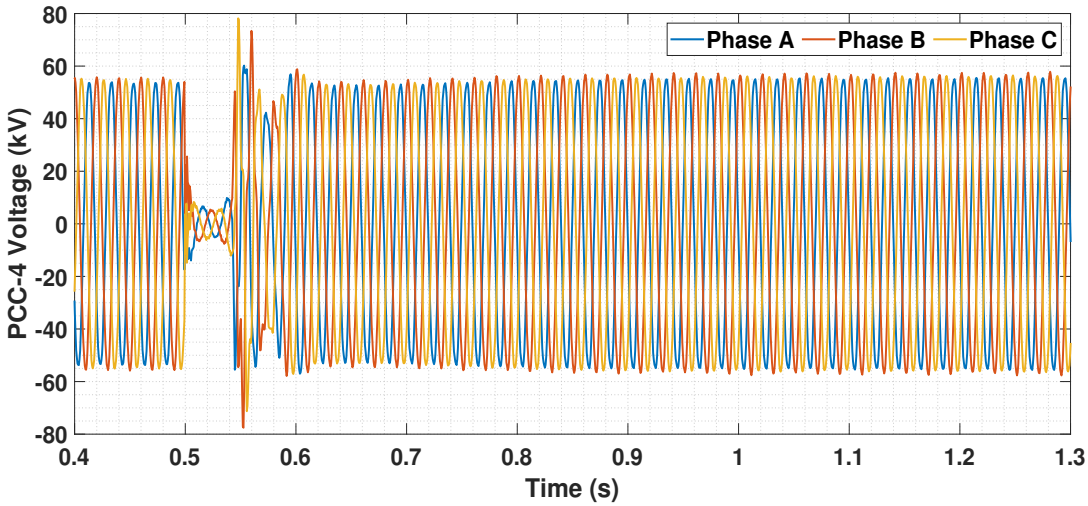

Figure C.18: Voltages at PCC-4 upon three-phase line to ground fault in the middle of cable-1

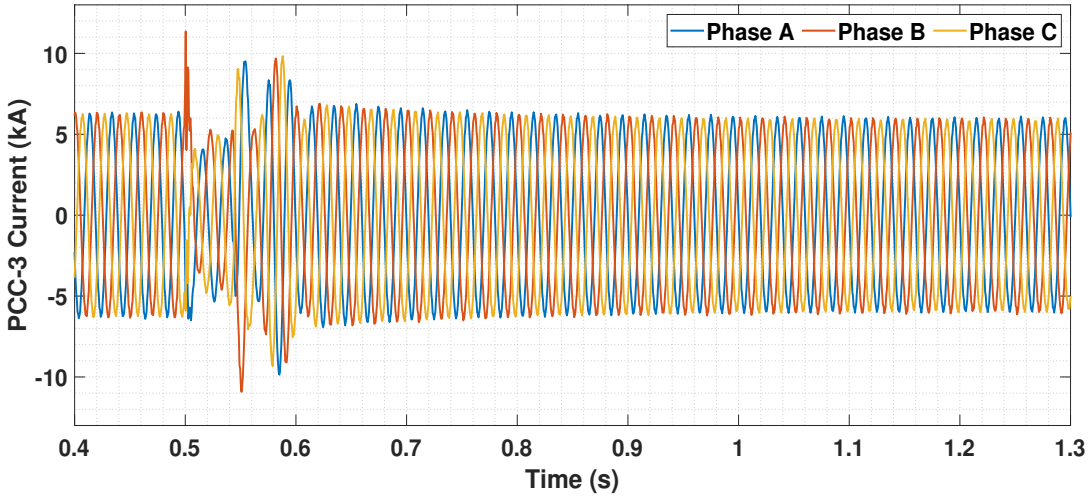

Figure C.19: Currents in PCC-3 upon three-phase line to ground fault in the middle of cable-1

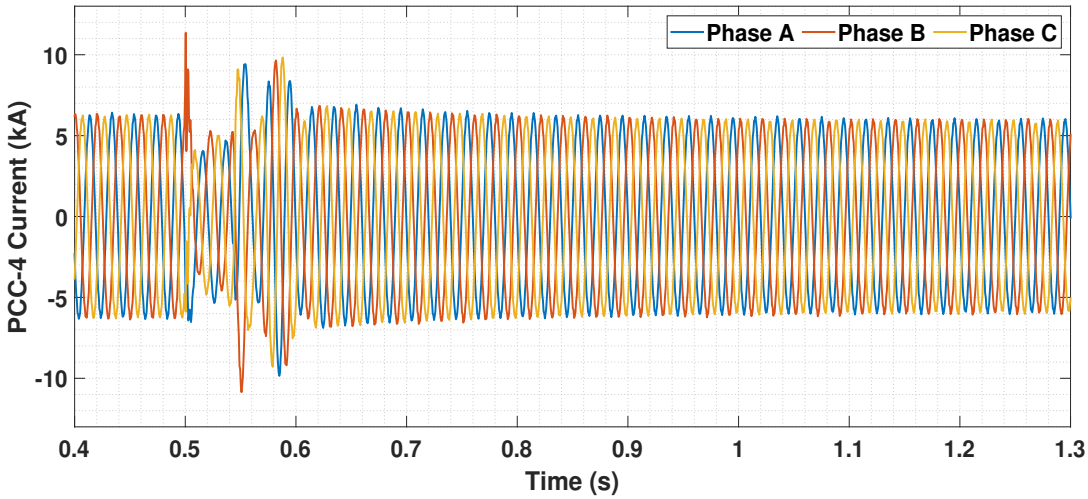

Figure C.20: Currents in PCC-4 upon three-phase line to ground fault in the middle of cable-1

D

Parameters and Configurations in RSCAD

D.1. Reactive power control parameters in DVC

Parameter	Description	Unit	Value
k_{QV}	Static gain for slow global reactive power control	p.u.	6.6
$q_{max/min}$	Maximum/minimum reactive power	p.u.	0.31
k_Q	Slow global reactive power control proportional gain	p.u.	0.002
T_Q	Slow global reactive power control integral time constant	s	15
k_V	Fast local voltage control proportional gain	p.u.	0.2
x	Converter reactance	p.u.	0.1
k_P	Washout filter proportional gain	p.u.	0.05
T_w	Washout filter time constant	s	0.01

Table D.1: Parameters of reactive power control loop in DVC [38]

D.2. Active power control parameters in DVC

Parameter	Description	Unit	Value
k_S	DC voltage control proportional gain	p.u.	1
T_S	DC voltage control integral time constant	p.u.	0.1
k_{Rf}	Proportional gain for direct frequency control	p.u.	1
T_{Rf}	First order delay for direct frequency control	s	0.2
T_{U_v}	Washout time constant for the voltage dependent active power reduction	s	60
k_{Ufv}	Proportional gain for voltage dependent active power reduction	p.u.	2
T_{Ufv}	First order delay for the voltage dependent active power reduction	s	0.005
x	Converter reactance	p.u.	0.1
k_Q	Washout filter proportional gain	p.u.	0.05
T_w	Washout filter time constant	s	0.01
T_a	Voltage measurement delay	s	5
	Deadband for direct frequency control	Hz	0.2
	Deadband for voltage dependent active power reduction	p.u.	0.1

Table D.2: Parameters of active power control loop in DVC [38]

D.3. V/F control parameters

Parameter	Unit	Value
k_{p_vf}	p.u.	0.2
k_{i_vf}	p.u.	30

Table D.3: Parameters for PI gains in V/F control loop [48]

D.4. Cable module configuration

The cable module opens a cable setup popup menu into which the cable parameters are added. The file is then compiled and saved in a ".clo" file format. The cable parameters are referenced through the external file previously created using the cable module. In RSCAD, Pi cable models are derived from Bergeron cable model. Initially, a Bergeron cable model is created with RLC parameters and then the option to make it work as a Pi model is chosen. The ".clo" file must be added first using the 'Dnm1' option, which is obtained by double-clicking on the calculation box (Figure D.1(a)). The cable constants are of type Bergeron as chosen in the 'cntyp' parameter in Figure D.1(a). The 'frcpi' parameter available in the "Options when using Bergeron data" tab, forces the use of Pi section model manually by the user. The selection is made, as shown by the red box in Figure D.1(b). The terminal block must be specified as either the sending or receiving end as shown in Figure D.2 and the cable name provided in the calculation block has to be entered in the terminal blocks as well.

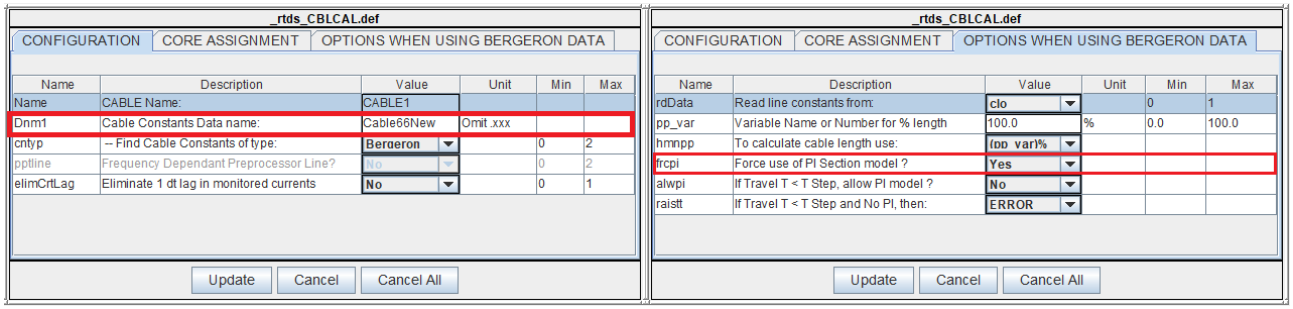

(a) Cable configuration

(b) Additional options

Figure D.1: Configuration of the calculation block

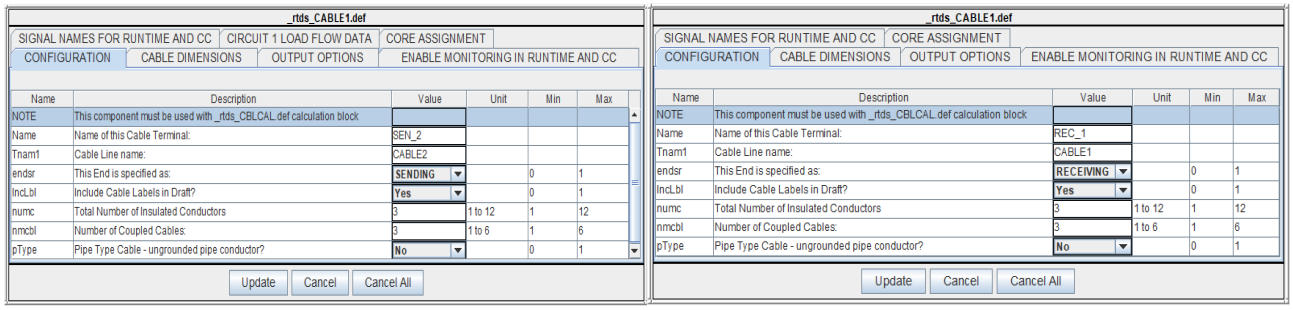

(a) Sending end terminal

(b) Receiving end terminal

Figure D.2: Configuration of the terminal blocks

D.5. Core assignment in RSCAD

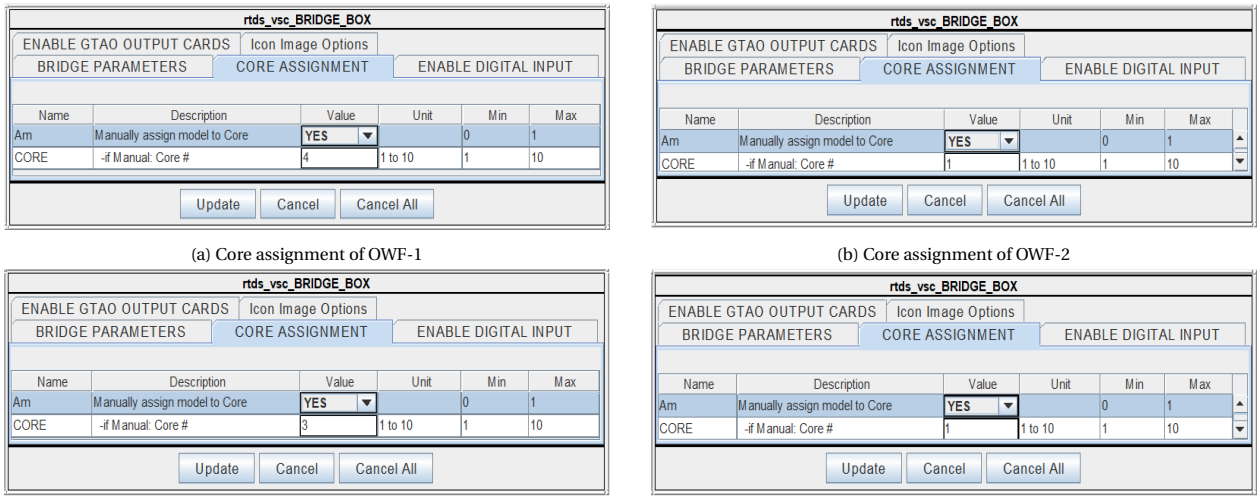

(a) Core assignment of OWF-1

(b) Core assignment of OWF-2

(c) Core assignment of OWF-3

(d) Core assignment of OWF-4

Figure D.3: Core assignment of the 4 small time step boxes representing 4 OWFs

After assigning the cores for the small time step blocks, the processor assignment for subsystem 2 is as illustrated in Figure D.4. The 'Core Assignment' tab is available by right-clicking the small time block and choosing "Edit" and then "Parameters" as shown in Figure D.3. Setting the 'Am' parameter to 'No' for all the small time blocks causes all the available cores to be full and leaving no room for a processor to allocate control signals. Hence these cores should be manually assigned, and proper allocation has to be done.

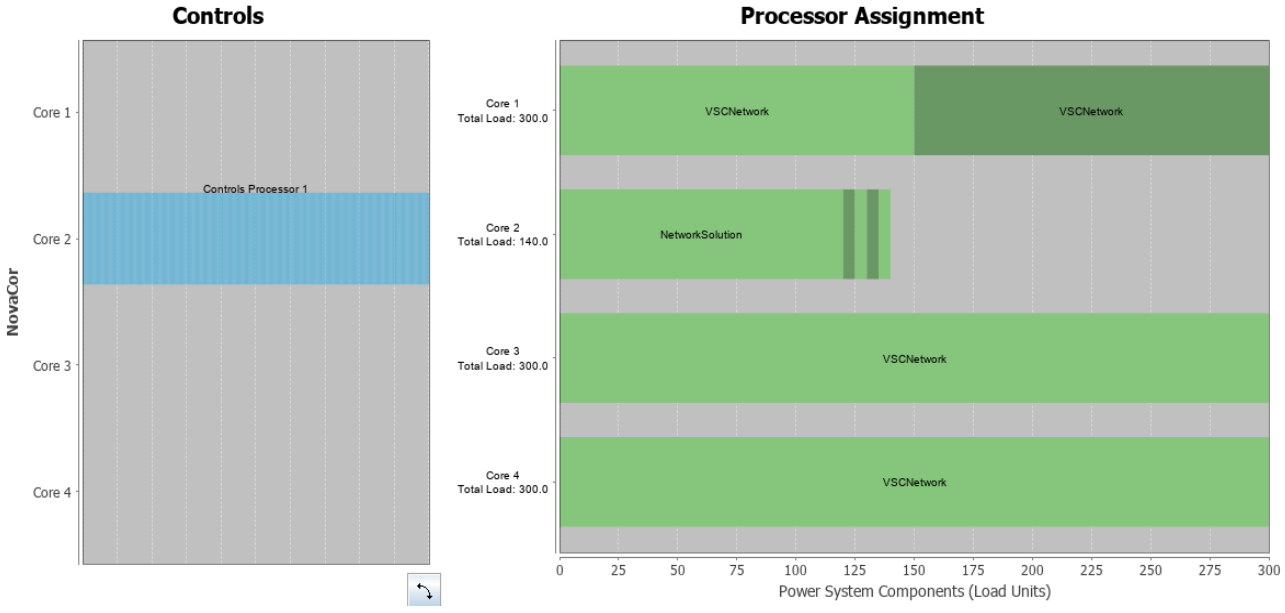

Figure D.4: Processor assignment chart for subsystem 2

D.6. Tline module configuration

The parameters are entered in the Tline popup menu, and the file is compiled and saved in a ".clo" format.

The cable parameters are referenced through the external file previously created using the cable module. The ".clo" file must be added first using the 'Dnm1' option, which is obtained by double-clicking on the calculation box (Figure 4.8). The cable constants are of type Bergeron as chosen in the 'cntyp' parameter in Figure D.1(a).

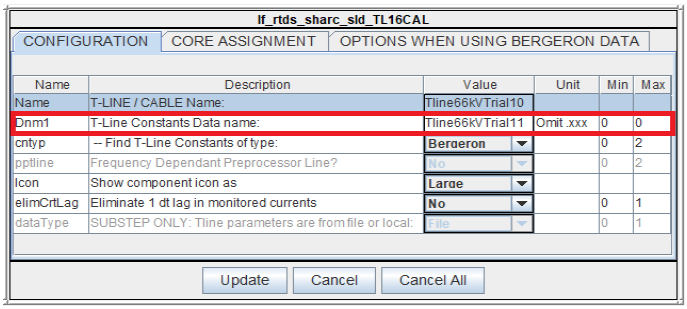

Figure D.5: Configuring Tline model in RSCAD

D.7. Representation of symmetrical monopole configuration in RSCAD

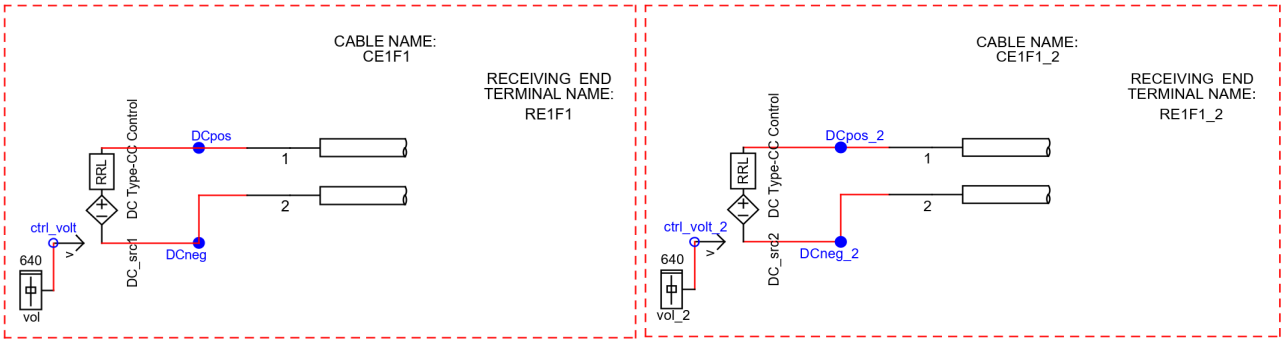

(a) DC source-1 connected to the receiving end of HVDC cable-1

(b) DC source-2 connected to the receiving end of HVDC cable-2

Figure D.6: Onshore converter stations representation using DC sources in RSCAD

Bibliography

[1] UNFCCC, "Adoption of the Paris agreement. COP," *25th session Paris*, vol. 30, 2015.

[2] "Vision – Northseawindpowerhub," 2020. [Online]. Available: https://northseawindpowerhub.eu/vision/

[3] "TenneT develops first 2GW offshore grid connection with suppliers," Feb. 2020. [Online]. Available: https://www.tennet.eu/news/detail/tennet-develops-first-2gw-offshore-grid-connection-with-suppliers/

[4] "The first Hub-and-Spoke energy island – Northseawindpowerhub," 2020. [Online]. Available: https://northseawindpowerhub.eu/the-first-hub-and-spoke-energy-island/

[5] G. Denis, T. Prevost, M.-S. Debry, F. Xavier, X. Guillaud, and A. Menze, "The Migrate project: the challenges of operating a transmission grid with only inverter-based generation. A grid-forming control improvement with transient current-limiting control," *IET Renewable Power Generation*, vol. 12, no. 5, pp. 523–529, Apr. 2018. [Online]. Available: https://digital-library.theiet.org/content/journals/10.1049/iet-rpg.2017.0369

[6] Ecofys, "Translate COP21: 2045 outlook and implications for offshore wind in the North Seas," Technical Report, 2017.

[7] "HVDC Connection of Offshore Wind Power Plants," CIGRE Working Group B4.55, Technical Brochure 619, 2015.

[8] J. Peralta, H. Saad, S. Dennetière, J. Mahseredjian, and S. Nguefeu, "Detailed and Averaged Models for a 401-level MMC-HVDC system," *IEEE Transactions on Power Delivery*, vol. 27, no. 3, pp. 1501–1508, 2012.

[9] E. Telaretti, G. Graditi, M. Ippolito, and G. Zizzo, "Economic feasibility of stationary electrochemical storages for electric bill management applications: The Italian scenario," *Energy Policy*, vol. 94, pp. 126–137, Jul. 2016. [Online]. Available: https://linkinghub.elsevier.com/retrieve/pii/S0301421516301707

[10] Abdelwahed, Mohamed Abdelaziz and El-Saadany, Ehab F, "Power Sharing Control Strategy of Multiterminal VSC-HVDC Transmission Systems Utilizing Adaptive Voltage Droop," *IEEE Transactions on Sustainable Energy*, vol. 8, no. 2, pp. 605–615, 2016.

[11] DNV.GL, "66 kV Systems for Offshore Wind Farms," Technical Brochure, 2015.

[12] M. Mohseni and S. M. Islam, "Review of international grid codes for wind power integration: Diversity, technology and a case for global standard," *Renewable and Sustainable Energy Reviews*, vol. 16, no. 6, pp. 3876–3890, Aug. 2012. [Online]. Available: https://linkinghub.elsevier.com/retrieve/pii/S1364032112002225

[13] K. Sharifabadi, L. Harnefors, H.-P. Nee, S. Norrga, and R. Teodorescu, *Design, Control, and Application of Modular Multilevel Converters for HVDC Transmission Systems*. John Wiley & Sons, 2016.

[14] P. Lozada Ayala, "Dynamic System Performance Analysis of a Novel Grid Connection Topology for Offshore Wind Farms Using MMC-HVDC Transmission," 2018. [Online]. Available: https://repository.tudelft.nl/islandora/object/uuid%3Abfd0ac94-fc5b-46e4-a049-742c5249138a

[15] B. Weise, A. Korai, and A. Constantin, "Comparison of Selected Grid-Forming Converter Control Strategies for Use in Power Electronic Dominated Power Systems," in *Proceedings of the 18th Wind Integration Workshop, Dublin, Ireland*, 2019, pp. 16–18.

[16] U. Markovic, Z. Chu, P. Aristidou, and G. Hug, "LQR-Based Adaptive Virtual Synchronous Machine for Power Systems with High Inverter Penetration," *IEEE Transactions on Sustainable Energy*, vol. 10, no. 3, pp. 1501–1512, 2018.

[17] D. Duckwitz, F. Welck, and C. Glöckler, "Operational Behavior of the Virtual Synchronous Machine," *Fachtagung Netzregelung und Systemführung*, 2017.

[18] L. Lu and N. A. Cutululis, "Virtual synchronous machine control for wind turbines: a review," *Journal of Physics: Conference Series*, vol. 1356, p. 012028, Oct. 2019. [Online]. Available: https://iopscience.iop.org/article/10.1088/1742-6596/1356/1/012028

[19] A. E. M. Bouzid, P. Sicard, A. Yamane, and J.-N. Paquin, "Simulation of droop control strategy for parallel inverters in autonomous ac microgrids," in *2016 8th International Conference on Modelling, Identification and Control (ICMIC)*. IEEE, 2016, pp. 701–706.

[20] M. Yu, A. J. Roscoe, C. D. Booth, A. Dysko, R. Ierna, J. Zhu, and H. Urdal, "Use of an inertia-less Virtual Synchronous Machine within future power networks with high penetrations of converters," in *2016 Power Systems Computation Conference (PSCC)*. IEEE, 2016, pp. 1–7.

[21] A. W. Korai, "Dynamic Performance of Electrical Power Systems with High Penetration of Power Electronic Converters: Analysis and New Control Methods for Mitigation of Instability Threats and Restoration," 2019. [Online]. Available: https://duepublico2.uni-due.de/receive/duepublico_mods_00048074

[22] I. Erlich, A. Korai, T. Neumann, M. Koochack Zadeh, S. Vogt, C. Buchhagen, C. Rauscher, A. Menze, and J. Jung, "New Control of Wind Turbines Ensuring Stable and Secure Operation Following Islanding of Wind Farms," *IEEE Transactions on Energy Conversion*, vol. 32, no. 3, pp. 1263–1271, Sep. 2017. [Online]. Available: http://ieeexplore.ieee.org/document/7990199/

[23] D. Duckwitz, "Derivation of Requirements and Comparison of Inertia Emulation Methods for Converter-based Power PlantsPower System Inertia," Ph.D. dissertation, Universität Kassel, 2019. [Online]. Available: https://kobra.uni-kassel.de/handle/123456789/11261

[24] X. Liu and A. Lindemann, "Control of VSC-HVDC Connected Offshore Windfarms for Providing Synthetic Inertia," *IEEE Journal of Emerging and Selected Topics in Power Electronics*, vol. 6, no. 3, pp. 1407–1417, 2017.

[25] S. Sethi, "Real-Time implementation for Gird Forming Control of Type-4 Wind Turbine to mitigate voltage and frequency instabilities in high renewable penetration." Master's thesis, NTNU, 2019.

[26] J. F. Manwell, J. G. McGowan, and A. L. Rogers, *Wind Energy Explained: Theory, Design and Application*. John Wiley & Sons, 2010.

[27] V. Yaramasu, B. Wu, P. C. Sen, S. Kouro, and M. Narimani, "High-power wind energy conversion systems: State-of-the-art and emerging technologies," *Proceedings of the IEEE*, vol. 103, no. 5, pp. 740–788, May 2015. [Online]. Available: http://ieeexplore.ieee.org/document/7109820/

[28] M. Ali, *Wind energy systems: Solutions for power quality and stabilization*. Boca Raton, FL: CRC Press, 2012.

[29] T. Sebastian and G. Slemon, "Transient modeling and performance of variable-speed permanent-magnet motors," *IEEE Transactions on Industry Applications*, vol. 25, no. 1, pp. 101–106, Jan. 1989. [Online]. Available: http://ieeexplore.ieee.org/document/18878/

[30] RTDS Technologies, "RSCAD Modules," 2020. [Online]. Available: https://knowledge.rtds.com/hc/en-us/articles/360037537653

[31] "Appendix A: Voltage Source Converter Topologies," in *Offshore Wind Energy Generation*. John Wiley & Sons, Ltd, 2014, pp. 223–269, _eprint: https://onlinelibrary.wiley.com/doi/pdf/10.1002/9781118701638.app1. [Online]. Available: https://onlinelibrary.wiley.com/doi/abs/10.1002/9781118701638.app1

[32] M. Ndreko, "Offshore wind power plants with VSC-HVDC transmission: Grid code compliance optimization and the effect on high voltage ac transmission system," Ph.D. dissertation, Delft University of Technology, 2017.

[33] N. P. W. Strachan and D. Jovcic, "Stability of a Variable-Speed Permanent Magnet Wind Generator With Weak AC Grids," *IEEE Transactions on Power Delivery*, vol. 25, no. 4, pp. 2779–2788, Oct. 2010. [Online]. Available: http://ieeexplore.ieee.org/document/5570107/

[34] "Variable-Speed Wind Energy Systems with Synchronous Generators," in *Power Conversion and Control of Wind Energy Systems*. Hoboken, NJ, USA: John Wiley & Sons, Inc., Sep. 2011, pp. 275–316. [Online]. Available: http://doi.wiley.com/10.1002/9781118029008.ch9

[35] "ABB review : Special report 60 years of HVDC," ABB, Geneva, Switzerland, Corporate Technical Journal ISSN: 1013-3119, 2014.

[36] "VSC Transmission," CIGRE Working Group B4.37, Technical Brochure 269, 2005.

[37] O. Peake, "The History of High Voltage Direct Current Transmission," *Australian Journal of Multi-Disciplinary Engineering*, vol. 8, no. 1, pp. 47–55, Jan. 2010. [Online]. Available: https://www.tandfonline.com/doi/full/10.1080/14488388.2010.11464824

[38] I. Erlich and A. Korai, "Description, Modelling and Simulation of a Benchmark System for Converter Dominated Grids (Part I)," 2018. [Online]. Available: https://www.digsilent.de/en/faq-reader-powerfactory/do-you-have-an-example-of-a-fault-tolerant-power-system-with-98-share-of-renewables.html

[39] RTDS Technologies, "Simulator Hardware," 2020. [Online]. Available: https://knowledge.rtds.com/hc/en-us/articles/360037038514-Hardware-in-the-loop-Testing-for-Microgrids

[40] "The MIGRATE Project, AN EU-FUNDED PROJECT UNDER THE FRAMEWORK OF EUROPEAN UNION'S HORIZON 2020," 2020. [Online]. Available: https://www.h2020-migrate.eu/

[41] R. N. Beres, X. Wang, M. Liserre, F. Blaabjerg, and C. L. Bak, "A Review of Passive Power Filters for Three-Phase Grid-Connected Voltage-Source Converters," *IEEE Journal of Emerging and Selected Topics in Power Electronics*, vol. 4, no. 1, pp. 54–69, Mar. 2016. [Online]. Available: http://ieeexplore.ieee.org/document/7350094/

[42] D. P. Kothari and I. Nagrath, *Modern power system analysis*. Tata McGraw-Hill Education, 2003.

[43] "Guide for the Development of Models for HVDC Converters in a HVDC grid," CIGRE Working Group B4.57, Technical Brochure, 2014.

[44] PowerFactory, "User manual, 2019." [Online]. Available: http://79.101.33.142/DIgSILENT%20PowerFactory%202019%20User%20Manual/UserManual_2019_en.pdf

[45] RTDS Technologies, "Novacor," 2020. [Online]. Available: https://knowledge.rtds.com/hc/en-us/articles/360034290474

[46] ABB, "HVDC technology for offshore wind is maturing," 2018. [Online]. Available: https://new.abb.com/news/detail/8270/hvdc-technology-for-offshore-wind-is-maturing

[47] V. Lescale, P. Holmberg, R. Ottersten, and Y. Hafner, "Parallelling offshore wind farms HVDC ties on offshore side," *Proceedings of CIGRE 2012*, (2012).

[48] T. K. Vrana, Y. Yang, D. Jovcic, S. Dennetière, J. Jardini, and H. Saad, "The CIGRE B4 DC grid test system," *Electra*, vol. 270, no. 1, pp. 10–19, 2013.

[49] "World's Most Powerful Offshore Wind Turbine: Haliade-X 12 MW | GE Renewable Energy," 2020. [Online]. Available: https://www.ge.com/renewableenergy/wind-energy/offshore-wind/haliade-x-offshore-turbine

[50] RTDS Technologies, "PB5 Card," 2020. [Online]. Available: http://knowledge.rtds.com/hc/en-us/articles/360034285894

[51] R. Ryndzionek and Sienkiewicz, "Evolution of the HVDC Link Connecting Offshore Wind Farms to Onshore Power Systems," *Energies*, vol. 13, no. 8, p. 1914, Apr. 2020. [Online]. Available: https://www.mdpi.com/1996-1073/13/8/1914

[52] RTDS Technologies, "MMC Modeling," 2020. [Online]. Available: http://knowledge.rtds.com/hc/en-us/articles/360039628773

[53] H. A. Saad, "MODÉLISATION ET SIMULATION D'UNE LIAISON HVDC DE TYPE VSC-MMC," Ph.D. dissertation, École Polytechnique de Montréal, 2015.